UDK 62
DOI: http://doi.org/10.21857/9xn31cv46y

ISSN 1848-8935 (Online)
ISSN 1330-0822 (Tisak)

RAD

HRVATSKE AKADEMIJE
ZNANOSTI I UMJETNOSTI

536

TEHNIČKE ZNANOSTI
19

ZAGREB, 2018.

RAD HRVATSKE AKADEMIJE ZNANOSTI I UMJETNOSTI
KNJIGA 536

HRVATSKA AKADEMIJA ZNANOSTI I UMJETNOSTI
RAZRED ZA TEHNIČKE ZNANOSTI

CROATIAN ACADEMY OF SCIENCES AND ARTS
DEPARTMENT OF TECHNICAL SCIENCES

Razred za tehničke znanosti
Trg Nikole Šubića Zrinskog 11, 10000 Zagreb
sivcic@hazu.hr

Elektronička inačica svih tekstova objavljenih u časopisu dostupna je na središnjem portalu hrvatskih znanstvenih i stručnih časopisa HRČAK na e-adresi http://hrcak.srce.hr/rtz

The electronic versions of all texts published in the journal are available on HRČAK, the central portal for Croatian scientific and expert journals. Link http://hrcak.srce.hr/rtz

UDK 62
DOI: http://doi.org/10.21857/9xn31cv46y

ISSN 1848-8935 (Online)
ISSN 1330-0822 (Tisak)

R A D

HRVATSKE AKADEMIJE
ZNANOSTI I UMJETNOSTI

536

TEHNIČKE ZNANOSTI

19

ZAGREB, 2018.

CONTENTS / SADRŽAJ

UDK / UDC 531/534
DOI: 10.21857/ypn4oc8nw9

Pregledni članak / Review paper
Prihvaćeno / Accepted: 18. 12. 2018.

COMPUTATIONAL MECHANICS IN SCIENCE AND ENGINEERING – QUO VADIS

Peter Wriggers, Fadi Aldakheel, Michele Marino, Christian Weißenfels

Abstract

Computational Mechanics has many applications in science and engineering. Its range of application has been enlarged widely in the recent decades. Hence, nowadays areas such as biomechanics and additive manufacturing are among the new research topics, in which computational mechanics helps solve complex problems and processes. In this contribution, these emerging areas will be discussed together with new discretization schemes, e. g. virtual element method and particle methods, whereby the latter need high performance computing facilities in order to solve problems such as mixing in an accurate way. Failure analysis of structures and components is another topic that is developing fast. Here, modern computational approaches rely on the phase field method that simplifies discretizations schemes. All these approaches and methods are discussed and evaluated by means of examples.

Keywords: virtual element methods; biomechanics; additive manufacturing; phase field methods; discrete element methods; fluid-particle interaction.

1. INTRODUCTION

The phrase ”computational mechanics” comprises two words. The second one is associated with an ”old” part of physics, which is brought by the first word into a modern multidisciplinary area. Computational mechanics nowadays plays a key role in solving problems in Engineering, Science and Medicine (Biomechanics). It combines Continuum Mechanics, Applied Mathematics, Computer Science and Modeling Techniques, and hence merges different fields and methodologies in a multidisciplinary sense to a scientific approach that helps understand physical, chemical and other phenomena in science and engineering. These types of multidisciplinary applications are today a necessity for scientific and engineering advancement. The basic phases in a computational mechanics

process are modeling, selection of a discretization scheme, software development, numerical simulation, and validation.

In this contribution, we will discuss recent developments with respect to discretization techniques and future trends in Computational Mechanics that are related to modeling and multiphysics applications.

2. MODELING

Models are required for the prediction of processes, developments and durability in science, business and engineering. In engineering and science, it is generally not possible to apply a full-scale model for a problem at hand, which is due to the large structures that have to be designed. Here the length scale difference can easily be of the order of 1000. The same is due for time scales, since processes at microstructural or atomistic level are a lot shorter than at macroscopic level when describing the behavior of a material. Hence, models have to be derived for different length scales. In engineering and science, one could start from an atomistic description of materials. However, due to the complexity and size of the problems, this is often not the adequate modeling approach. Furthermore, the molecular dynamics approach which is related to nano- and micrometer scales, is not always feasible. Thus, there is need for a continuum approach based on the theory of continuum mechanics. Even with these – in general three-dimensional – models, it is generally not possible to design real engineering structures. Thus, reduced models –such as trusses, beam, plates and shells – derived from the general three-dimensional continuum equations or other techniques to reduce the order of a complex, have to be applied to be able to reproduce the main structural behavior of the building. They are consistent with the model assumptions and may be validated by experimental data.

Model development in science and engineering is related to the length and time scales that have to be considered. If the interaction of atoms is of relevance, then the Schrödinger equations have to be solved. This is very complex and time-consuming, and is hence only used if the interaction forces between atoms are of interest. The next length scale is provided by molecular dynamics of atoms with known force relations between the atoms. Here, large dynamical systems of many molecules also have to be solved at a length scale of nanometers. Additionally, also a correct time resolution has to be considered when solving these equation set; thus, only shorter time periods can be predicted. Such models can be applied to model chemical reactions, biological cells or material behavior at atomic length scale. The models are very accurate, but due to their complexity, they cannot be used as predictive tools for many applications. In order

to overcome this difficulty, it is necessary to coarsen such models, which lead to continuum models that include atomistic or molecular structures in a smeared way within the constitutive relations. These models are classically applied for most predictions in engineering, biomechanics and physics.

In the next step, we focus on the modeling process in engineering.

Modeling Process. Engineers have to make prediction for objects such as structures, machines, cars, airplanes, but also medical devices and structures in biomechanics. This starts with a design goal, and then the real physical behavior of the object has to be projected onto a model that can accurately predict the response of the object in the application range that is set by the design goals. Often the model will not lead to the expected results, and a different or refined model will have to be generated. A generic cycle is depicted in Fig. 1. It includes the steps leading to a proper model.

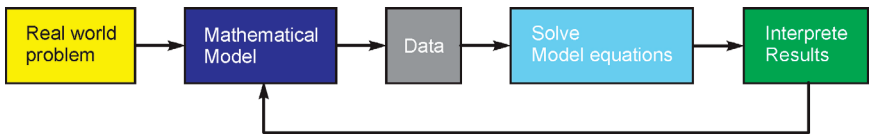

Fig. 1. Model development from the real world to mathematics.

Sl. 1. Razvoj od realnog problema do matematičkog modela.

One of the main steps in this process is the construction of the model. Most frequently, an existing model is used – amended in such a way that it reproduces the behavior of the real world object. However, the development of a completely new model is also possible when the real world problem demands a new approach.

Another major step is the collection of proper data. In engineering, this includes the action of a surrounding medium, dead loads and other loads. Additionally, initial conditions of states and boundary conditions have to be considered. These data often have random character and thus bring uncertainties into the model. Data collection can also invoke a refined process when it turns out that e.g. actions of the surrounding medium – air or water – have to be predicted by a model itself, that has then to be coupled with the structure leading to a so called fluid-structure-interaction problem.

Once the mathematical formulation of the model is finished the set of algebraic or differential equations has to be solved. For this purpose, a proper method has to be selected. Here, the engineer needs sufficient mathematical background and knowledge in engineering theory, such as continuum mechanics, in order to select a solution scheme that provides reliable results in the most efficient way when e.g. nonlinear problems are addressed. Here, we have to ask the question: *Do we solve the equations right?*

Within the last step, the model results have to be interpreted and validated. This is of utmost importance, since the reliability of a model depends on good validation. The latter word means: *Are the model equations correct?* This question can be answered by experiments if possible or by the knowledge of the engineer who can judge the results by experience. Furthermore, simplified models can be used to access general correctness.

On a first view, it seems that all steps can be carried out one after another. However, it is obvious that the last and the first step are connected, since a change in the model can be caused by the validation. However, the mathematical model might also have to be changed if the interpretation of results suggests a new mathematical model. Thus, instead of going back to the first step, the loop is now just from the fourth to the third step. And again, the loop can also be formed from the validation step to the data collection, and thus different paths might have to be followed in the process of projecting real world problems onto a model.

Theoretical background. New models have to rely on a sound theoretical formulation that leads in general to a set of partial differential equations. The general equation set formulates time-dependent problems in three-dimensional space. The basis for setting up the correct equation set for a continuum mechanics problem is given by the following general structure:

- **Kinematics**: deformation, displacements, rotations and velocities.
- **Balance laws**: balance of mass, momentum, momentum of momentum, the first and the second law of thermodynamics.
- **Constitutive relations**: assign quantities from kinematics to stresses. These equations have to be selected related to the material under consideration and can thus only be determined from experimental data or from atomistic scale computations with respective homogenization.

All of these laws and relations lead to partial differential equations that are in general nonlinear. The general formulation can be specialized for solids and fluids. But often, for more complex applications, coupled sets of equations are needed in order to include multi-physics like temperature, diffusion and other transport phenomena.

Many current topics need new modeling processes. Here, we chose to focus on several topics that are associated with emerging areas, such as special discretization techniques, discrete element method and particle-laden flows, as well as new models for additive manufacturing and biomechanics.

3. DISCRETIZATION TECHNIQUES

During the last sixty years, the finite difference method, the finite element method, and the boundary element method were developed; they are now ready for application in engineering design problems. Many of these methods cover the problem ranges that are described above (e.g. small/large strains, different constitutive equations or coupled field equations). Additionally, new approaches, such as meshless methods for arbitrary deformations, isogeometric analysis, and the extended finite element method (XFEM) for fracture mechanics problems evolved and can be efficiently used within a specific problem range. Thus, the art of modeling means here picking the right numerical solution method that provides accurate results in the most time-efficient way.

Each of the methods described above has its own specifications and thus needs experts for correct and efficient application. As an example: within the finite element method, there are hundreds of different finite element formulations for different applications that can even fail when applied to an inadequate problem. The same is true for all the other methods.

Here, a relatively new method – the virtual element method, which can be an alternative for specific problems – will be presented. The authors of the method were F. Brezzi and coworkers, see [5].

3.1 Virtual Element Method (VEM)

The virtual element method was developed during the last decade and applied to problems in elasticity for small strains and other areas in the linear range. Extensions of the virtual element method to problems of compressible and incompressible nonlinear elasticity and finite plasticity have been reported in the last years. Low-order formulations for problems in two and three dimensions, with elements being arbitrary polygons or polyhydra, are considered. Various formulations considered are based on the minimization of energy, with a novel construction of the stabilization energy.

The structure of the VEM typically comprises a term in the weak formulation or energy functional, in which the displacement $\boldsymbol{u}_h$ (with the nodal degrees of freedom $\boldsymbol{u}_I$), being sought, is replaced by its projection $\boldsymbol{u}_\pi$ onto a polynomial space (see Fig. 2).

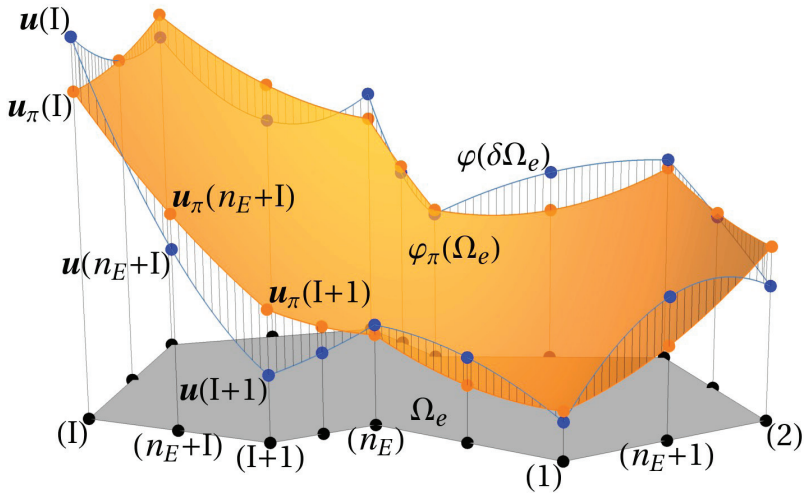

Fig. 2. Projection of an arbitrarily shaped element onto an ansatz space using a quadratic polynomial.

Sl. 2. Projekcija elementa proizvoljnog oblika u područje interpolacije korištenjem polinoma drugog stupnja.

This results in a rank-deficient structure, so that it is necessary to add a stabilization term to the formulation. The stabilization term is generally a function of the difference $\boldsymbol{u}_h - \boldsymbol{u}_\pi$ between the original variable and its projection. In order to adhere to a fundamental aspect of VEM, in which all integrations take place on element boundaries, the stabilization term proposed (see e.g. [5]) takes the form of a sum of a function of nodal variables. This is the approach adopted in some nonlinear investigations with the scalar stabilization parameter of the linear case being replaced by one that depends on the trace of the fourth-order elasticity tensor.

For another formulation of VEM that uses a different stabilization technique, see [24]. The essence of the method is the addition to the positive semi-definite mean strain energy Ψ a positive-definite energy $\hat{\Psi}$, which is evaluated using full quadrature, and for consistency subtraction of a term involving $\hat{\Psi}$ as a function of the mean strain. The strain energy is then the sum of $\Psi(\boldsymbol{u}_\pi) + [\hat{\Psi}(\boldsymbol{u}_h) - \hat{\Psi}(\boldsymbol{u}_\pi)]$, the original energy as a function of the projected displacement, and a term in which a positive definite stabilization energy as a function of the displacement and its projection are respectively added and subtracted. The second term vanishes when the element size goes to zero.

The methodology can be applied for compressible and incompressible elastic and inelastic materials. Some examples of this new promising discretization scheme are discussed below.

3.2 VEM for hyperelasticity

Once the projection of the virtual element method is known, which in case of linear polynomials can be computed directly (see [24]), it is simple to compute the constant deformation gradient related to the projection $\boldsymbol{u}_\pi$ within a virtual element. This computation only involves an integral over the boundary of the virtual element. Once the deformation gradient is known, quantities like the left Cauchy Green tensor and its invariants that enter the strain energy function can be easily obtained. Hence, the strain energy $\Psi(\boldsymbol{u}_\pi)$ can be computed, and by using the software tool AceGen (see [13]), the residual and tangent stiffness related to that strain energy function follow.

The stabilization needed to obtain a virtual element with correct rank is based on the strain energy difference $\hat{\Psi}(\boldsymbol{u}_h) - \hat{\Psi}(\boldsymbol{u}_\pi)$, see [24]. The second term can be computed in the same way as $\Psi(\boldsymbol{u}_\pi)$. For the first term of the stabilization part, internal triangularization is used, which involves only the boundary nodes of the virtual element. Here, linear triangles or tetraheders are used, which again leads to constant strains per internal element and yield an efficient formulation of the virtual element.

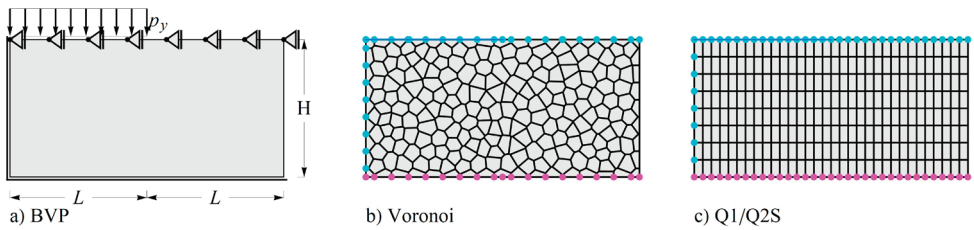

Fig. 3. Punch problem and different mesh types.

Sl. 3. Problem utiskivanja i različite vrste mreža.

As an example, we consider the punch problem depicted on the left side in Fig. 3. The punch is on rollers at the bottom and the left side. The displacement at the top is restricted, so that it can only deform vertically. A uniform load is applied at the top on the left half of the punch. A Neo-Hookean strain energy is used with a Young's modulus of E = 240 kN/mm^2 and a Poisson ratio of ν = 0.3. The length L and height H have the same value of 1 mm. A total load of 800 kN/mm is applied leading to the deformed configurations shown in Fig. 4.

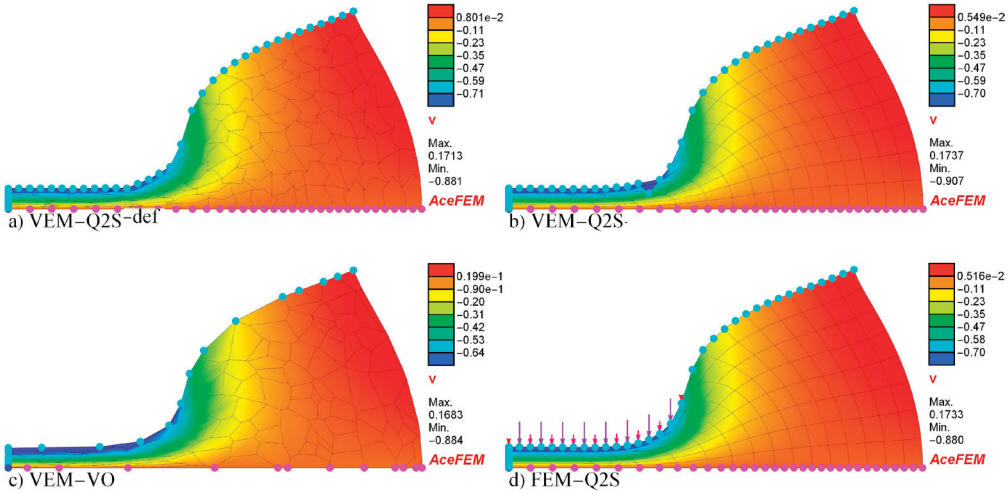

Fig. 4. Comparison of different discretizations.

Sl. 4. Usporedba različitih diskretizacija.

Different types of meshes were used, as can be seen in Fig. 3 b) and c) on the right side. The meshes consist of 8 noded quadrilateral elements that are standard for a serendipity finite element mesh, here denoted by Q2S. The results for this type of mesh can be seen in Fig. 4 b) and d), whereby b) relates to a solution using the linear virtual elements with eight nodes, and d) depicts the solution when using quadratic serendipity finite elements. In Fig. 4 a), the Q2S mesh is distorted by randomly positioning the nodes of a Q2S serendipity mesh. This leads even to non-convex elements. The solution is here obtained with virtual elements that directly discretize these elements. Finally, in Fig. 4 c), a randomly generated Voronoi mesh consisting of elements with different sizes was used.

All discretizations converge for a mesh size of 32 × 16 elements to the same solution, however, even when the meshes have only 8 × 4 elements, the deviation of the final vertical displacement under the load is less than 1 % with respect to the converged solution.

3.3 VEM for finite strain elasto-plasticity

In contribution [12], the virtual element method using linear polynomial approximations was applied to finite strain plasticity. As an example, the torsion of a bar with square cross section was considered in [12].

The bar is subjected to a torsional load around z-axis at the center. The geometrical setup and the loading conditions of the specimen are depicted in Fig. 5(a). The height along the third direction z is chosen to be $H = 5$ mm, and the length of the square cross-section is set to $L = 1$ mm. At the boundaries, we fixed the bottom end of the bar and applied torsion to the top end, as depicted in Fig. 5(a). The elongation along the third direction z at the top surface is linked, i.e. $\Delta w_{ij} = w_i - w_j = 0$. Different element formulations are studied to illustrate the robustness of the proposed virtual element method. A Voronoi mesh of about $9 \times 9 \times 36$ elements was used; this is depicted in Fig. 5(b).

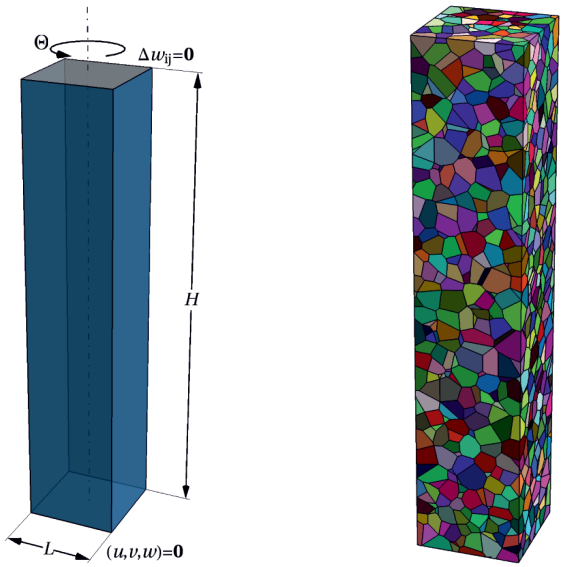

Fig. 5. Numerical torsion test of a square-section bar. (a) Geometry and boundary conditions; (b) Voronoi mesh used in the numerical analysis for $9 \times 9 \times 36$ elements.

Sl. 5. Numerički test uvijanja štapa kvadratnog presjeka. (a) Geometrija i rubni uvjeti (b) Voronoijeva mreža korištena u numeričkoj analizi za $9 \times 9 \times 36$ elemenata.

Figure 6 demonstrates the distribution of the equivalent plastic strain α using VEM-VO for different rotation angles until one cycle $\Theta = 360^{\circ}$ is completed. In comparison with the standard, the virtual element formulation provides as good solutions as a H1-P0 element. A cut through the bar was made in both the contour plots (results: Figure 6) to illustrate the plastic evolution inside the specimen along with the deformed elements.

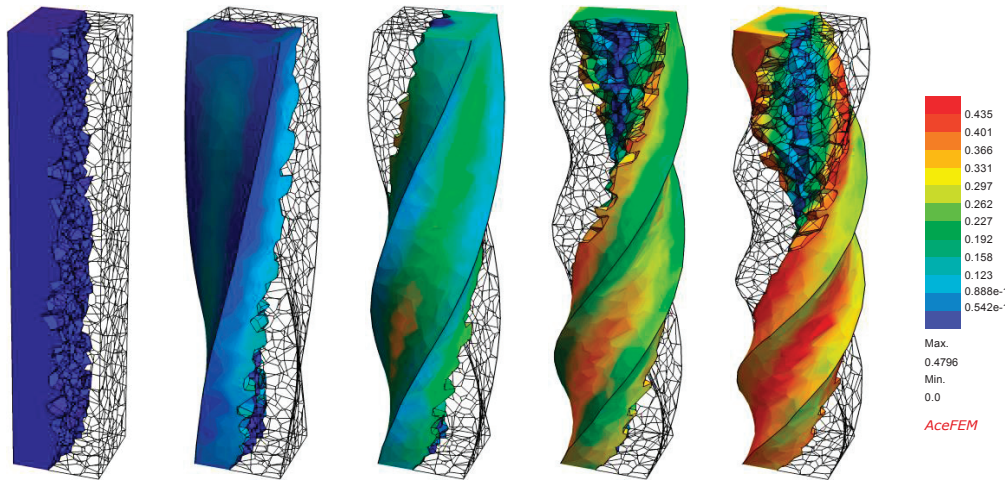

Fig. 6. Numerical torsion test of a square-section bar. Distribution of the equivalent plastic strain for different rotations angles until the cycle is completed using the VEM-VO element.

Sl. 6. Numerički test uvijanja štapa kvadratnog presjeka. Raspodjela ekvivalentne plastične deformacije za različite kutove rotacije do postizanja punog ciklusa primjenom VEM-VO elementa.

4. VARIATIONAL PHASE-FIELD MODELING

The analysis of crack initiation and propagation in ductile materials has been a topic of intensive research recently, to predict failure mechanisms for various engineering applications. Machining, cutting and forming ductile materials are at the core of automobile, aerospace, medical fields, bridges or heavy industries. These applications can significantly benefit from a precisely predictive computational tool to model ductile fracture in the design phase of products.

Numerical tools for the prediction of fracture initiation and propagation are numerous (see [15]). Besides boundary and finite element methods for linear elastic fracture analysis, different versions of the so-called eXtended Finite Element Method (XFEM) are applied. The underlying methodology is based on the enhancement of the internal element shape functions by modes that account for the fracture. This method is well developed and even used in the context of multiscale applications in which micro cracks are modeled; they can later grow into macro cracks leading to failure of a structural element; for details see e.g. [11].

Starting with the work of [7], fracture processes were modeled by a phase-field approach. Due to its simplicity, this methodology has gained wide interest und has been used in the engineering community since 2008. From there on, many scientists have worked in this field and developed phase-field approaches for finite elements, isogeometric analysis, and lately also virtual element technology (see [3]). The main driving force for these developments is the possibility to handle complex fracture phenomena within numerical methods in three dimensions. Thus, research on phase-field approaches is still vivid and points in many different directions. Three applications can be found in the next sessions.

4.1 Brittle fracture

The phase-field approach regularizes sharp crack surfaces within a pure continuum setting by a specific gradient damage modeling with constitutive terms rooted in fracture mechanics. The key goal of the development is to present a consistent variation-based framework for the phase-field modeling of isotropic brittle fracture. It is based on a constitutive work density function and a dissipation function with threshold for fracture, which together define a minimization principle for the coupled problem. The work density function is decomposed into: (i) An energetic part defined to be exclusively elastic in nature, which represents a degraded elastic free energy density. Besides the constitutive expression for the stresses, it also provides a locally energetic driving force for regularized fracture. (ii) The dissipative part governs fracture resistance with the inclusion of a fracture length scale parameter. For brittle fracture, the material response corresponds to the sequence: E(elastic) - F (fracture).

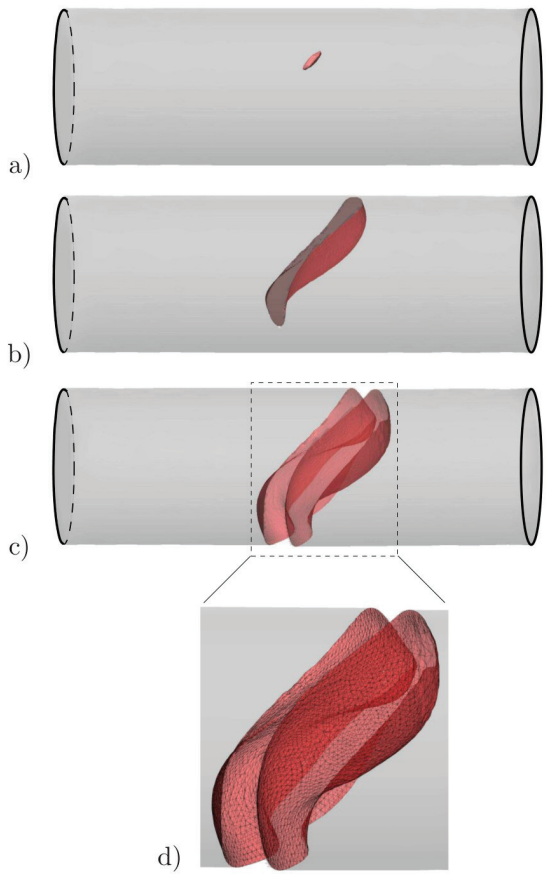

Fig. 7. Three-dimensional torsion test of a cylindrical bar. (a)–(c) Contour plots of the fracture phase-field *d* evolution in brittle (Elastic-Fracture) cast-iron for a twist loading. (d) Visualization of the crack faces.

Sl. 7. Trodimenzijski test uvijanja cilindričnog štapa. (a)-(c) konturni prikaz razvoja lomnog faznog polja *d* u krtom (elastični lom) lijevanom željezu za opterećenje uvijanja. (d) Prikaz lomnih ploha.

On the computational side, one may employ either a monolithic or a staggered algorithm to compute the unknowns, in which the displacement and the crack phase-field are computed simultaneously or alternatively, respectively. Herein, a robust and efficient monolithic scheme is employed in the numerical implementation using the software tool AceGen (see [13]).

As an example, the three dimensional torsion test of a cylindrical bar was considered in [2]. The evolution of the crack phase fi *d* for the cast-iron bar is depicted in Fig. 7. The crack starts to initiate at a point on the surface near the center of the specimen at an angle of twist of 1.1° (see Fig. 7a). Then it propagates from the surface inwards until final rupture in Fig. 7c. To illustrate the crack surface, we zoomed out the fractured area as shown in Fig. 7d. Since the fracture path is about 45° from the longitudinal direction, the fracture surface is complicated and looks like a helicoids. Here, we used a transparency effect to show the failure surface for $d \geq c \approx 1$.

4.2 Ductile fracture

Most metals fail in a ductile fracture mode, preceded by considerable plastic deformation, in contrast to brittle or quasi-brittle materials, where fracture occurs without noticeable permanent deformation, as discussed above. The modeling of failure in ductile materials must account for complex phenomena at micro-scale, such as void nucleation, growth and coalescence, the formation of micro-shear-bands and micro-cracks, as well as the final rupture at the macro-scale.

A large number of phenomenological and micro-mechanical approaches exist for the continuum modeling of ductile fracture. From the computational point of view, the tracking of sharp crack surfaces provides substantial difficulties and is often restricted to simple crack topologies. This difficulty can be overcome by recently developed phase-field approaches to fracture, based on the regularization of sharp crack discontinuities.

The novel aspect of this research is a precise representation of the framework in a canonical format governed by variation principles. The coupling of plasticity to fracture mechanics is realized by a constitutive work density function that includes the stored elastic energy and the dissipated work due to plasticity and fracture. The latter represents coupled resistance to plasticity and fracture, depending on the internal variables that enter plastic yield function and fracture threshold function.

In Fig. 8, the experimentally observed cup–cone failure mechanism of porous plastic solids in a round tensile bar is analyzed numerically. A huge plastic deformation as a necking zone with concentration hardening in Fig. 8a and void fraction in Fig. 8d at the specimen center, resulting in crack initiation at the center zone, as demonstrated in Fig. 8f. The crack phase field *d* then propagates horizontally from the center outward along a zig-zag path. Thereafter, the failure mode changes to a shear mode, and the crack continues propagating at about 135° from the loading direction to follow the equivalent plastic strain evolution path in Fig. 8c and the void volume fraction path in Fig. 8e, giving rise to the final cup–cone fracture surface. For visualization of crack surface, deformed regions with a crack phase-field $d \approx 1$ are not plotted. For details on phase-field porous ductile fracture, we refer the interested reader to Aldakheel et al. [1].

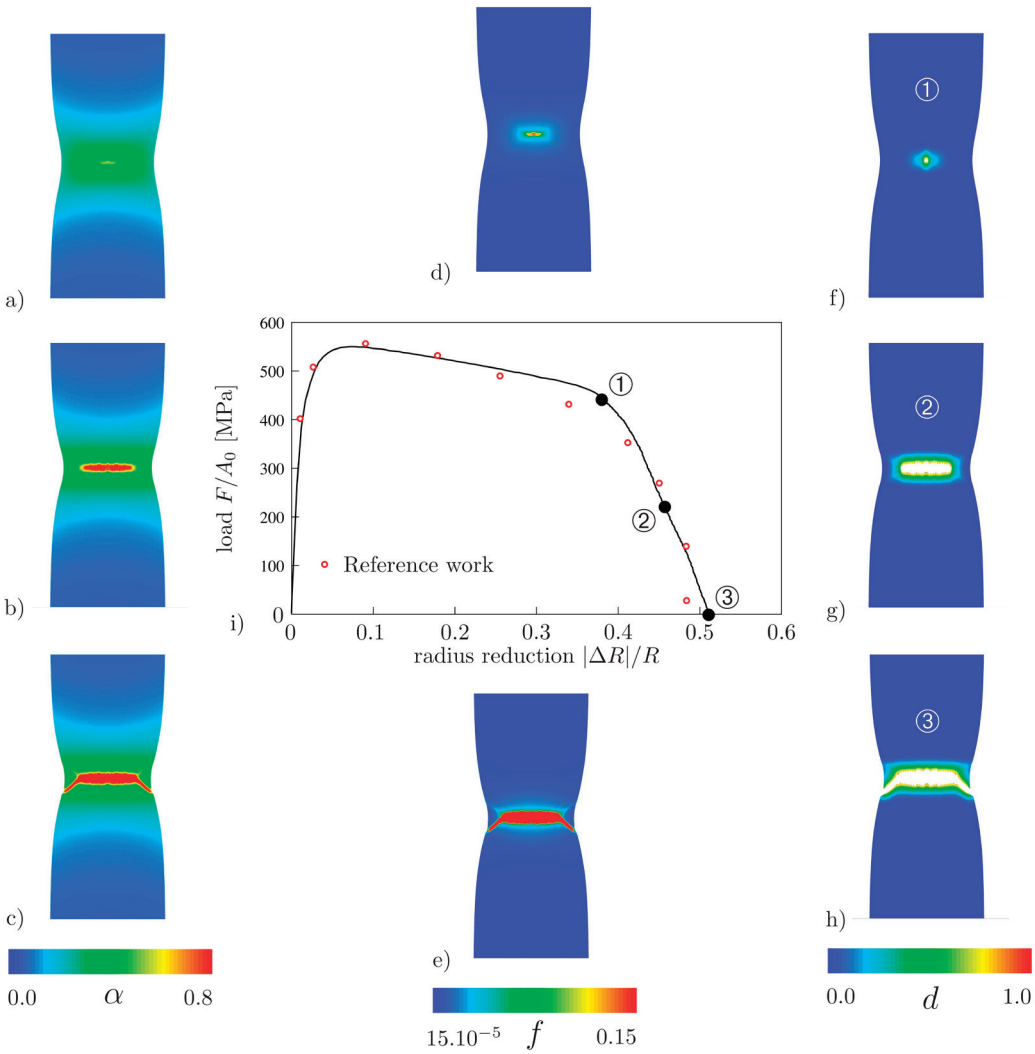

Fig. 8. Cup–cone formation in axis-symmetric tension test. Contour plots of the hardening variable in (a)-(c); the void volume fraction *f* in (d)-(e) and the fracture phase-field *d* in (f)-(h). Load (force *F* / initial cross sectional area A_0) versus magnitude of the radius reduction $|\Delta R|/R$ curve in comparison with the reference work of Besson et al. [2001] is shown in (i).

Sl. 8. Nastajanje Cup-cone oblika pri osnosimetričnom vlačnom testu. Konturni prikaz varijable očvršćenja u (a)-(c); volumni udio šupljina *f* u (d) i (e) i fazno polje *d* u (f) i (h). Krivulja medusobne ovisnosti opterećenja (sila F/početna površina poprečnog presjeka) i veličine redukcijskog polumjera $|\Delta R|/R$ u usporedbi s referenciranim radom Besson i drugi [2001] je prikazana u (i).

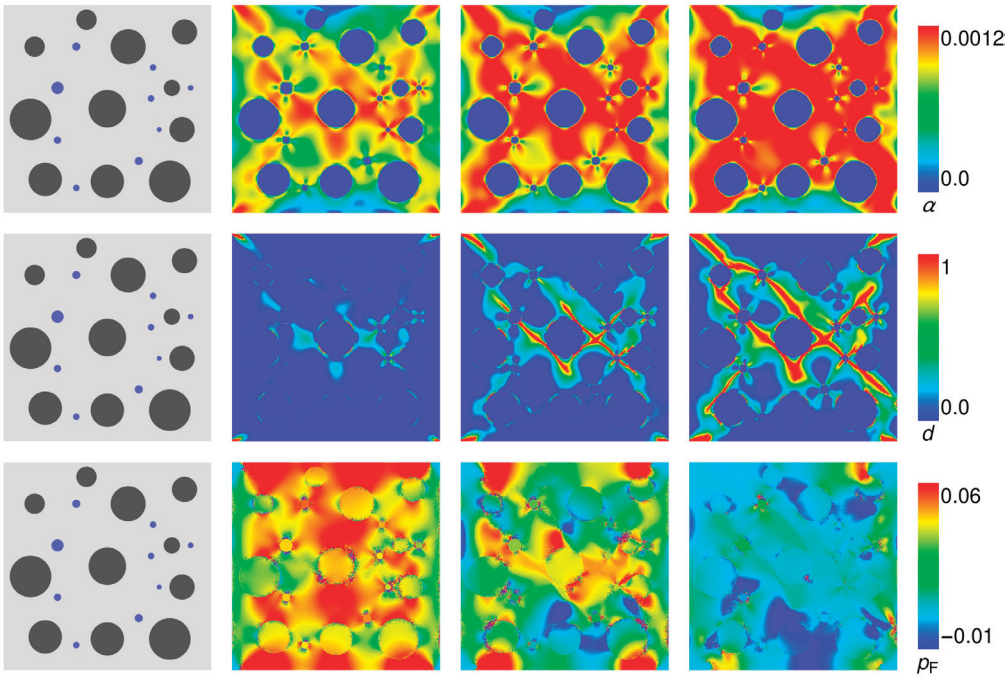

Fig. 9. Compression test for idealized microstructure of concrete specimen under water. Dark gray circles represent the stones, blue circles stand for water (saturated voids), and the rest with light gray color stands for the cement paste (mixture). Evolution of the hardening variable , crack phase-field d and fluid pressure p_F .

Sl. 9. Tlačni test idealizirane mikrostrukture betonskog uzorka pod vodom. Tamnosivi krugovi predstavljaju kamenje, plavi krugovi su voda (natopljene šupljine) i ostatak označen svjetlo sivo je cementna pasta (mješavina). Nastajanje varijable očvršćenja , pukotina faznog polja d i tlak fluida p_F .

4.3 Multi-physics problems at fracture

For new applications in multi-phase problems, water-induced failure mechanics for concrete based on the phase-field approach is investigated. The concrete has a highly hetero-geneous structure on different scales, and its composite behavior is very complex. Due to this, a variety of effects ought to be considered for analyzing failure response at micro-scale, e.g. modeling the solid skeleton, fl bulk phases and their interaction. To this end, the fracture phase-field formulations are extended towards Darcy-Biot-type fluid-saturated heterogeneous porous media at micro-to-macro-scale, see Fig. 9 as a preliminary result in this direction.

The evolution of the equivalent plastic strain α (first row), the crack phase-field d (second row) and the fluid pressure pF (third row) are depicted in Fig. 9. The plasticity starts to accumulate around the stiff gravel, and the fluid pressure increases from the saturated voids. The crack starts to initiate in the plastic zones when the elasto-plastic energies reach a critical value. As expected, the fluid pressure however drops in the fractured areas as shown in Fig. 9.

5. DISCRETE ELEMENT METHODS

Discrete element methods are becoming an increasingly powerful tool, especially for the treatment of granular materials and in process engineering. The method can nowadays be applied to problems that need more than 10 million particles for an accurate model. These processes are run on high-performance parallel computers or GPU systems. The problem of the interchanging contact conditions due to large particle motions presents a challenge for the development of algorithms that scale well for large numbers of processors.

5.1 Mixing of particles

Here, we will focus on an application that uses the discrete element method to model the mixing process of different particles in a drum. In this application, the particles are mixed by rigid blades that rotate about the middle axis. The blades move up and down to perform the mixing. Here, millions of particles have to be considered, and many small time steps have to be executed to follow the complex motion of the particles in a mixer. Such problems necessitate the use of parallel computing machines with many cores. The problem is depicted in Fig. 10 a), which also shows the allocation of parts of the particles to a specific core of the parallel computer. In Fig 10 b), the velocity distribution during the mixing process is depicted. One can easily observe the complex movement of the particles that change locations and come into contact with other particles, thus leaving the location of the initial allocation and having to be moved to another core. This usually requires a reallocation and slows down the computation. In order to get good performance, sophisticated algorithms have to be used, which on the one hand have to be fast, and on the other limit data transfer. Thereby, a linear speed-up, even for a large number of processors, can be achieved (see Fig. 11). The blue curve shows the theoretical limit for a speed-up investigation up to 3500 processors. The red curve shows the performance for one algorithm, while the more sophisticated algorithm and related data handling amount to the green curve that produces an extremely good linear speed-up over all number of processors that reaches 66 % of the theoretical limit.

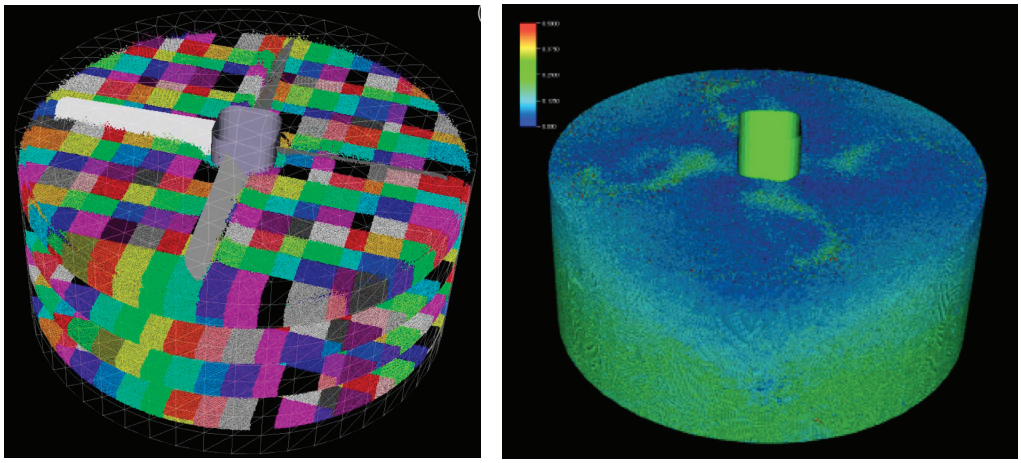

Fig. 10. a) Set-up of the particles in the mixer. The color code shows the allocation to a core in the parallel computer. b) Velocity distribution of the particles during mixing.

Sl. 10. a) Postavljene čestice u mikseru. Bojom označeni dijelovi pokazuju razmještaj u jezgri paralelnog računala. b) Raspodjela brzine čestica za vrijeme mješanja.

5.2 Particle Flow

Particle flow is governed by combining fluid mechanics with particle mechanics. Thus, the field of Computational Fluid Dynamics (CFD) is combined here with a discrete scheme based on the motion of distinct particles. Modeling of such flows requires different steps. On the one hand, the CFD model has to describe the fl using the Navier-Stokes equations. On the other hand, the motion of the particles has to be characterized by the classical equations for rigid bodies.

Different discretization schemes for the fluid can be employed. Among them are: finite difference schemes (see e.g. [8]), the finite volume approach (see. e.g. [10]), the Lattice Boltzmann method (see e.g. [14]), or the finite element method – to name only a few. In our approach, we use a finite element approach as developed in [20] leading to a computational fluid dynamics model, which has to be solved as an initial value problem (see [4]). The equations of motions describing the particle motion can be solved directly by a numerical integration scheme in time.

The interaction between the particles and rigid walls – describing the boundary of the fluid domain – is described by constitutive equations that take care of the approach of the particles, the friction at the interface and adhesive forces. The interaction between fluid and particles is modeled using an immersed technique, in which the fluid forces acting

on the particle are considered as well as the obstacle resulting from particle geometry that influences the flow.

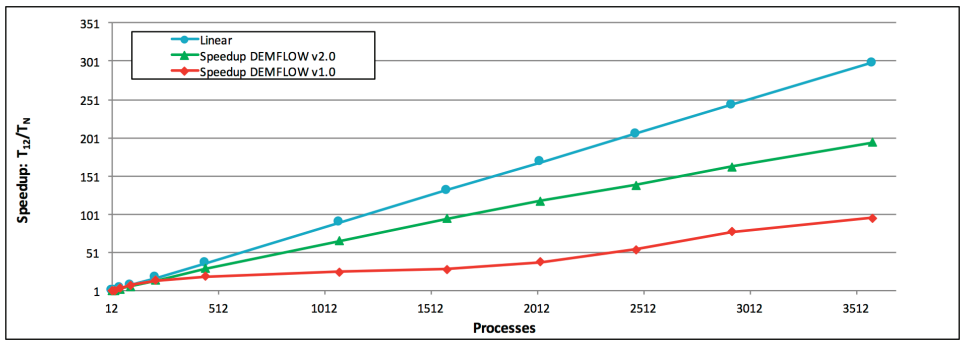

Fig. 11. Speed-up for different algorithmic treatments.

Sl. 11. Ubrzanja za različite algoritamske postupke.

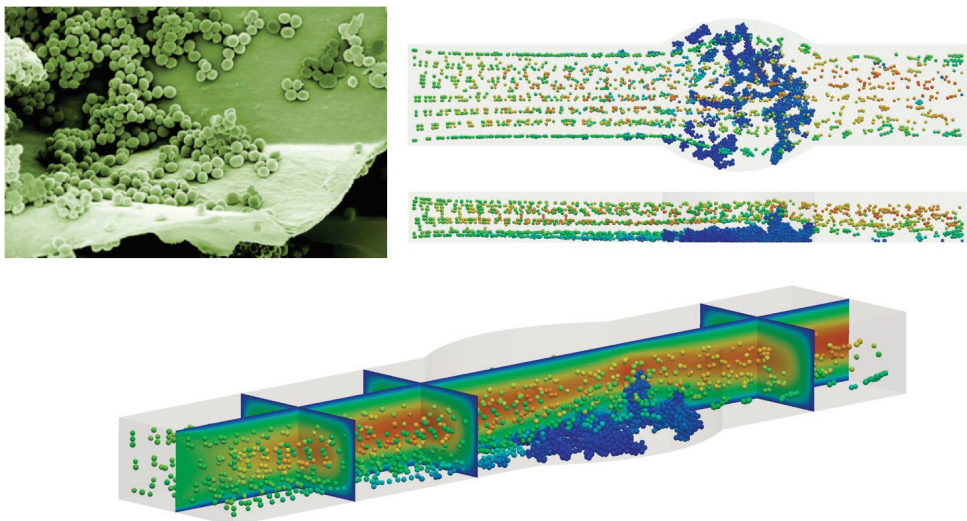

Fig. 12. Modeling biofilm growth using a particulate flow mode.

Sl. 12. Modeliranje rasta biofilma korištenjem čestičnog strujnog moda.

The particulate flow model is now applied to the growth of a biofilm, where the molecules are approximated by rigid particles. Adhesion between particles and walls is considered such that particles in the fluid can adhere to each other and also to the walls.

The channel (see Fig. 12) has a wider cross-section in the middle. Due to this, one can observe in Fig. 12 that the biofilm represented by the particles attaches to the surfaces in the middle of the channels, where the velocity of the flow is reduced. This is related to the decreased shear forces enforced by the flow on the particles.

6. ADDITIVE MANUFACTURING

Following the strategies of several governments, additive manufacturing will play a significant role in the digitalization of industry. This layer-by-layer 3D-printing process allows the production of mass customized products, e.g. patient specific implants, the building on demand of spare parts for aircraft or vintage cars, or the generation of new materials that exhibit desired mechanical, thermal, electrical, magnetic or optical behavior. The only input in this process is the data triple consisting of the digital model, the material composition and the process parameters. However, the physics of the whole process is not fully understood. Reproducibility, the control of the final physical properties, the quality assurance, and the automatization of the process chain are still barriers that limit comprehensive use in industry. The increase in computational power for mathematical modeling and simulation opens the possibility for scientific computing to play a significant role in the design of advanced manufacturing processes. However, classical simulation software, as the Finite Element Method for example, are ill-suited to simulate systems that are inherently discontinuous, such as additive manufacturing processes. However, meshfree computational methods are being developed – e.g. the stabilized Optimal Transportation Meshfree (OTM) method ([23]) or Smooth Particle Hydrodynamics (SPH), which are ideal for the simulation of these processes.

Fig. 13. Selective Laser Melting on the particle scale using
"Implicit Smooth Particle Hydrodynamics"

Sl. 13. Selektivno lasersko taljenje na skali čestice korištenjem metode
"Implicit Smooth Particle Hydrodynamics"

6.1 Multi-physical modeling

For including simulation software into the virtual development process, high fidelity models, which represent all the physical phenomena, are indispensable. In Selective Laser Melting (SLM) processes, the main interacting phenomena are laser matter interaction, heat transfer, phase transition, residual stress formation, and surface tension. The interaction with the process parameters laser power, scan rate, laser beam diameter, particle size, height particle layer and hatch spacing determine the quality of the printed component. Due to temperature, the state of each particle changes from solid to fluid and back to solid. The phase change approach, which models the whole solidification in a finite deformation framework suited to represent this effect in the SLM processes, can be found in [22]. Based on this, it can be demonstrated that the most important physical effect in Selective Laser Melting is surface tension. This effect is responsible for the fusion of two particles as shown in Fig. 15. If surface tension is neglected, only the thermal expansion of the particles can be observed.

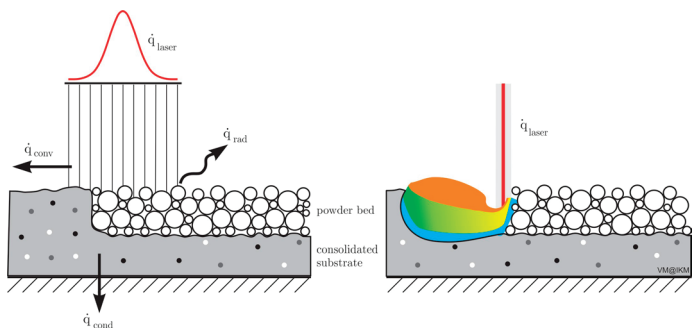

Fig. 14. (Left) Laser irradiation is emitted by thermal conduction, convection and radiation. (Right) Melt pool due to molten particles.

Sl. 14. (Lijevo) Lasersko zračenje uslijed toplinskog provodenja, konvekcije i radijacije. (Desno) bazen s talinom uslijed rastaljenih čestica.

6.2 Influence of laser heat source modeling

The laser matter interaction plays another central role in additive manufacturing processes. Laser emits power in pulses or continuously. Four stages of sophistication of laser modeling can be distinguished. The simplest form is the estimation of heating from the absorbed energy. Another simplification is a volumetric heat source model.

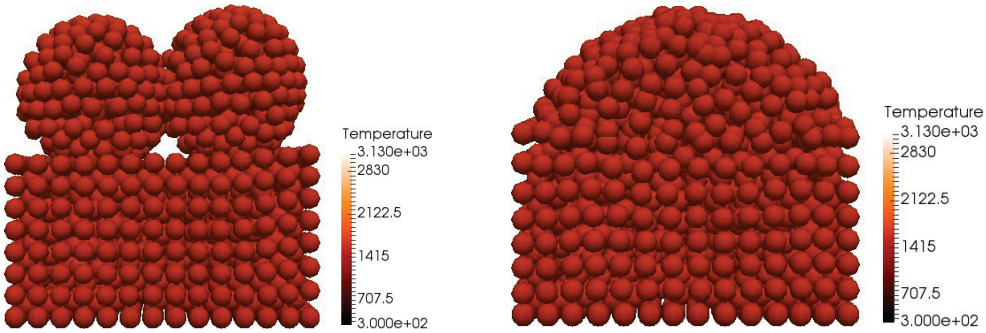

Fig. 15. Melting and solidification of two laser-irradiated particles using the stabilized OTM method, (left) neglecting and (right) including the surface tension effect.

Sl. 15. Taljenje i skrućivanje dviju čestica ozračenih laserom korištenjem stabilizirane OTM metode (lijevo) zanemarivanjem i (desno) uključivanjem efekta površinske napetosti.

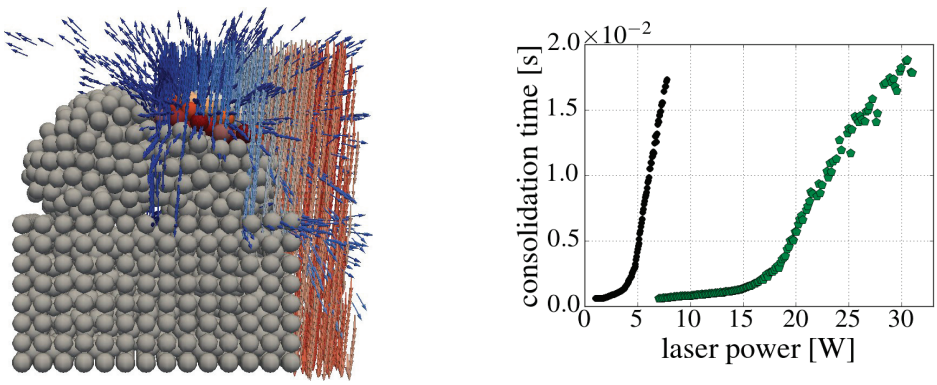

Fig. 16. (Left) Ray tracing approach coupled with the stabilized OTM method. (Right) Comparison of consolidation time between volumetric heat source model of [9] (green dots) and ray tracing approach (black circles).

Sl. 16. (Lijevo) Postupak provlačenja zraka u spoju sa stabiliziranom OTM metodom. (Desno) Usporedba vremena konsolidacije izmedu modela toplinskog izvora [9] (zelene točke) i postupka provlačenja zraka (crni kružići).

Discretizing the laser into rays is the next step of sophistication. The electro-magnetic Maxwell equations provide high accuracy of laser propagation, but the computational cost thereof is very high.

A coupling algorithm of ray tracing with meshfree methods can be found in [21]. The influence of the heat source modeling on the fusion of particles is also investigated therein. As shown in Figure 16, comparison between the volumetric heat source model for the SLM processes given in [9] and the ray tracing approach shows a different response behavior, although the absorbed energy is equivalent in both cases.

7. COMPUTATIONAL BIOMECHANICS

Advancements in computational methods for biomechanical applications can speed up the rate of scientific discovery in medicine and improve the effectiveness of clinical approaches. *In silico* analyses indeed reduce the need for experimental clinical trials, allowing to reproduce different pathophysiological scenarios in a rapid and low-cost way. In particular, computational biomechanics helps: (i) clarify the complex mechanobiological equilibrium that maintains physiological behavior; (ii) identify the relationships between histological and biochemical alterations with pathologies; (iii) gain a better understanding of the etiology of diseases; (iv) support the tailoring of clinical treatments to patient-specific features.

Personalized and effective numerical simulations for clinical applications need the patient-specific definition of geometry, applied loads/boundary conditions and material properties. While better While better patient-specific geometries are essentially related to progress in medical imaging technologies and reconstruction algorithms, advances in computational mechanics techniques can significantly increase the reliability of personalized boundary conditions and mate rialm properties.

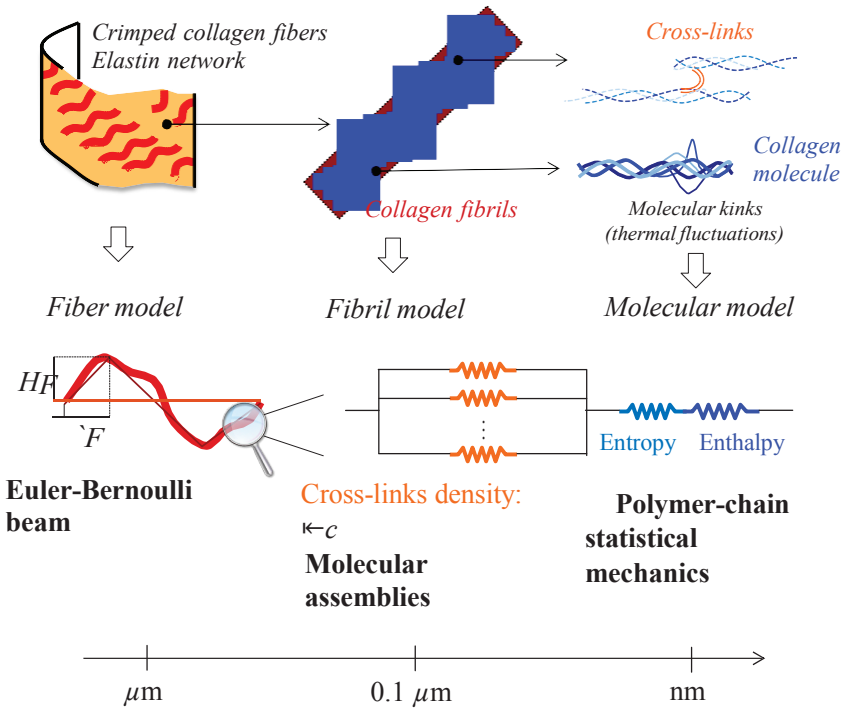

Fig. 17. Multiscale homogenization rationale for tissue constitutive nonlinearities: analytical description of crimped fibers (microscale), cross-linked molecular assemblies (meso(nano-to-micro) scale), and molecular elongation mechanisms (nanoscale).

Sl. 17. Višeskalno homogenizacijsko načelo za konstitutivne nelinearnosti tkiva: analitički opis nabranih vlakana (mikroskala), poprečno povezani skupovi molekula (mezo (od nano do mikro) skala i mehanizmi izduženja molekula (nanoskala).

In order to introduce recent results in the field, an exemplary case of arterial blood vessels is addressed here. Computational analyses of arterial segments clearly require the solution of the fluid-structure interaction (FSI) problem. Nevertheless, with respect to a number of FSI problems in more traditional engineering contexts, these simulations are complicated due to the need of accounting for high constitutive nonlinearities and the complexity of the vascular system, which is made up by a series of interconnected branches. Indeed, accurate representations of both physiological and pathological flow conditions require a fine complete description of vessel wall mechanics and hemodynamics conditions. Moreover, pathologies are associated with an alteration of cell-cell signaling molecular pathways in tissues. Biochemical reactions indeed drive the concentrations

of biologically active molecules. These substances play a crucial role in the synthesis/degradation of the constituents of the extra-cellular matrix. Accordingly, they drive the growth and remodeling mechanisms of tissues in a complex balance that might bring to either tissue healing or pathological and uncontrolled modifications associated with mechanical dysfunctions.

In what follows, novel solutions for some computational challenges in biomechanics are discussed: multiscale homogenization approaches for tissue constitutive models; the FSI simulations accounting for constitutive nonlinearities and the up-/down-stream vasculature; multiphysics approaches for the chemo-mechano-biological description of growth and remodeling. Future trends in the field are also traced.

7.1 Multiscale homogenization approaches

The mechanical response of soft tissues is highly nonlinear and associated with a (quasi) incompressible behavior. The response is highly anisotropic and depending on the presence of collagen fibers embedded in an elastin network. Defects in the structure and arrangement of these constituents play a primary role in the onset and evolution of diseases. The challenge here is to incorporate structural information in constitutive models. In the state-of-the-art, widely-employed constitutive approaches are essentially based on phenomenological descriptions of the strain energy of collagen fibers, with their mean orientation being the only structural information [16]. Therefore, they generally exhibit a weak relationship between model parameters and tissue histological/biochemical features. Alternatively, multiscale homogenization approaches for soft tissues mechanics have been recently developed [16]. Among these, the rationale proposed by Marino and coworkers is based on an analytical description of the main mechanisms occurring down at the nanoscale (i.e. collagen triple helix elongation mechanisms), through the mesoscale (i.e. cross-linked molecular assemblies), up to the microscale (i.e. crimped fibers). The coupling of these models allocates macroscopic stress as function of micro- and nanostructural mechanisms (cf., Fig. 17). Hence, model parameters represent measurable histological and biochemical features across scales. This multiscale approach, originally developed in an updated-Lagrangian framework, has recently been formulated in a full-Lagrangian description by Marino and Wriggers [17].

7.2 Multiscale FSI simulations

The afore-introduced multiscale homogenization technique has also been implemented within FSI simulations. To this aim, an explicit time-marching approach has been adopted [6]. A physical coupling between the structural and the fl problem is performed by restoring compatibility and equilibrium relationships between the fl and solid

domain at discrete time intervals along the cardiac cycle. The macro-time interval is then subdivided in separate fl and structure sub-steps. An Euler formulation in a rigid domain is considered for the fl problem, which describes the blood flow within a single macro-step. Boundary conditions are enforced on the basis of a 3D-0D coupling, which introduces a multiscale fluid description: inflow boundary conditions are read from experimental velocity flow profiles from the upstream vasculature, while the outflow boundary conditions are obtained from a three-element Windkessel model that accounts for the downstream vessels. In this way, the arterial segment model under investigation is embedded in the entire circulatory system. A Lagrangian description is adopted for the wall mechanics, computing structural displacements as function of the fluid pressure at the beginning of the current macro-step. At the next macro-step, the fluid domain is updated on the basis of wall displacements (i.e. from the solution of the structural problem), and structural loads are updated on the basis of the fluid flow (i.e. from the solution of the fluid problem), guaranteeing the FSI coupling.

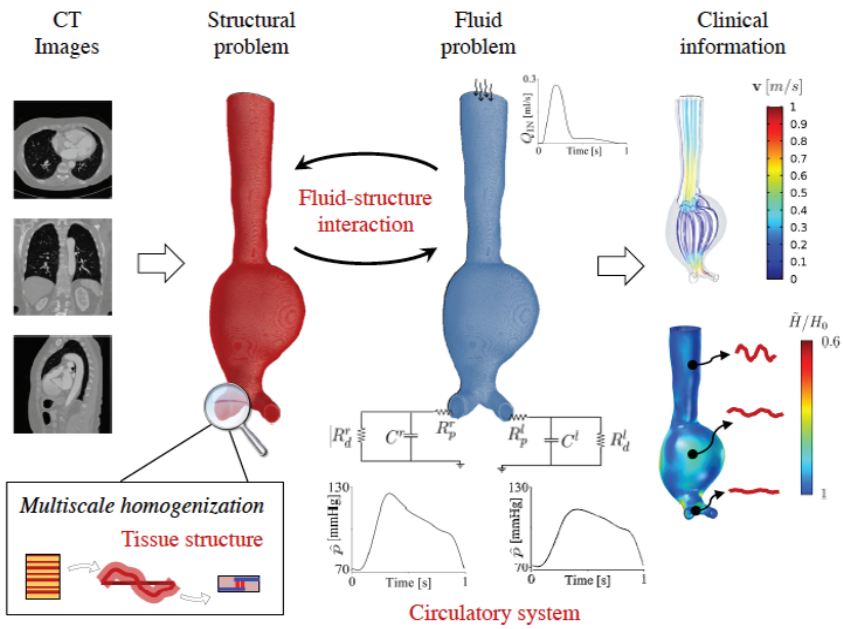

Fig. 18. Multiscale FSI simulations for clinical applications: coupling between the multiscale homogenization rationale for constitutive nonlinearities and a multiscale fluid description based on a 3D-0D definition of boundary conditions.

Sl. 18. Višeskalne FSI simulacije za kliničke primjene: spoj između homogenizacijkog načela za konstitutivne nelinearnosti i višeskalnog opisa fluida temeljenog na 3D-0D definiciji rubnih uvjeta.

Although the proposed strategy neglects advective effects induced by the wall moving within the fluid domain, the present approach has proved to be effective and accurate in a patient-specific model of aortic abdominal aneurysm (cf., Fig. 18). Thanks to the multiscale fluid rationale, the proposed strategy allows for obtaining classical fluid-related risk indices, as well as a novel insight on the coupling between tissue structural defects and the evolution of diseases or the rupture of blood vessels.

7.3 Chemo-mechano-biological modeling

The multiscale constitutive description of arterial tissues has also been coupled with a mechanistic modeling of cell-cell signaling pathways (modeled via transport diffusive equations) and biochemically-motivated remodeling laws of tissue structural features (inspired by the logistic function). The coupled multiphysical description has been solved by exploiting the separation of time scales between different phenomena. Therefore, staggered solution strategies have been implemented: the mechanical problem is assumed to be at steady-state for the transport problem, whose steady-state, in turn, influences tissue remodeling (cf., Fig. 19). Numerical results have been obtained by addressing a case study that shows the mechanical alteration of arterial physiological behavior as a consequence of tissue remodeling mechanisms induced by matrix metalloproteinases, transforming growth factors and interleukines [18].

8. OPEN CHALLENGES AND FUTURE DIRECTIONS

This overview tackled only some of the major areas within which Computational Mechanics moves. There are more complex models and refined discretization schemes that have to be robust and efficient in order to be applied in engineering and science. Some areas, such as material modeling at different length scales, fatigue modeling, stochastic analysis, and reduced order models have not been discussed in this contribution, though they too are of great interest.

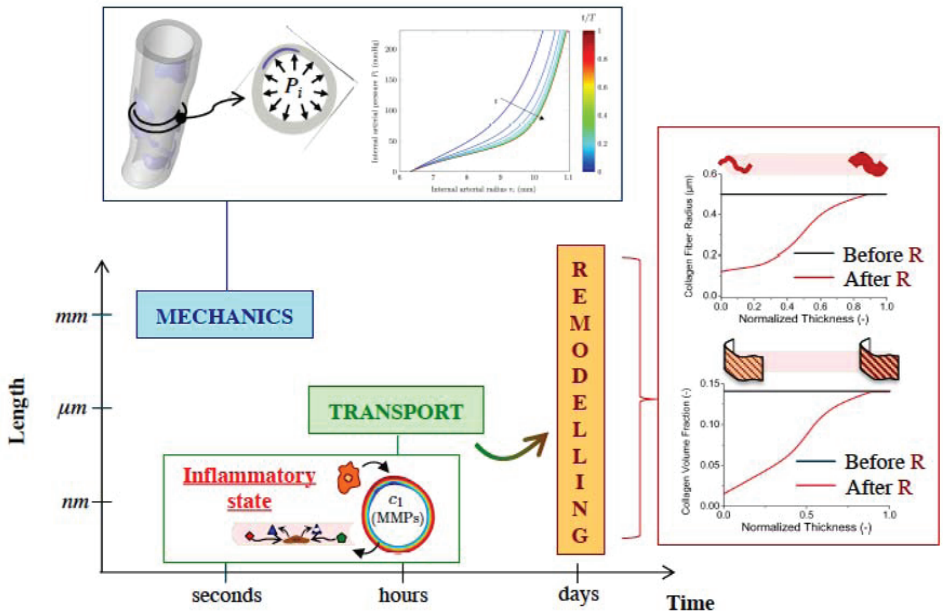

Fig. 19. Chemo-mechano-biological description of tissue remodeling: transport diffusive equations describe cell-cell signaling pathways; a logistic function introduces biochemically-motivated remodeling laws; the effects on arterial mechanics are analyzed thanks to the multiscale homogenization modeling rationale for tissue constitutive response. In the figure, c_1 denotes the concentration of matrix metalloproteinases (MMPs) as a consequence of an inflammatory state that triggers the mechanical dysfunction.

Sl. 19. Kemijsko-mehaničko-biološko opisivanje remodeliranja tkiva: prijenosno difuzijske jednadžbe opisuju signalizirane putanje izmedu stanica; logističke funkcije uvode biokemijski motivirane zakone remodeliranja; djelovanja na mehaniku arterija su analizirana zahvaljujući načelu višeskalnog homogenizacijskog modeliranja konstitutivnog odziva tkiva. Na slici c_1 označava koncentraciju matrice metaloproteinasa (MMPs) kao posljedicu upalnog stanja koje pokreće mehaničku disfunkciju.

8.1 Discretization techniques

Numerous discretization methods exist and are applied in the design of structures, components and processes. In mechanics, this means more complex tasks that models have to solve, including, inter alia, finite strains, nonlinear material response, and multi-physics. This means there does not exist one numerical method that could solve all problems. Instead, there is a wide range of methods, such as finite elements, virtual elements, finite differences, finite volumes, boundary elements, least square methods,

fast Fourier transforms spectral methods, and so forth. The development state of most methods is on a very good level, however there are still challenges for specific applications in nonlinear mechanics. These are related to internal constraints, stability of formulations for finite deformations, etc. Among others, the research is conducted on high-order continuous and discontinuous Galerkin methods that offer high convergence rates. Furthermore, the virtual element method has to be further developed for applications in nonlinear mechanics and multi-physics.

8.2 Phase-field approaches

The phase-field approach has been proven to be a very powerful technique for simulating complex crack phenomena in multi-physical environments. In [3], the 2D phase-field approach was extended towards the recently developed virtual element formulation as outlined in Section 3, due to the flexible choice of nodes number in an element that can easily be changed during the simulation process. As a future direction, the 2D model of [3] will be further extended to a three-dimensional setting at finite strains. Open challenges due to this extension are: (i) the extra computational costs due to the additional amount of data required in the stabilization term to store the triangulation; and (ii) the preprocessing of meshes is more demanding in VEM (e.g. Voronoi 3D cells). These challenges will be investigated in future works.

8.3 Modeling in biomechanics

In terms of constitutive modeling approaches, current studies aim at optimizing the computational cost of multiscale descriptions. Moreover, the description of damage with a multiscale rationale would be a major advancement (see [19]). Addressing the FSI studies, a stronger coupling between the structural and fl problems might lead to more accurate evaluations when bigger movements of the solid within the fl are expected (e.g., dissections). In order to overcome this issue, future investigations will address the coupling of continuum-based and discrete-based approaches when both the structural and fluid problems are described by the means of a multiscale approach (see[4]). Finally, addressing the chemo-mechano-biological description of remodeling, monolithic solution strategies are being investigated, together with its coupling with a kinematic description of growth. Moreover, a better description of tissue reaction to injuries, and hence coupling with damage across scales, stays an open issue under investigation.

8.4 Additive Manufacturing

To simulate the whole 3D-printing process based on the fusion of all individual particles is beyond the processing power of current computers. The multiscale approach (Fig. 20) is one option to evaluate the quality of the final manufacturing component by means of computational modeling. However, the selection of suitable data to be transferred from the particle- to the macroscale is a still an open question. On the other hand, in order to provide a high fidelity model for additive manufacturing, the information of the microscale have to be included into model. Another important step in finding the optimal model for additive manufacturing is the validation by the means of experimental observations. Therefore, a suitable benchmark test case has to be developed.

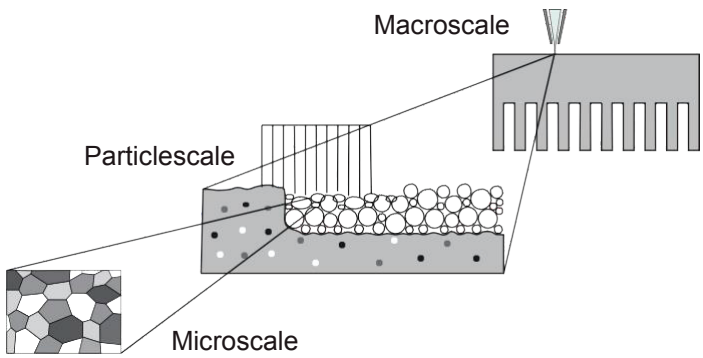

Fig. 20. Multiscale approach for modeling additive manufacturing processes.

Sl. 20. Višeskalni postupak za modeliranje aditivnih proizvodnih procesa.

8.5 Emerging Areas

Other areas that are under investigation in different research groups are numerous. Among them are fictitious domain methods that allow for the efficient discretization of very complex problems, for which meshing with finite elements is very difficult. For fluid lattice Boltzmann methods offer a very efficient solution for a wide range of problems, even exceeding the limits of the Navier-Stokes equations. Non-intrusive coupling methods allow for performing model-adaptive simulations based on the existing, well-developed solvers. Uncertainty modeling and stochastic approaches are necessary for obtaining more reliable predictions in engineering, science and medicine.

Finally, a tremendous development of Artificial Intelligence (AI) techniques influenced the development of many fields in the previous decades. Machine learning and manifold

learning, and, notably, deep learning techniques, have contributed to an unprecedented growth in the wide range of engineering applications as well. This might lead to a change in the way design of engineering structures and processes is performed. Hence, data-enabled science and engineering can be today looked at as a symbiosis of theory, experiments, simulation and artificial intelligence.

References

[1] Aldakheel, F., Wriggers, P., Miehe, C. A modified Gurson-type plasticity model at finite strains: formulation, numerical analysis and phase-field coupling. *Computational Mechanics*, https://doi.org/10.1007/s00466-017-1530-0, 2017.

[2] Aldakheel, F. Mechanics of nonlocal dissipative solids: gradient plasticity and phase field modeling of ductile fracture. Ph.D. thesis, Institute of Applied Mechanics (CE), Chair I, University of Stuttgart. https://doi.org/10.18419/opus-8803, 2016.

[3] Aldakheel, F., Hudobivnik, B., Hussein, A., Wriggers, P. Phase-Field Modeling of Brittle Fracture Using an Efficient Virtual Element Scheme, Computer Methods in Applied Mechanics and Engineering 341, 443-466, 2018.

[4] Avci B., Wriggers P. A DEM-FEM coupling approach for the direct numerical simulation of 3D particulate flows. J Applied Mechanics 79, 010901-(1-7), 2012.

[5] Beirão Da Veiga, L., Brezzi, F., Marini, L.D. Virtual Elements for linear elasticity problem, SIAM Journal on Numerical Analysis 51(2), 794-812, 2013.

[6] Bianchi D., Monaldo E., Gizzi A., Marino M., Filippi S., Vairo G. A FSI computational framework for vascular physiopathology: A novel flow-tissue multiscale strategy. Med. Eng. Phys. 47, 25–37, 2017.

[7] Bourdin, B., Francfort, G.A., Marigo, J.J. Numerical experiments in revisited brittle fracture Journal of the Mechanics and Physics of Solids 48, 797-826, 2000.

[8] Ferziger, J.H., Peric, M. Computational methods for fluid dynamics, 3rd ed., Springer, Heidelberg, 2012

[9] Gusarov, A.V., Yadroitsev, I., Bertrand, P., Smurov, I. Model of radiation and heat transfer in laser-powder interaction zone at selective laser melting. Journal of Heat Transfer, 131(7):072101, 2009.

[10] Jasak, H. OpenFOAM: open source CFD in research and industry, International Journal of Naval Architecture and Ocean Engineering, 2, 89-94, 2009.

[11] Holl, M, Loehnert, S, Wriggers, P. An adaptive multiscale method for crack propagation and crack coalescence International Journal for Numerical Methods in Engineering 93 (1), 23-51, 2013.

[12] Hudobivnik, B, Aldakheel, F, Wriggers, P. Low order 3D virtual element formulation for finite elastoplastic deformations, Computational Mechanics https://doi.org/10.1007/s00466-018-1593-6, 2018.

[13] Korelc, J, Wriggers, P. Automation of Finite Element Methods, Springer, Berlin, 2016.

[14] Krafczyk, M., Tölke, J., Luo, L.S. Large-eddy simulations with a multiple-relaxation-time LBE model, International Journal of Modern Physics B 17, 33-39, 2003.

[15] Kuna, M. Numerische Beanspruchungsanalyse von Rissen, Vieweg & Teubner, 2008.

[16] Marino M. Constitutive Modeling of Soft Tissues. In: Hellmich C. (Ed.), Encyclopedia of Biomedical Engineering – Biomechanics, Elsevier. doi: 10.1016/B978-0-12- 801238-3.99926-4, 2018.

[17] Marino M, Wriggers P. Finite strain response of crimped fibers under uniaxial traction: an analytical approach applied to collagen. Journal of the Mechanics and Physics of Solids. 98, 429–453, 2017.

[18] Marino M, Pontrelli G, Vairo G, Wriggers P. A chemo-mechano-biological formulation for the effects of biochemical alterations on arterial mechanics: the role of molecular transport and multiscale tissue remodelling. Journal of the Royal Society, Interface 14: 20170615, 2017.

[19] Marino M. Molecular and intermolecular effects in collagen fibril mechanics: a multiscale analytical model compared with atomistic and experimental studies. Biomechanics and Modeling in Mechanobiology 15, 133–154, 2016.

[20] Hron, J., Turek, S. A monolithic FEM/multigrid solver for an ALE formulation of fluid-structure interaction with applications in biomechanics, Fluid-structure interaction, 2006.

[21] Wessels, H., Bode, T., Weißenfels, C., Wriggers, P., Zohdi, T.I. Invetigation of heat source modeling for selective laser melting. Computational Mechanics, accepted for publication, 2018.

[22] Wessels, H., Weißenfels, C., Wriggers, P. Metal particle fusion analysis for additive manufacturing using the stabilized optimal transportation meshfree method. Computer Methods in Applied Mechanics and Engineering, 339:91114, 2018.

[23] Weißenfels, C., Wriggers, P. Stabilization algorithm for the optimal transportation meshfree approximation scheme. Computer Methods in Applied Mechanics and Engineering, 286:87106, 2017.

[24] Wriggers, P., Reddy, B.D., Rust, W., Hudobivnik, B. Efficient virtual element formulations for compressible and incompressible finite deformations, Computational Mechanics 60, 253-268, 2017.

RAČUNALNA MEHANIKA U ZNANOSTI I INŽENJERSTVU – QUO VADIS

Sažetak

Računalna mehanika ima široku primjenu u znanosti i inženjerstvu. Njeno područje primjene se znatno povećalo u zadnjim desetljećima. Danas polja kao biomehanika i aditivna proizvodnja nova su područja istraživanja u kojima računalna mehanika pomaže rješavati složene probleme i procese. U radu se razmatraju ova granična područja zajedno s novim diskretizacijskim postupcima kao što su metoda virtualnih elemenata i metoda čestica, gdje potonja zahtijeva moćnu računalnu opremu da bi se mogli točno riješiti problemi kao što je miješanje. Analiza oštećenja konstrukcija i njenih komponenata je drugo područje koje se brzo razvija, pa se ovdje moderni računalni postupci odnose na metodu faznih polja koja pojednostavljuje diskretizacijske sheme. Svi navedeni postupci i metode su razmatrani i vrednovani u numeričkim primjerima.

Ključne riječi: Metoda virtualnih elemenata, biomehanika, aditivna proizvodnja, metoda faznih polja, metoda diskretnih elemenata, medusobno djelovanje fluida i čestice

Peter Wriggers*, Fadi Aldakheel, Michele Marino, Christian Weißenfels

Leibniz Universität Hannover
Institute for Continuum Mechanics, Faculty of Mechanical Engineering, Appelstr. 11, 30161 Hannover,
E-mail: wriggers@ikm.uni-hannover.de; aldakheel@ikm.uni-hannover.de; marino@ikm.uni-hannover.de; weissenfels@ikm.uni-hannover.de
* corresponding member HAZU

UDK / UDC 531/534
DOI: 10.21857/94kl4cxkjm

Izvorni znanstveni članak / Original scientific paper
Prihvaćeno / Accepted: 17. 1. 2019.

MESHLESS APPROACH AS AN ALTERNATIVE TO FINITE ELEMENT METHOD IN SOLID MECHANICS NUMERICAL MODELING

Jurica Sorić, Boris Jalušić, Tomislav Jarak

Summary

Meshless approaches enable discretizations of a computational model only by a set of nodes, which do not need to be connected to elements. This paper presents the meshless local Petrov-Galerkin method, which belongs to truly meshless approaches, as it does not require any kind of mesh or background cells for either interpolation or integration. Full displacement and mixed formulations are presented. The full displacement approach is used for the solution of a three-dimensional elasto-static problem, while the mixed approach is applied for the modeling of deformation responses of shell-like structures. The modeling of material discontinuities is performed by the mixed meshless local Petrov-Galerkin approach by employing the collocation method. The efficiency and accuracy of all the presented methods are tested and compared with finite element formulations in numerical examples. It is demonstrated that the meshless approaches may be considered an alternative to the well-known finite element method regarding certain problems.

Keywords: meshless method; local Petrov-Galerkin formulation; mixed meshless approach; collocation meshless approach.

1. INTRODUCTION

In the recent years, meshless approaches have been proposed as an alternative to the well-known finite element method. These relatively new computational strategies have attracted considerable attention due to their capability to solve a boundary value problem without a meshing procedure. In contrast to the finite element formulation, computational model may be discretized only by nodes, which do not need to be connected to elements. Thus, the nodes can be easily added and removed without burdensome remeshing of

the entire structure. Furthermore, some issues associated with the mesh-based finite element method (FEM), such as a time-consuming mesh generation or element distortion problems, may be efficiently overcome by using meshless formulations. On the other hand, the derivation of interpolation functions in the meshless formulations is more complex than in the finite element approach.

Nowadays, there are a large number of meshless methods as a result of intense development over the last two decades. They can be divided into three basic groups according to the manner of obtaining and solving the discretized system of equations: the strong form; the weak form; and the weak-strong form methods.

The strong form approaches are based on the strong form of differential equations and are usually referred to as collocation methods. Herein, the governing equations are written and imposed in discretization nodes of the numerical model, and accordingly, there is no numerical integration. Some of the representatives of these methods are the Finite difference method [1]; and the Radial basis collocation method [2,3]. Although the strong form methods possess several attractive characteristics, e.g. a simple algorithm for assembling a solvable system of equations, speed and computational efficiency, they may have some numerical stability problems that can lead to inaccuracies.

In the weak form methods, the partial differential equations with the accompanied natural boundary conditions are expressed in an integral form using different numerical approaches. The weak forms are then used to obtain the system of algebraic equations through the numerical integration procedure, using predetermined background cells that can be defined globally – over the entire problem domain [4] or locally – over a part of the computational domain [5]. The operation of integration smudges the error within the integrated area; this increases the accuracy and stability of solutions. Integration acts as a kind of regularization to stabilize the numerical solution.

The meshless global weak form methods are based on the integration of the global Galerkin weighted residual equations and the use of meshless approximations functions. The background cells are required over the entire computational domain for the purpose of the integration. The Element Free Galerkin (EFG) [4] and the Reproducing Kernel Particle Method (RKPM) [6] can be mentioned as representatives of the global weak form methods. The meshless local weak form methods are based on the integration of the so-called local weak forms of Galerkin equations. Herein, local integration areas are often very simple – e.g. spherical, circular, or rectangular in shape. They may mutually overlap, and are automatically built during the calculation process. Some of the representatives of these methods are the HP-Cloud method [7] and the Meshless Local Petrov-Galerkin (MLPG) method [8]. Numerical integration makes the weak form methods computationally more expensive than the collocation methods.

The weak-strong form methods have been designed to utilize the advantages of the weak and strong methods, and to avoid their disadvantages [9,10]. They have been created for the purpose of removing the need for background integration cells as much as possible, and at the same time to provide stable and accurate solutions, even for problems in which the derivative boundary conditions are present. The main idea of this type of methods is to create a system of discretized equations, where weak and strong methods are used selectively, depending on the placement of the discretization nodes. The weak form methods are mostly used at the nodes where the derivative boundary conditions (natural boundary conditions) are prescribed. The strong form methods are utilized in all the remaining nodes of the computational model.

In this contribution, the MLPG method is applied to solve various physical problems. In 3-D elasticity, the Boussinesq problem involving concentrated load acting on a semi-infinite elastic medium is solved [11]. The mixed MLPG method developed in [12] for the analysis of shell-like structures is presented next. Thereby, undesired thickness and shear locking phenomena are eliminated in an efficient way. In addition, the mixed MLPG method employing the collocation approach [13] is used for the modeling of material discontinuity in two-dimensional heterogeneous structures. All the meshless approaches considered demonstrate superiority in comparison with the standard finite element formulation in terms of accuracy and convergence rates.

2. MESHLESS FORMULATION FOR THREE-DIMENSIONAL ELASTICITY

According to the three-dimensional solid concept, the equilibrium equations in a domain of the volume Ω, which is bounded by the surface Γ, are given by

$$\sigma_{ij,j} + b_i = 0, \text{ in } \Omega, \tag{1}$$

where σ_{ij} are the stress tensor components and b_i denotes the body forces. The indices i, j, which take the values 1,2,3, refer to the Cartesian coordinates x, y, z. On the boundary Γ, the following boundary conditions are assumed:

$$\begin{aligned} u_i &= \bar{u}_i, \text{ on } \Gamma_u, \\ t_i &= \sigma_{ij} n_j = \bar{t}_i \text{ on } \Gamma_t, \end{aligned} \tag{2}$$

where u_i are the displacement components and t_i stands for the surface traction components. Γ_u and Γ_t are parts of the global boundary with prescribed displacements $\bar{u}_i$ and tractions $\bar{t}_i$, respectively. n_j denotes direction cosines of the outward normal on the boundary Γ of the volume Ω.

In the MLPG method, the equilibrium equations may be written in a weak form over a local sub-domain Ω^I_s defined around a grid node I, which may be expressed in the following form:

$$\int_{\Omega^I_s} \left(\sigma_{ij,j} + b_i\right) v_i \mathrm{d}\Omega - \alpha \int_{\Gamma^I_{su}} (u_i - \bar{u}_i) v_i \mathrm{d}\Gamma = 0 \cdot \tag{3}$$

Herein, u_i is the trial function describing the displacement field, while v_i is the test function. In the MLPG method applied, the test and trial functions may be chosen from different functional spaces. The local sub-domain Ω^I_s is a small region inside the domain Ω and could be of any geometric shape and size, Fig. 1. Here in the 3D analysis, the local sub-domains are taken to be of spherical shape. The local sub-domains may overlap, and they cover the whole global domain Ω. Γ^I_{su} is a part of the boundary $\partial\Omega^I_s$ of the local sub-domain with the prescribed displacement $\bar{u}_i$, and α denotes a penalty parameter, α>>1, which is introduced in order to satisfy the geometric boundary conditions.

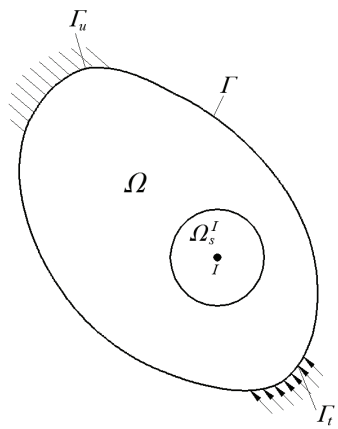

Fig. 1. Definition of local sub-domain
Sl. 1. Određivanje lokalnog potpodručja

Using the divergence theorem and some mathematical manipulation according to [11], the local symmetric weak form (LSWF) for linear elasticity may be expressed as:

$$\int_{\Omega^I_s} \sigma_{ij} v_{i,j} \mathrm{d}\Omega - \int_{L^I_s} t_i v_i \mathrm{d}\Gamma - \int_{\Gamma^I_{su}} t_i v_i \mathrm{d}\Gamma + \alpha \int_{\Gamma^I_{su}} u_i v_i \mathrm{d}\Gamma = \int_{\Gamma^I_{su}} \bar{t}_j v_i \mathrm{d}\Gamma + \alpha \int_{\Gamma^I_{su}} \bar{u}_i v_i \mathrm{d}\Gamma + \int_{\Omega^I_s} b_i v_i \mathrm{d}\Omega \,. \tag{4}$$

Herein, L^I_s is the part of the local boundary $\partial\Omega^I_s$ that is totally inside the global domain, Γ^I_{st} is the part of $\partial\Omega^I_s$ that coincides with the global traction boundary, i.e., $\Gamma^I_{st} = \partial\Omega^I_s \cap \Gamma_t$, and L^I_{su} is the part of $\partial\Omega^I_s$ that coincides with the global geometric boun-

dary, i.e., $\Gamma^I_{st} = \partial\Omega^I_s \cap \Gamma_u$. If the Heaviside step function is chosen as the test function in each local sub-domain, defined as

$$v(x) = \begin{cases} 1 & \text{at } x \in \Omega_s \\ 0 & \text{at } x \notin \Omega_s \end{cases}, \tag{5}$$

the LSWF (4) may be simplified as

$$-\int_{L^I_s} t_i \mathrm{d}\Gamma - \int_{\Gamma^I_{su}} t_i \mathrm{d}\Gamma + \alpha \int_{\Gamma^I_{su}} u_i \mathrm{d}\Gamma = \int_{\Gamma^I_{st}} \bar{t}_j \mathrm{d}\Gamma + \alpha \int_{\Gamma^I_{st}} \bar{u}_i \mathrm{d}\Gamma + \int_{\Omega^I_s} b_i \mathrm{d}\Omega \,. \tag{6}$$

As evident from equation (6), there is no domain integration involved in the left-hand side. Under the assumption of zero body force, the domain integration is totally eliminated.

The trial function is chosen to be the moving least square (MLS) approximation [14], defined over a number of nodes within the domain of influence. While the local sub-domain Ω^I_s is defined as the region over which the integration around node *I* is carried out, and in this text, it is set to be equal to the support of the nodal test function, the domain of influence is defined as the region that includes all the nodes whose MLS nodal trial shape functions do not vanish in the local sub-domain of the current node *I*. In other words, the domain of influence contains all the nodes that have a non-zero coupling in the stiffness matrix with the current node *I* as shown in Fig. 2.

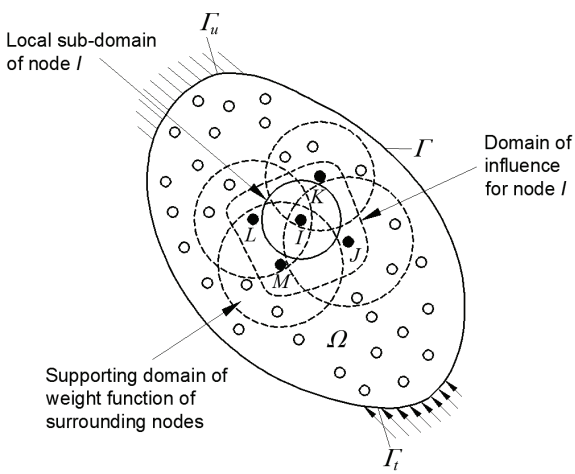

Fig. 2. MLPG trial and test domain

Sl. 2. Interpolacijsko i testno područje u MLPG (bezmrežnoj lokalnoj Petrov-Galerkinovoj) formulaciji

In Fig. 2, the solid-lined sphere surrounding the node *I* represents the local sub-domain, where integration is carried out. The dashed spheres surrounding the nodes *J*, *K*, *L*, *M*… represent the supporting domains of the MLS weight functions of the nodes whose weight functions do not vanish in the local sub-domain of the node *I*. The volume surrounded by the dashed curve represents the domain of influence of the node *I*.

The MLS method is generally considered to be one of useful interpolation schemes that approximate random data with reasonable accuracy. The characteristics of the MLS have been widely discussed in literature [15,16]. Accordingly, the displacement distribution in three-dimensional space may be expressed as

$$\mathbf{u} = \sum_{J=1}^{N} \phi_J(x, y, z)\, \hat{\mathbf{v}}_J\,, \tag{7}$$

where

$$\mathbf{u}^T = \begin{bmatrix} u & v & w \end{bmatrix}, \tag{8}$$

$$\hat{\mathbf{v}}_J^T = \begin{bmatrix} \hat{u} & \hat{v} & \hat{w} \end{bmatrix}_J, \tag{9}$$

$\hat{\mathbf{v}}_J$ is the vector with the fictitious nodal displacement components, and N is the total number of nodes. In relation (7), $\phi_J(x, y, z)$ stands for the shape function of the MLS approximation associated with the node *J*. It should be stressed that in the general case, the MLS approximation function does not interpolate the nodal values, and therefore, they are called fictitious values. In other words, it does not possess the Kronecker delta property. This is the reason why the penalty parameter is introduced in (3) in order to impose the displacement boundary condition. Using the derivation procedure described in [11] and [17], the nodal shape function is obtained in the following form:

$$\phi_J(\mathbf{x}) = \sum_{i=1}^{m} p_i(\mathbf{x}) \left[\mathbf{A}^{-1}(\mathbf{x})\mathbf{B}(\mathbf{x})\right]_{iJ} \tag{10}$$

with the matrices **A(x)** and **B(x)** defined as

$$\mathbf{A}(\mathbf{x}) = \sum_{J=1}^{N} W_J(\mathbf{x})\mathbf{p}(\mathbf{x}_J)\mathbf{p}^T(\mathbf{x}_J)\,, \tag{11}$$

$$\mathbf{B}(\mathbf{x}) = \begin{bmatrix} W_1(\mathbf{x})\mathbf{p}(\mathbf{x}_1) & W_2(\mathbf{x})\mathbf{p}(\mathbf{x}_2) & \dots & W_J(\mathbf{x})\mathbf{p}(\mathbf{x}_J) & \dots & W_N(\mathbf{x})\mathbf{p}(\mathbf{x}_N) \end{bmatrix}. \tag{12}$$

In the above relations, $W_J(\mathbf{x})$ is the weight function associated with the node *J*, and $\mathbf{p}(\mathbf{x})$ denotes a vector comprising a complete monomial basis of order *m*, $\mathbf{p}^T(\mathbf{x}) = [p_1(\mathbf{x})\ p_2(\mathbf{x})\ \dots\ p_i(\mathbf{x})\ \dots\ p_m(\mathbf{x})]$. $\mathbf{x}$ is the vector which contains coordinates, $\mathbf{x}^T = [x\ y\ z]$. The

linear basis is expressed as

$$\mathbf{p}^T(\mathbf{x}) = \begin{bmatrix} 1 & x & y & z \end{bmatrix}, \tag{13}$$

and the quadratic basis is

$$\mathbf{p}^T(\mathbf{x}) = \begin{bmatrix} 1 & x & y & z & x^2 & y^2 & z^2 & xy & yz & zx \end{bmatrix}. \tag{14}$$

In this text, the 4th order spline type weight function [17] is assumed

$$W_J(\mathbf{x}) = \begin{cases} 1 - 6\left(\dfrac{d_J}{r_J}\right)^2 + 8\left(\dfrac{d_J}{r_J}\right)^3 - 3\left(\dfrac{d_J}{r_J}\right)^4 & 0 \le d_J \le r_J \\ 0 & d_J > r_J \end{cases}. \tag{15}$$

By substituting the MLS interpolation function (7) into the formulation (6), the following discretized system of linear equations is obtained:

$$\sum_{J=1}^{N} \left[\int_{\Omega_s} \mathbf{N}\mathbf{D}\mathbf{B}_J \mathrm{d}\Gamma + \int_{\Gamma_{su}} \mathbf{S}\mathbf{N}\mathbf{D}\mathbf{B}_J \mathrm{d}\Gamma - \alpha \int_{\Gamma_{su}} \mathbf{S}\mathbf{\Phi}_J \mathrm{d}\Gamma \right] \mathbf{v}_J = -\int_{\Gamma_{st}} \bar{\mathbf{t}} \, \mathrm{d}\Gamma - \int_{\Omega_s} \mathbf{b} \, \mathrm{d}\Omega - \alpha \int_{\Gamma_{su}} \bar{\mathbf{u}} \, \mathrm{d}\Gamma, \tag{16}$$

where, in the three-dimensional space,

$$\mathbf{N} = \begin{bmatrix} n_1 & 0 & 0 & n_2 & 0 & n_3 \\ 0 & n_2 & 0 & n_1 & n_3 & 0 \\ 0 & 0 & n_3 & 0 & n_2 & n_1 \end{bmatrix}, \quad \mathbf{B}_J = \begin{bmatrix} \phi_{J,1} & 0 & 0 \\ 0 & \phi_{J,2} & 0 \\ 0 & 0 & \phi_{J,3} \\ \phi_{J,2} & \phi_{J,1} & 0 \\ 0 & \phi_{J,3} & \phi_{J,2} \\ \phi_{J,3} & 0 & \phi_{J,1} \end{bmatrix}, \quad \mathbf{\Phi}_J = \begin{bmatrix} \phi_J & 0 & 0 \\ 0 & \phi_J & 0 \\ 0 & 0 & \phi_J \end{bmatrix},$$

$$\mathbf{S} = \begin{bmatrix} S_1 & 0 & 0 \\ 0 & S_2 & 0 \\ 0 & 0 & \mathrm{S}_3 \end{bmatrix} \quad \text{with} \, S_i = \begin{cases} 1 & \text{if } u_i \text{ is prescribed on } \Gamma_u \\ 0 & \text{if } u_i \text{ is not prescribed on } \Gamma_u \end{cases}, \quad i = 1,3,$$

and **D** stands for the standard three-dimensional elasticity matrix. Using the standard well-known numerical procedures, the global set of equations is derived, which is as usually expressed in the following matrix form

$$\mathbf{KV} = \mathbf{F}, \tag{17}$$

where **K** is the stiffness matrix, **V** is the vector of nodal displacements, and **F** stands for the prescribed loading.

Three-Dimensional Boussinesq Problem

The Boussinesq problem is a classical problem for the study of contact, penetration, and impact problems. The problem can be simply described as concentrated load acting on a semi-infinite elastic medium with no body force. Because of the strong singularity in the Boussinesq problem, it is very difficult to get an accurate result using domain discretization methodology such as the finite element method. The exact displacement field within the semi-infinite medium is given by [18].

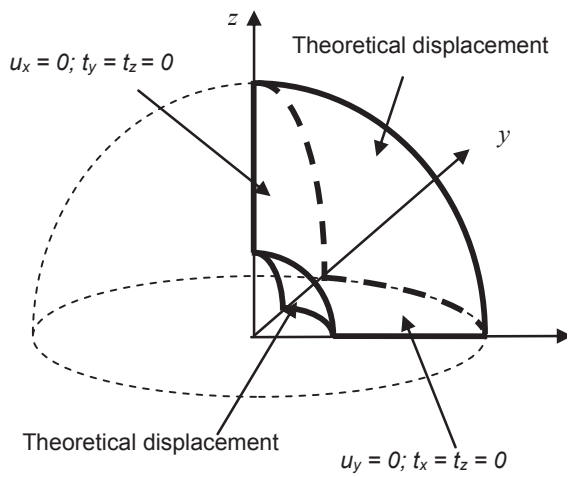

Fig. 3. Simulation model for Boussinesq Problem
Sl. 3. Simulacijski model za Boussinesqov problem

A one-eighth of a sphere is used to simulate the semi-infinite continuum. In order to avoid direct encounter with the singular loading point, the theoretical displacement is applied on a small spherical surface with the radius as low as 2.5% of the total radius of the sphere. The symmetric boundary conditions are applied on the surfaces of the one-eighth sphere, Fig. 3. An isotropic material of $E = 1{,}000$ and $\nu = 0.25$ is used in the simulation. The 1,177-node MLPG model and 1,159 node FEM model are shown in Figs. 4 and 5.

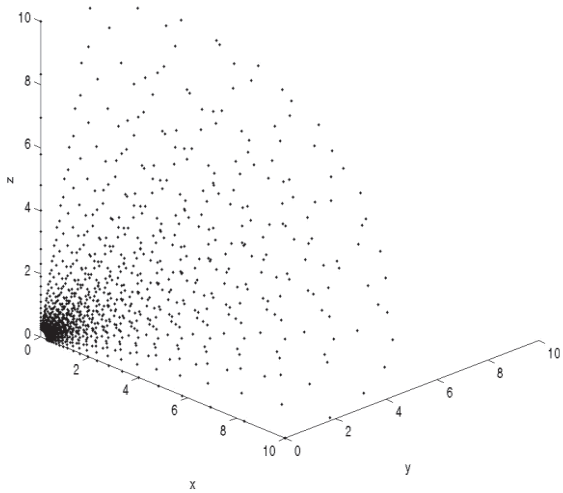

Fig. 4. MLPG model with 1,177 Nodes for Boussinesq problem [11]

Sl. 4. MLPG model s 1177 čvorova za Boussinesqov problem [11]

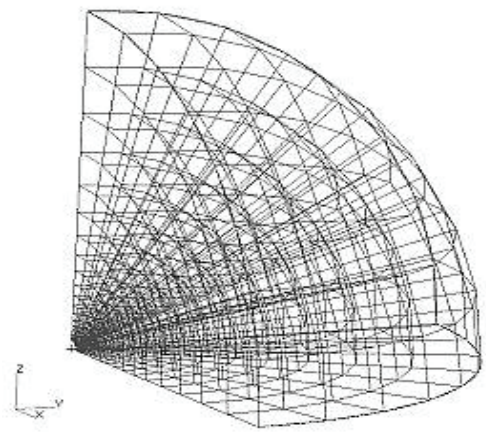

Fig. 5. FEM model with 1,159 nodes for Boussinesq problem [11]

Sl. 5. Model metode konačnih elemenata s 1159 čvorova za Boussinesqov problem [11]

The two models have similar nodal distances at the stress-concentrated area. However, it can be seen that a lot more nodes need to be added in the FEM model in order to prevent element distortion and maintain a reasonable element aspect ratio. In Fig. 6, the

relative errors of von Mises stress and strain energy for both the MLPG and the FEM method are plotted. It can be seen that even with a node number as high as 11,112, the accuracy of the finite element method is still far less than the MLPG method.

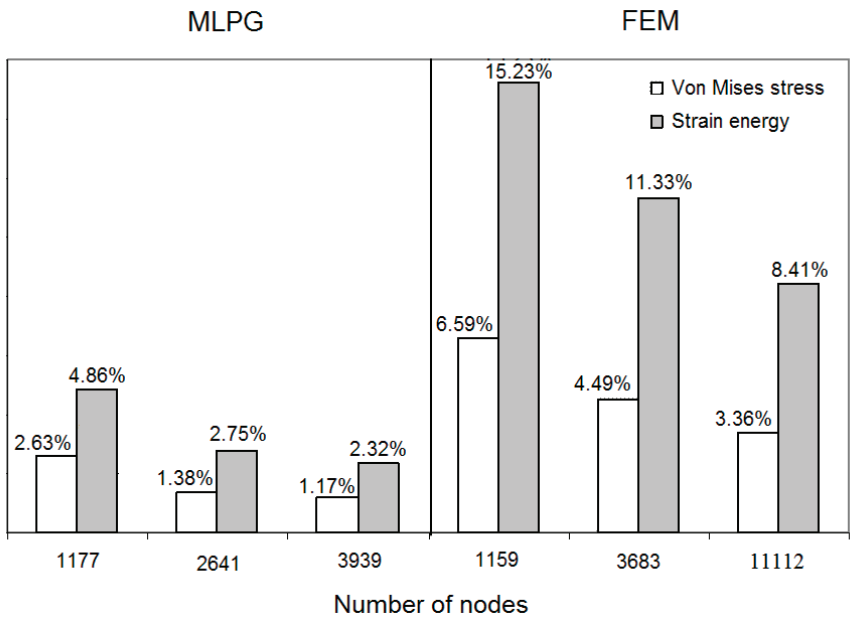

Fig. 6. Von Mises and strain energy relative error vs. node number [11]

Sl. 6. Relativne greške za von Misesovo naprezanje i energiju deformiranja u odnosu na broj čvorova [11]

3. MIXED MLPG METHOD FOR THE ANALYSIS OF SHELL-LIKE STRUCTURES

An efficient mixed meshless formulation based on the Local Petrov-Galerkin approach described above has been developed for the analysis of shell-like structures. The 3-D solid-shell concept used in the finite element formulations [19] and [20] is adopted, and the shell geometry, which can be described exactly, is analyzed. Plate structures may be considered a special case of the shell geometry defined by the zero value of the Gaussian curvature. Discretization is performed by the nodes located on the upper and lower surfaces, and the local weak form of the equilibrium over the prismatic local

sub-domain, surrounding the couple of nodes positioned on the opposite surfaces, is derived. Certain strain and stress components are first approximated independently, but their nodal values are eliminated from the discretized equation system locally, yielding a global system of equations with only nodal displacements as unknowns [12]. This is achieved by enforcing the kinematic relations between approximated strains and displacements at the nodes by means of a collocation approach. Instead of the standard MLS interpolation functions, a new modified MLS shape function, proposed in [21] and [22], obeying the interpolation condition with high accuracy, is implemented. Thus, a penalty approach for imposing the essential boundary conditions is avoided. Furthermore, the thickness and shear locking phenomena are fully suppressed due to the employed mixed numerical strategy.

According to the formulation presented in [12], the shell structure is described by the curvilinear coordinates θ^k, k = 1, 2, 3, defined into the global Cartesian space, and then mapped into a parametric space, where the curved middle surface is transformed into the two-dimensional unit square in the ζ^1, ζ^2 - parametric plane. ζ^1 and ζ^2 are the normalized parametric coordinates defined as $\zeta^\alpha = \frac{\theta^\alpha}{\theta^\alpha_{\max}}$, and thus their range is $0 \le \zeta^\alpha \le 1$ as shown in Fig. 7. Herein, θ^α denotes the middle surface convective coordinates, and θ^3 is the local coordinate in the thickness direction. The nodes are uniformly generated on the upper and lower surfaces in the parametric space, and then mapped into the global Cartesian coordinates. The prismatic local sub-domains are defined in the parametric space around each couple of nodes positioned on the opposite discretized surfaces. All interpolations are performed by using the parametric coordinates ζ^i.

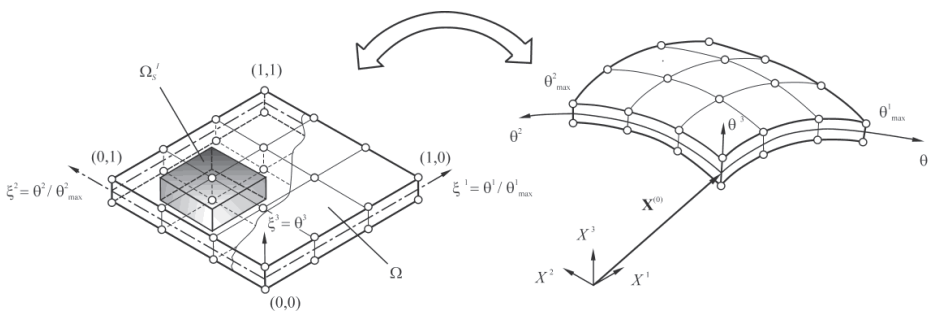

Fig. 7. Parametric representation and discretization of shell geometry

Sl. 7. Parametarski prikaz i diskretizacija ljuskaste geometrije

The derivation of the governing equation is based on the 3D meshless formulation presented in the previous section. Instead of the standard 3D discretization, here the nodes are distributed over the opposite surface, forming shell-like structures with arbitrary thickness as shown in Fig. 7. Accordingly, the test function is approximated over the thickness, and here the linear distribution is assumed as

$$v\left(\xi^j\right)=c_0+c_1(\xi^3), \tag{18}$$

with c_0 and c_1 as arbitrarily chosen real constants. Using the procedure described in the previous section, the governing equations for the local sub-domain Ω^I_s are derived in the following form:

$$-\int_{L^I_s} n_j\sigma_{ij}\mathrm{d}\Gamma-\int_{\Gamma^I_{su}} n_j\sigma_{ij}\mathrm{d}\Gamma=\int_{\Omega^I_s} b_i\,\mathrm{d}\Omega+\int_{\Gamma^I_{st}}\overline{t}_i\mathrm{d}\Gamma, \tag{19}$$

$$\int_{\Omega^I_s}\xi^3{}_{,j}\,\sigma_{ij}\mathrm{d}\Omega-\int_{L^I_s}\xi^3\,n_j\sigma_{ij}\mathrm{d}\Gamma-\int_{\Gamma^I_{su}}\xi^3\,n_j\sigma_{ij}\mathrm{d}\Gamma=\int_{\Omega^I_s}\xi^3\,b_i\,\mathrm{d}\Omega+\int_{\Gamma^I_{st}}\xi^3\,\overline{t}_i\,\mathrm{d}\Gamma\,. \tag{20}$$

Here, all tensor and vector components are defined in the Cartesian coordinates, i.e. $\boldsymbol{\sigma}=\sigma_{ij}\,\mathbf{e}_i\otimes\mathbf{e}_j$, $\mathbf{t}=t_i\,\mathbf{e}_i$, $\mathbf{n}=n_i\,e_i$. However, the integration over the local sub-domain is performed in the parametric coordinates, where the volume element is expressed as

$$\mathrm{d}\Omega=(\bar{\mathbf{G}}_1\times\bar{\mathbf{G}}_2)\cdot\bar{\mathbf{G}}_3\;\mathrm{d}\xi^1\,\mathrm{d}\xi^2\,\mathrm{d}\xi^3\,. \tag{21}$$

Herein, $\bar{\mathbf{G}}_i$ are the base vectors defined by $\bar{\mathbf{G}}_i=\mathbf{G}_k\frac{\partial\theta^k}{\partial\xi^i}$ with $\mathbf{G}_k=\frac{\partial\mathbf{X}}{\partial\theta^k}$, where $\mathbf{X}$ is the position vector. As known in the theory of shells, the base vectors describe the shell geometry [23]. As evident from (19) and (20), a set of six equations for each local sub-domain Ω^I_s is obtained.

The next step is the discretization of the governing equations. In contrast to the standard displacement based formulation, here the displacement field, the strain components consisting of the three in-plane and the two transversal shear components, and the transversal normal stress component are approximated independently, by using the same in-plane interpolation functions. Linear polynomials are used for the distribution over the thickness, and the approximation in the in-plane directions is performed by means of the MLS functions. The displacement components are written in the directions of the Cartesian coordinates, $\mathbf{u}=u_i\,\mathbf{e}_i$, while the strain and stress tensors are expressed in the parametric space as $\varepsilon=\varepsilon_{ij}\,\bar{\mathbf{G}}^i\otimes\bar{\mathbf{G}}^j$ and $\boldsymbol{\sigma}=\sigma^{ij}\,\bar{\mathbf{G}}_i\otimes\bar{\mathbf{G}}_j$. The undesired shear locking effect in the thin structural limit is suppressed by using the strain interpolation, and the transversal stress interpolation is applied for elimination of the thickness locking phenomena.

As mentioned above, the modified MLS shape function with the interpolation property is used for the discretization. The Kronecker delta property is fulfilled with high accuracy; therefore, the penalty approach for imposing the displacement boundary conditions is not required. The interpolation condition is achieved by the modification of the weight function, which is now expressed in the following form:

$$W_J(\xi^\delta) = \begin{cases} w_{SJ} w_{RJ}, & 0 \le d_J \le r_J \\ 0, & d_J > r_J \end{cases}. \tag{22}$$

As evident, the weight function is computed as a product of the two functions, w_{SJ} and w_{RJ}, where w_{SJ} stands for the 4th-order spline function:

$$w_{SJ} = 1 - 6\left(\frac{d_J}{r_J}\right)^2 + 8\left(\frac{d_J}{r_J}\right)^3 - 3\left(\frac{d_J}{r_J}\right)^4, \tag{23}$$

and w_{RJ} denotes the regularized weight function expressed as

$$w_{RJ} = \frac{\left(\left(\frac{d_J}{r_J}\right)^4 + \varepsilon\right)^{-2} - (1+\varepsilon)^{-2}}{\varepsilon^{-2} - (1+\varepsilon)^{-2}}. \tag{24}$$

In the above relations, $d_J = \left|\xi^\gamma - \xi_J{}^\gamma\right|$ is the distance between the node couple J and the current sample point in the parametric space, while r_J represents the support domain of the weight function. ε is the regularization parameter, which should be very small and here it is assumed to be $\varepsilon = 10^{-5}$.

Analogous to relation (10), the MLS nodal shape function is now expressed in the parametric plane as

$$\phi_J\left(\xi^\gamma\right) = \sum_{i=1}^{m} p_i(\bar{\xi}^\gamma)\left[\mathbf{A}^{-1}\mathbf{B}\right]_{iJ}. \tag{25}$$

The matrices **A** and **B** are also derived in the in-plane parametric space. Using relation (25) and employing the linear polynomial interpolation in the ζ^3 direction, the 3D shape function matrix $\mathbf{\Phi}_J^\omega\left(\xi^i\right)$ for the strain and the stress tensor components, as well as the matrix $\mathbf{\Phi}_J^u\left(\xi^i\right)$ for the displacement components, are derived. In the derivation procedure, which is described in detail in [12], the nodal strain values are computed by the well-known kinematic relations, and then expressed in terms of the nodal displacement components, in order to obtain a closed global system of equation with only the nodal displacements as unknown variables. After relatively complicated mathematical mani-

pulations, the following final discretized form of the governing equations on the domain of influence level is obtained:

$$\sum_{J=1}^{N_J}\left[\int_{L_S^I}\mathbf{N}\,\mathbf{T}^{\sigma}\tilde{\mathbf{C}}\,\boldsymbol{\Phi}_J^{\omega}\,\mathrm{d}\Gamma+\int_{\Gamma_{Su}^I}\mathbf{N}\,\mathbf{T}^{\sigma}\tilde{\mathbf{C}}\,\boldsymbol{\Phi}_J^{\omega}\mathrm{d}\Gamma\right]\sum_{K=1}^{\tilde{n}_J}\tilde{\mathbf{B}}_{KJ}\hat{\mathbf{v}}_K=$$
$$=-\int_{L_{St}^I}\overline{\mathbf{t}}\,\mathrm{d}\Gamma-\int_{\Omega_s^I}\mathbf{b}\,\mathrm{d}\Omega, \tag{26}$$

$$\sum_{J=1}^{N_J}\left[\int_{L_S^I}\xi^3\mathbf{N}\,\mathbf{T}^{\sigma}\tilde{\mathbf{C}}\,\boldsymbol{\Phi}_J^{\varepsilon}\,\mathrm{d}\Gamma+\int_{\Gamma_{Su}^I}\xi^3\mathbf{N}\,\mathbf{T}^{\sigma}\,\tilde{\mathbf{C}}\,\boldsymbol{\Phi}_J^{\omega}\mathrm{d}\Gamma-\int_{\Omega_s^I}\nabla\mathbf{d}^T\mathbf{T}^{\sigma}\tilde{\mathbf{C}}\,\boldsymbol{\Phi}_J^{\omega}\mathrm{d}\Omega\right]$$
$$\cdot\sum_{K=1}^{\tilde{n}_J}\tilde{\mathbf{B}}_{KJ}\hat{\mathbf{v}}_K=-\int_{L_{St}^I}\xi^3\,\overline{\mathbf{t}}\,\mathrm{d}\Gamma-\int_{\Omega_s^I}\xi^3\,\mathbf{b}\,\mathrm{d}\Omega, \tag{27}$$

where $\tilde{\mathbf{B}}_{KJ}$ is the matrix containing derivatives of the 3-D shape functions; it is analogous to the standard strain-displacement matrix [24]. $\tilde{\mathbf{C}}$ is the material matrix, $\mathbf{T}^{\sigma}$ is the transformation matrix between the parametric space and the global Cartesian coordinates, and $\hat{\mathbf{v}}_J$ is the vector of the unknown displacement components in the directions of the global Cartesian coordinates at the upper and lower surface, respectively. $\mathbf{N}$ is the matrix containing the components of the outward unit normal vector $\mathbf{n}=n_i\,\mathbf{e}_i$ on the local sub-domain boundary, and $\nabla\mathbf{d}$ comprises the derivatives of ξ^3 with respect to the global Cartesian coordinates. $\tilde{n}_J$ denotes the number of nodes in the domain of influence of the node couple *J*. The closed global system of equations on the structural level is derived by using well-known numerical node-by-node assemblage procedures. The body forces are usually neglected in engineering computations, and therefore, all terms containing the body force vector **b** can be omitted.

Cylindrical shell subjected to uniform line load

As an example, a horizontal thin cylindrical shell subjected to the uniform line load of $q=1$ along the upper and lower generatrix is analyzed as shown in Fig. 8. The material data are the Young's modulus $E=210000$ and the Poisson's ratio $\nu=0.3$. The shell thickness is $h=0.9$, with the radius to thickness ratio of $R/h=100$. The length of the cylinder is $L=300$. Due to symmetry, only one octant of the shell is discretized by a uniform grid.

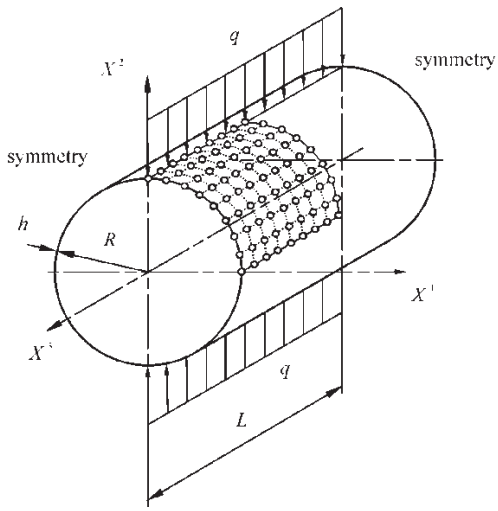

Fig. 8. Geometry and discretization of cylindrical shell

Sl. 8. Geometrija i diskretizacija cilindrične ljuske

The computation is performed by the proposed mixed formulation, using the second- and third-order polynomial bases of the MLS function. The convergence of the vertical displacement at the shell middle surface under the line load, which is normalized by the analytical solution from [18], is presented in Fig. 9. The results are again compared with the values obtained by the full displacement approach taken from [24], as well as with the parabolic 3D finite elements from the MSC/NASTRAN program package [25]. As obvious from Fig. 9, the mixed meshless formulation is superior to other formulations displayed. The fifth-order basis function in the MLS interpolation has to be used in the full displacement approach in order to achieve the convergence, which significantly decreases numerical efficiency as mentioned before. Furthermore, it is again to note that the computation by the means of the third-order MLS basis function in the mixed approach yields the exact displacement values, even for the relatively coarse discretization.

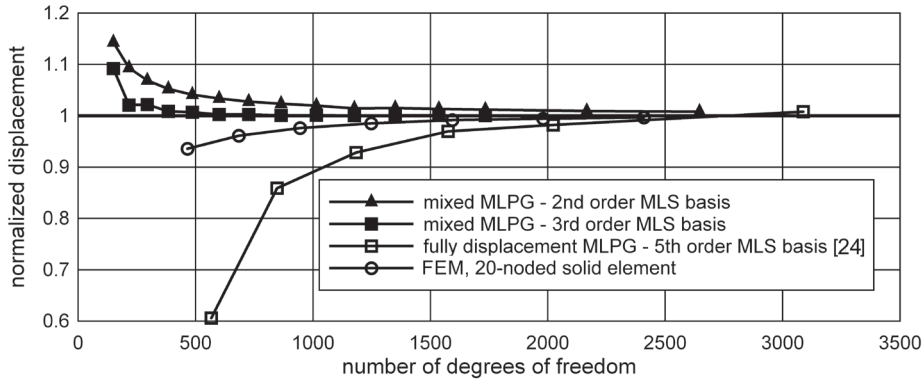

Fig. 9. Convergence of vertical displacement under line load for cylindrical shell

Sl. 9. Konvergencija vertikalnog pomaka pod linijskim opterećenjem za cilindričnu ljusku

Furthermore, the sensitivity of the mixed approach to the shear locking effect has been tested by increasing the shell radius to thickness ratio, and the results are shown in Fig. 10. As evident, by using the second order MLS polynomial basis, the shear locking is again completely eliminated, even if very thin shells are considered.

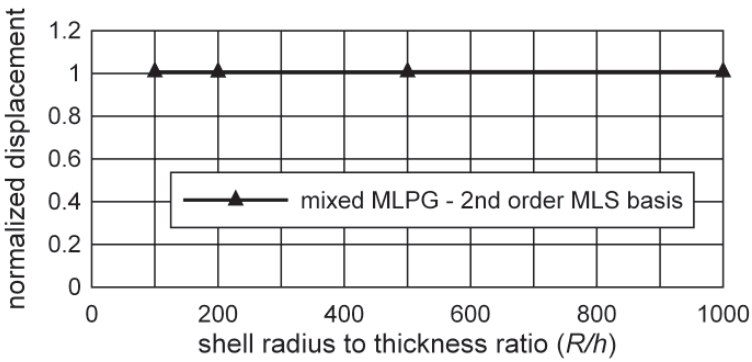

Fig. 10. Vertical displacement under line load vs. radius to thickness ratio for cylindrical shell

Sl. 10. Vertikalni pomak pod linijskim opterećenjem u odnosu na omjer polumjera i debljine stijenke za cilindričnu ljusku

4. MODELING MATERIAL DISCONTINUITY BY THE MEANS OF THE MESHLESS COLLOCATION METHOD

The collocation mixed MLPG method is applied here for the modeling of material discontinuity. Instead of the previously described weak formulations, here the Dirac delta function is used as the test function in the local weak form. Each homogeneous region is discretized by using independent interpolations of both displacements and stress components. The MLS shape functions with interpolation property are used, which allows for a simple and direct imposition of the displacement and traction boundary conditions at the discretization nodes positioned on the global boundary, as well as the imposition of appropriate conditions at the nodes stationed at the material interface. No additional treatment or parameter determination at the material interface is needed. The final closed global system of discretized governing equations with the displacements as unknown variables is obtained through the kinematic and constitutive relations, similar as in the previous section. The details of this approach are given in [13].

A two-dimensional heterogeneous structure representing the global domain, which consists of two homogeneous parts Ω ($\Omega = \Omega^+ \cup \Omega^-$) bounded by the global outer boundary Γ ($\Gamma = \Gamma^+ \cup \Gamma^-$), is considered as shown in Fig. 11. The boundary Γ_s represents the interface between two homogeneous isotropic materials, represented by domains Ω^+ and Ω^-, with different linear elastic material properties, while $\mathbf{n}^+$ and $\mathbf{n}^-$ denote unit outward normal vectors on their outer boundaries, Γ^+ and Γ^-, and on the interface boundary Γ_s.

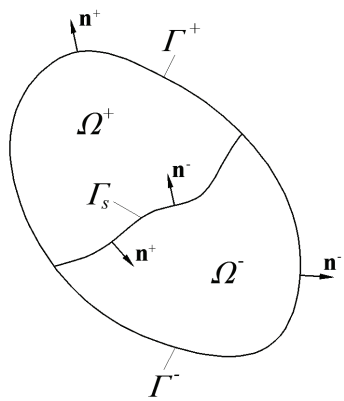

Fig. 11. Heterogeneous structure consisting of two homogeneous materials

Sl. 11. Heterogena struktura koja se sastoji od dva homogena materijala

The strong form of elasto-static governing equations can be defined for each homogeneous material separately, and accordingly the equilibrium equation for the homogeneous domain Ω^+ may be written as

$$\sigma^+_{ij,x_j} + b^+_i = 0, \quad \text{within } \Omega^+, \tag{28}$$

where σ^+_{ij} are the Cauchy stress tensor components, while b^+_i denotes body forces. On the outer boundaries Γ^+ and Γ^-, the following displacement and traction boundary conditions have to be satisfied. Thus, for Γ^+, they are expressed as

$$u^+_i = \overline{u}^+_i, \quad \text{on } \Gamma^+_u, \tag{29}$$

$$t^+_i = \sigma^+_{ij} n^+_j = \overline{t}^+_i, \quad \text{on } \Gamma^+_t. \tag{30}$$

Herein, Γ^+_u represents the part of the boundary Γ^+, where the displacement condition is prescribed, and Γ^+_t denotes the part where the traction boundary condition is imposed. The barred variables stand for the prescribed values of displacements and tractions. Analogous relations may be written for another homogeneous domain Ω^- and its boundaries Γ^-_u and Γ^-_t. In order to obtain the solution for the entire heterogeneous structure, the interface conditions on the boundary Γ_s should also be applied. These conditions are needed to impose the continuity of the displacement field along with the discontinuity (jump) in the displacement derivative field across the interface boundary Γ_s. This is fullfiled in a simple manner by enforcing the following equations at all nodes stationed on Γ_s

$$u^+_i - u^-_i = 0, \tag{31}$$

$$\sigma^+_{ij} n^+_j + \sigma^-_{ij} n^-_j = 0. \tag{32}$$

The discretization of the global computational domain Ω is performed by two different sets of nodes, $I = 1,2,...,N$ and $M = 1,2,...,P$, where N and P indicate the total number of nodes within homogeneous materials Ω^+ and Ω^-, respectively. The interface boundary Γ_s is discretized by overlapping nodes belonging to different homogeneous domains. The state fields at the discretization nodes associated with the material domain Ω^+ can only be influenced by the nodes from this domain. The same applies to the nodes belonging to the domain Ω^-.

According to the standard collocation approach, the strong form equilibrium equations at the discretization nodes are expressed as follows:

$$\sigma^{+}_{ij,x_j}\left(\mathbf{x}_I\right)+b^{+}_{i}\left(\mathbf{x}_I\right)=0, \qquad \text{within } \Omega^{+}, \tag{33}$$

$$\sigma^{-}_{ij,x_j}\left(\mathbf{x}_M\right)+b^{-}_{i}\left(\mathbf{x}_M\right)=0, \qquad \text{within } \Omega^{-}. \tag{34}$$

The associated boundary and interface conditions can be written analogously. Like in the mixed approach proposed in [26], the displacement and stress components are chosen as the unknown field variables which are approximated separately within the homogeneous materials Ω^{+} and Ω^{-}, using the same field approximation functions. Hence, for the homogeneous material Ω^{+} the approximated fields can be written as

$$u^{+(h)}_{i}\left(\mathbf{x}_I\right)=\sum_{J=1}^{N_{\Omega_s}}\phi_J\left(\mathbf{x}_I\right)\left(\hat{u}^{+}_{i}\right)_J, \qquad \text{within } \Omega^{+}, \tag{35}$$

$$\sigma^{+(h)}_{ij}\left(\mathbf{x}_I\right)=\sum_{J=1}^{N_{\Omega_s}}\phi_J\left(\mathbf{x}_I\right)\left(\hat{\sigma}^{+}_{ij}\right)_J, \qquad \text{within } \Omega^{+}, \tag{36}$$

where ϕ_J represents the nodal value of the two-dimensional shape function for node J, N_{Ω_s} stands for the number of nodes within the approximation domain, while $\left(\hat{u}^{+}_{i}\right)_J$ and $\left(\hat{\sigma}^{+}_{ij}\right)_J$ denote the nodal values of displacement and stress components. The displacement and stress components over the material domain Ω^{-} are analogously approximated. The MLS approximation scheme with the interpolation property is used, which has already been described in the previous section.

According to the mixed MLPG paradigm, the equilibrium collocation equations (33) and (34) are first discretized by the stress approximations leading to the system of equations with the stress nodal variables, as presented in [13]. Then, in order to obtain the closed system of the governing equations with the displacement components as unknown nodal variables, the nodal stress components are expressed by means of the constitutive relations and the kinematic equations. Accordingly, for one homogeneous region Ω^{+} the following matrix relation may be derived:

$$\hat{\boldsymbol{\sigma}}^{+}_{J}=\mathbf{D}^{+}\sum_{L=1}^{N_{\Omega_s}}\mathbf{B}^{+}_{JL}\hat{\mathbf{u}}^{+}_{L}, \qquad \text{within } \Omega^{+}, \tag{37}$$

where $\mathbf{D}^{+}$ denotes the elasticity matrix, and $\mathbf{B}^{+}_{JL}$ is the matrix composed of first-order spatial derivatives of the nodal shape functions for the J^{th} node influencing the approximation at node L. $\hat{\mathbf{u}}^{+}_{L}$ stands for the nodal values of displacements. Analogous relations are derived for another homogeneous region Ω^{-}.

Finally, the discretized system of equations can be written for the nodes of each homogeneous domain Ω^+ and Ω^- as

$$\sum_{J=1}^{N_{\Omega_s}} \mathbf{K}_{IJ}^{+}\hat{\mathbf{u}}_J^{+} = \mathbf{R}_I^{+}, \quad I = 1,2,...,N, \quad \text{within } \Omega^+, \tag{38}$$

$$\sum_{J=1}^{N_{\Omega_s}} \mathbf{K}_{MJ}^{-}\hat{\mathbf{u}}_J^{-} = \mathbf{R}_M^{-}, \quad M = 1,2,...,P, \quad \text{within } \Omega^-, \tag{39}$$

where $\mathbf{K}_{IJ}^{+}$ and $\mathbf{K}_{MJ}^{-}$ are the nodal stiffness matrices, while $\mathbf{R}_I^{+}$ and $\mathbf{R}_M^{-}$ stand for the nodal force vectors. The discretized displacement boundary conditions can be written simply as

$$\overline{\mathbf{u}}_I^{+} = \sum_{L=1}^{N_{\Omega_s}} \phi_L \hat{\mathbf{u}}_L^{+}, \quad \text{on } \Gamma_u^{+}, \tag{40}$$

$$\overline{\mathbf{u}}_M^{-} = \sum_{L=1}^{N_{\Omega_s}} \phi_L \hat{\mathbf{u}}_L^{-}, \quad \text{on } \Gamma_u^{-}, \tag{41}$$

and the discretized traction boundary conditions are computed as

$$\overline{\mathbf{t}}_I^{+} = \mathbf{N}_I^{+}\mathbf{D}^{+}\sum_{L=1}^{N_{\Omega_s}} \mathbf{B}_{IL}^{+}\hat{\mathbf{u}}_L^{+}, \quad \text{on } \Gamma_t^{+}, \tag{42}$$

$$\overline{\mathbf{t}}_M^{-} = \mathbf{N}_M^{-}\mathbf{D}^{-}\sum_{L=1}^{N_{\Omega_s}} \mathbf{B}_{ML}^{-}\hat{\mathbf{u}}_L^{-}, \quad \text{on } \Gamma_t^{-}, \tag{43}$$

where $\mathbf{N}_I^{+}$ and $\mathbf{N}_M^{-}$ denote the matrices containing outward unit normal vector components to Γ_t^{+} or Γ_t^{-}. The following discretized interface boundary conditions may be written as

$$\sum_{L=1}^{N_{\Omega_s}} \phi_L \hat{\mathbf{u}}_L^{+} = \sum_{L=1}^{N_{\Omega_s}} \phi_L \hat{\mathbf{u}}_L^{-}, \quad \text{on } \Gamma_s, \tag{44}$$

$$\mathbf{N}_I^{+}\mathbf{D}^{+}\sum_{L=1}^{N_{\Omega_s}} \mathbf{B}_{IL}^{+}\hat{\mathbf{u}}_L^{+} = \mathbf{N}_M^{-}\mathbf{D}^{-}\sum_{L=1}^{N_{\Omega_s}} \mathbf{B}_{ML}^{-}\hat{\mathbf{u}}_L^{-}, \quad \text{on } \Gamma_s. \tag{45}$$

The global system of equations for the entire heterogeneous structure is obtained by looping through all the nodes belonging to the material sub-domains Ω^+ and Ω^- using the standard well-known procedure.

Plate with circular inclusion

As an example, a rectangular square plate with dimensions $2L \times 2L$ and the circular inclusion with radius $R = 1$ subjected to the unit horizontal traction t^0 is considered as depicted in Fig. 12.

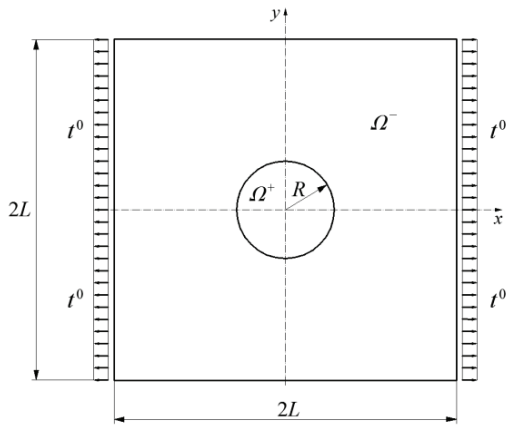

Fig. 12. Plate with circular inclusion subjected to uniform traction

Sl. 12. Ploča s okruglim umetkom podvrgnuta jednolikom istezanju

Due to the symmetry, only one quarter of the plate consisting of the two sub-domains Ω^- and Ω^+ has been discretized as shown in Fig. 13. As obvious, the symmetry boundary conditions are used along the left and bottom edges, while the tractions $\bar{t}_x^{\mathrm{a}}$ and $\bar{t}_y^{\mathrm{a}}$, taken from the analytical solution [27], are prescribed on all outer edges. The material properties of the plate are $E^+ = 1000$, $\nu^+ = 0.25$, while the values of $E^- = 10000$ and $\nu^- = 0.3$ have been chosen for the inclusion.

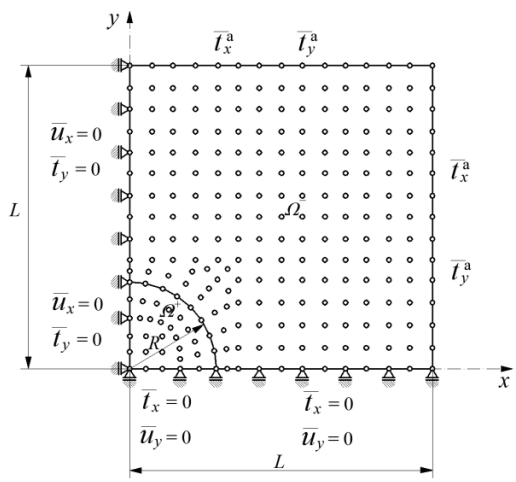

Fig. 13. Computational model of plate with circular inclusion with boundary conditions

Sl. 13. Računalni model ploče s okruglim umetkom i rubnim uvjetima

The computation is performed by using the MLS interpolation functions employing the second- and third-order basis (IMLS2, IMLS3). The accuracy of the numerical solutions is again compared to the analytical solutions [27]. The distributions of the strain components ε_x and the stress component σ_x for $x = 0$ are presented in Figs 14 and 15. The results obtained by the proposed mixed formulation by using the second- (IMLS2-M) and third-order (IMLS3-M) functions are also compared with the solutions obtained by the full displacement (primal) approach [5], using the same order basis (IMLS2-P and IMLS3-P). The superiority of the proposed mixed approach is evident.

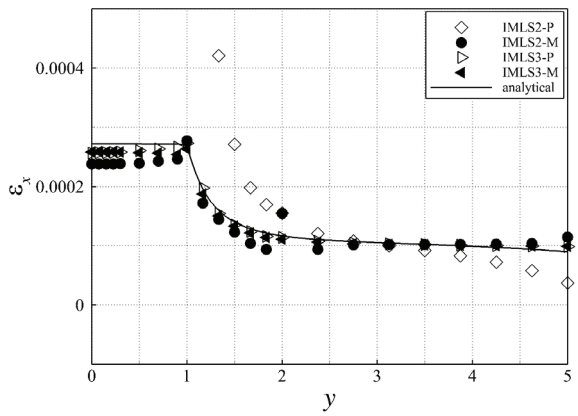

Fig. 14. Plate with circular inclusion – distribution of strain ε_x za $x = 0$

Sl. 14. Ploča s okruglim umetkom – raspodjela deformacije ε_x za $x = 0$

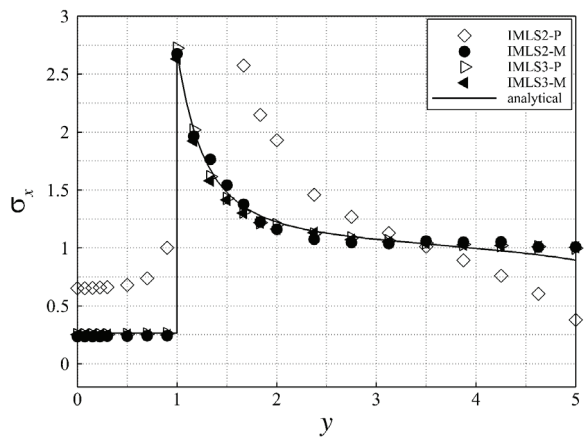

Fig. 15. Plate with circular inclusion – distribution of stress σ_x for $x = 0$

Sl. 15. Ploča s okruglim umetkom – raspodjela naprezanja σ_x za $x = 0$

Finally, the numerical efficiency of the proposed collocation formulation has been tested by investigating the convergence rate and computational time, and the results have been compared to those obtained by the FEM. The global stress convergence rates are portrayed in Fig. 16. Herein, the results obtained by the first-order triangular (CPS3), the first-order quadrilateral (CPS4), the second-order triangular (CPS6) and the quadrilateral (CPS8) elements from the ABAQUS [28] are compared to those computed by the proposed mixed MLPG collocation utilizing the second- and third-order MLS functions (IMLS2 and IMLS3, respectively). The available analytical solutions from [27] are used as the referent values. The discretized L_2 norm expressed as

$$e_\sigma = \sum_{k=1}^{N} \sqrt{\frac{\left(\sigma_x^{\mathrm{NUM}} - \sigma_x^{\mathrm{ANAL}}\right)_k^2 + \left(\sigma_y^{\mathrm{NUM}} - \sigma_y^{\mathrm{ANAL}}\right)_k^2 + \left(\tau_{xy}^{\mathrm{NUM}} - \tau_{xy}^{\mathrm{ANAL}}\right)_k^2}{\left(\sigma_x^{\mathrm{ANAL}}\right)_k^2 + \left(\sigma_y^{\mathrm{ANAL}}\right)_k^2 + \left(\tau_{xy}^{\mathrm{ANAL}}\right)_k^2}}, \tag{46}$$

is used as error indicator computed at all nodes of the numerical models considered. Here, σ_x and σ_y are normal stress components, while τ_{xy} represents the shear stress. The superscript NUM denotes numerical solutions, obtained either by FEM or by MLPG approach. The superscript ANAL stands for the analytical solutions. N denotes the number of nodes.

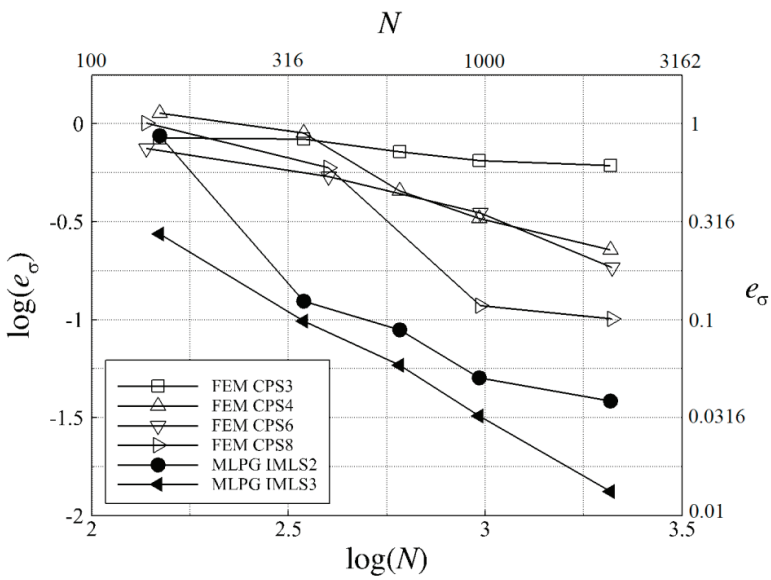

Fig. 16. Plate with circular inclusion – comparison of numerical stress accuracy with FEM

Sl. 16. Ploča s okruglim umetkom – usporedba točnosti naprezanja s FEM (metodom konačnih elemenata)

It can be seen from Fig. 16 that the meshless approach is superior to the above-mentioned finite element formulations with respect to the convergence rates and the numerical accuracy. The computational time for the meshless method is shorter than for the FEM, especially for the model with fewer nodes, indicating that the presented approach could be a potentially interesting alternative to the FEM in solving similar problems. It is important to emphasize that a further careful optimization of the developed meshless code is necessary in order to make a more trustworthy assessment about the numerical efficiency of the present approach.

5. CONCLUSIONS

Three different formulations of the meshless local Petrov-Galerkin approach are presented. The three-dimensional full displacement formulation is derived and applied for the solution of the elasto-static problem. It is evident that this approach is highly efficient in solving strongly singular problems, such as the Boussinesq problem. The presented method achieves significantly higher accuracy with only one-third as many nodes as compared to the finite element method. An efficient mixed meshless formulation based on the local Petrov-Galerkin approach for the analysis of plate and shell structures has been displayed. Here, the superiority of the mixed formulation in comparison to the standard full displacement approach is demonstrated. Using the strain and stress approximations, the undesired thickness and shear locking phenomena, which are a well-known drawback of the shell finite element formulations, are efficiently eliminated. The results also show that the accuracy and convergence of the mixed meshless formulation are better than that of the finite element used. The third meshless formulation is based on the mixed collocation approach. Therein, the deformation responses of heterogeneous structures are modeled. The discontinuities in the strain and stress fields due to the material heterogeneity are captured accurately. Again, the numerical efficiency of the proposed method is estimated by comparison to the FEM with respect to accuracy, convergence rates and computational time. The present method yields convergence rates, which are larger or comparable to those obtained by the FEM, while at the same time, it is more accurate for the same number of degrees of freedom. On the other hand, the FEM method is still faster for equal number of the degrees of freedom. Nevertheless, as the collocation method needs fewer nodes to achieve the same level of global accuracy as the FEM, the computational time required for solving an engineering problem might be shorter or comparable to that of the FEM.

It is to note that the construction of meshless shape functions is rather complex in nature in comparison to the polynomial functions within the mesh-based methods.

Thus, the number of integration points required for an exact calculation of the integrals in the meshless methods based on the weak forms may be higher than in the FEM, because the shape functions are often not of polynomial character.

References

[1] N. Perrone, R. Kao, A general finite difference method for arbitrary meshes, Computers & Structures, 5(1) (1975) 45-57.

[2] B. Šarler, J. Perko, C.-S. Chen, Radial basis function collocation method solution of natural convection in porous media, International Journal of Numerical Methods for Heat & Fluid Flow, 14(2) (2004) 187-212.

[3] H.-Y. Hu, Z.-C. Li, A. H.-D. Cheng, Radial basis collocation methods for elliptic boundary value problems, Computers & Mathematics with Applications, 50(1-2) (2005) 289-320.

[4] T. Belytschko, Y. Y. Lu, L. Gu, Element free Galerkin methods, International Journal for Numerical Methods in Engineering, 37(2) (1994) 229-256.

[5] S. N. Atluri, T. Zhu, A new Meshless Local Petrov-Galerkin (MLPG) approach in computational mechanics, Computational Mechanics, 22(2) (1998) 117-127.

[6] W. K. Liu, S. Jun, Y. F. Zhang, Reproducing kernel particle methods, International Journal for Numerical Methods in Fluids, 20(8-9) (1995) 1081-1106.

[7] C. A. Duarte, J. T. Oden, H-p Clouds – An h-p Meshless Method, Numerical Methods for Partial Differential Equations, 12(6) (1996) 673-705.

[8] S. N. Atluri, T.-L. Zhu, The meshless local Petrov-Galerkin (MLPG) approach for solving problems in elasto-statics, Computational Mechanics, 25(2-3) (2000) 169-179.

[9] G. R. Liu, Y. T. Gu, A meshfree method: meshfree weak-strong (MWS) form method for 2-D solids, Computational Mechanics, 33(1) (2203) 2-14.

[10] G. R. Liu, Y. L. Wu, H. Ding, Meshfree weak-strong (MWS) form method and its application to incompressible flow problems, International Journal for Numerical Methods in Fluids, 46(10) (2004) 1025-1047.

[11] Q. Li, S. Shen, Z. D. Han, S. N. Atluri, Application of Meshless Local Petrov-Galerkin (MLPG) to Problems with Singularities, and Material Discontinuities, in 3-D Elasticity, CMES: Computer Modeling in Engineering & Sciences, 4(5) (2003) 571-585.

[12] J. Sorić, T. Jarak, Mixed meshless formulation for analysis of shell-like structures, Computer Methods in Applied Mechanics and Engineering, 199 (17-20) (2010) 1153-1164.

[13] B. Jalušić, J. Sorić, T. Jarak, Mixed meshless local Petrov-Galerkin collocation method for modeling of material discontinuity, Computational Mechanics, 59 (1) (2017) 1-19.

[14] P. Lancaster, K. Salkauskas, Curve and surface fitting: an introduction. Academic Press Ltd, London (1986).

[15] S. N. Atluri, H.-G. Kim, J. Y. Cho, A critical assessment of the truly meshless local Petrov-Galerkin (MLPG) and Local Boundary Integral Equation (LBIE) methods, Computational Mechanics, 24(5) (1999) 348-372.

[16] P. Breikopf, A. Rassineux, G. Touzot, P. Villon, Explicit form and efficient computation of MLS shape functions and their derivatives, International Journal for Numerical Methods in Engineering, 48(3) (2000) 451-466.

[17] S. N. Atluri, S. Shen, The meshless local Petrov-Galerkin (MLPG) method, Tech Science Press, Encino, USA (2002).

[18] S. Timoshenko, J. N. Goodier, Theory of elasticity, McGraw-Hill Book Company, New York, USA (1951).

[19] R. Hauptmann, K. Schweizerhof, A systematic development of solid-shell element formulations for linear and non-linear analyses employing only displacement degrees of freedom, International Journal for Numerical Methods in Engineering, 42(1) (1998) 49-69.

[20] S. Klinkel, F. Gruttmann, W. Wagner, A robust non-linear solid shell element based on a mixed variational formulation, Computer Methods in Applied Mechanics and Engineering, 195(1-3) (2006) 179-201.

[21] T. Most, C. Bucher, A Moving Least Squares weighting function for the Element-free Galerkin Method which almost fulfills essential boundary conditions, Structural Engineering and Mechanics 21(3) (2005) 315-332.

[22] T. Most, A natural neighbour-based moving least-squares approach for the element-free Galerkin method, International Journal for Numerical Methods in Engineering,71(2) (2007) 224-252.

[23] Y. Basar, W.B. Krätzig, Theory of Shell Structures, VDI Verlag (2001).

[24] T. Jarak, J. Sorić, J. Hoster, Analysis of shell deformation responses by the Meshless Local Petrov-Galerkin (MLPG) approach, CMES: Computer Modeling in Engineering & Sciences, 18(3) (2007) 235-246.

[25] MSC.Software Corporation, MSC.Nastran 2005 Quick Reference Guide, MSC.Software Corporation, USA (2005).

[26] S. N. Atluri, H. T. Liu, Z. D., Meshless local Petrov-Galerkin (MLPG) mixed collocation method for elasticity problems, CMES: Computer Modeling in Engineering & Sciences 14(3) (2006) 141-152.

[27] M. Kachanov, B. Shafiro, I. Tsukrov, Handbook of Elasticity Solutions, Springer Science+Business Media, Dordrecht (2003).

[28] ABAQUS/Standard, Dassault Systemes, Providence, Rhode Island, USA (2014).

BEZMREŽNI POSTUPAK KAO ALTERNATIVA METODI KONAČNIH ELEMENATA PRI NUMERIČKOM MODELIRANJU U MEHANICI ČVRSTIH TIJELA

Sažetak

Bezmrežni postupak omogućuje diskretizaciju računalnog modela samo s čvorovima koji ne trebaju biti povezani s konačnim elementima. U ovom članku prikazuje se lokalna Petrov-Galerkinova formulacija koja u potpunosti spada u bezmrežne postupke jer ne zahtijeva niti jednu vrstu mreže ili tzv. popratnih ćelija, kako za interpolaciju tako i za integraciju. Prikazane su puna formulacija pomaka i mješovita formulacija. Postupak punog pomaka se primjenjuje za rješavanje trodimenzijskog elasto-statičkog problema, dok se mješovita formulacija koristi za modeliranje deformiranja ljuskastih konstrukcija. Modeliranje materijalnog diskontinuiteta se provodi mješovitim bezmrežnim lokalnim Petrov-Galerkinovim postupkom koji uključuje kolokacijsku metodu. U numeričkim primjerima, učinkovitost i točnost svih prikazanih metoda je testirana i uspoređena s formulacijama metode konačnih elemenata. Pokazano je da se bezmrežni postupci mogu smatrati alternativom za dobro poznatu metodu konačnih elemenata.

Ključne riječi: Bezmrežna metoda; lokalna Petrov-Galerkinova formulacija; mješoviti bezmrežni postupak; kolokacijski bezmrežni postupak.

Jurica Sorić*, Boris Jalušić, Tomislav Jarak

University of Zagreb
Faculty of Mechanical Engineering and Naval Architecture
Ivana Lučića 5, 10000 Zagreb,
E-mail: jurica.soric@fsb.hr; boris.jalusic@fsb.hr; tomislav.jarak@fsb.hr
* član suradnik HAZU

UDK / UDC 624.072.33:519.6
DOI: 10.21857/y26kec3z79

Izvorni znanstveni članak / Original scientific paper
Prihvaćeno / Accepted: 18. 12. 2018.

A NEW ROBUST AND COMPUTATIONALLY EFFICIENT NUMERICAL MODEL FOR THE ANALYSIS OF BEAM TYPE STRUCTURES

Ante Mihanović; Hrvoje Smoljanović;
Boris Trogrlić; Ante Munjiza

University of Split, Faculty of Civil Engineering, Architecture and Geodesy;
Matice hrvatske 15, 21000 Split, Croatia

Ab**strac**t

This paper presents a new numerical model for the analysis of beam type structures. The model uses two-noded rotation free finite elements and takes into account material non-linearity, finite displacements, finite rotations and finite strains. The presented numerical model has been implemented into the open source 'Yfdem', which is based on the Combined Finite Discrete Element Method. The performance of the new numerical model was demonstrated on simple benchmark tests, by a comparison with known experimental and analytical results.

Keywords: numerical model; beam structures; finite-discrete element method.

1. INTRODUCTION

Beam type structural elements, which are constituent elements of many constructions, are elements in which the length is considerably more pronounced than the width and the height of the cross-section. Beam elements can be flat, supporting transverse load through bending, or curved, supporting transverse loads trough a combined action of bending and axial force.

Throughout history, a number of numerical models have been developed for the analysis of beam structures, most of which are based on the finite element method (FEM). The finite element method formulation of the problem results in a system of algebraic equations. To solve the problem, it subdivides a large domain into smaller parts

that are called finite elements. The method yields approximate displacement field over finite elements at the finite number of points by using shape functions. Simple equations obtained over these finite elements are assembled into a larger system of equations that models the entire problem. Solving a large system of equations, especially if material non-linearity, finite rotations and finite displacements are taken into account, can become computationally very demanding and time-consuming, causing additionally problems due to numerical instabilities.

Due to its long tradition, a number of numerical models based on FEM have been developed and are distinguished in type of finite elements, the structure of which is discretized, and in type of constitutive law of materials that can be linear and non-linear.

The simplest element formulations, which use lower order polynomial as shape functions for approximating node displacement, result in overly stiff behaviour known as the locking phenomenon. This phenomenon arises due to an inability of the formulations to describe a pure bending deformation. The solution to this problem has emerged in the form of a coupled polynomial, mixed trigonometric polynomial and in higher-order-polynomial shape functions for approximating displacement field over finite elements [1-6]. Finite elements proposed so far are mainly dependent on the shape of the beam element. They are usually not established or are even found deficient for different beam configurations. In search for better computational efficiency, there has also been development in rotation-free finite elements [7-11]. These elements manage to remove rotational degrees of freedom by increasing the interpolation domain outside of the area of integration domain, and therefore achieve significant simplification of the initial problem.

The main purpose of this paper is to present a simple, robust and computationally efficient numerical model for the analysis of beam type structures. The model is based on two-noded rotation free finite elements taking into account non-linear material behaviour, finite displacements, finite rotations and finite strains. The discretization of the structure with a detailed description of the axial and bending carrying mechanism of finite elements are presented. Proposed numerical algorithms have been implemented into the open source 'Yfdem', which is based on combined finite discrete element method (FDEM) presented by Munjiza [12-15]. Subsequently, verification and validation of the proposed numerical model have been performed on several examples by comparing the obtained numerical results with the known analytical and experimental results from literature.

2. PROPOSED NUMERICAL MODEL

This chapter presents a numerical algorithm for the analysis of beam type structures, which, inter alia, takes into account material non-linearity, finite displacement and

finite rotations. Detailed information regarding the discretization of the structure and the calculation of nodal forces due to the bending and axial deformation are shown below.

2.1. Discretization of the structure

Within the presented numerical model, the structure has been discretized with two-noded finite elements. The mass of the structure is concentrated in the finite element nodes as shown in Fig. 1.

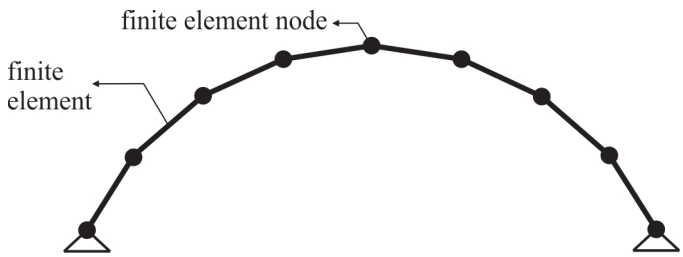

Fig. 1. Discretization of structure
Sl. 1. Diskretizacija konstrukcije

2.2. Calculation of nodal forces due to axial and bending carrying mechanisms

For the purposes of calculating the axial and bending deformation and the calculation of nodal forces, the observed node B is considered together with its two neighbouring nodes – A and C – as shown in Fig. 2.

Based on the known coordinates of the nodes at any time step, it is possible to calculate the radius of the curvature of the circle passing through the nodes A, B and C according to the relation:

$$r = \frac{d}{2 \sin \varphi} \tag{1}$$

Here, d and φ are the length between the adjacent nodes and the angle between the finite elements in the node B, respectively (see Fig. 2.).

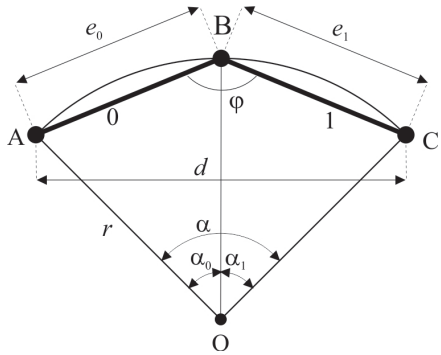

Fig. 2. Observed finite element node together with two neighbouring nodes
Sl. 2. Promatrani čvor konačnog elementa zajedno sa susjednim čvorovima

Based on the known radius of curvature of the circle and the distance between adjacent nodes, it is possible to calculate the angles α_0, α_1 and α (see Fig. 2.) at any time step according to the following relations:

$$\alpha_0 = \operatorname{acos}\left(\frac{1-e_0^2}{2r^2}\right)$$
$$\alpha_1 = \operatorname{acos}\left(\frac{1-e_1^2}{2r^2}\right)$$
$$\alpha = \alpha_0 + \alpha_1 \tag{2}$$

Within the presented numerical algorithm, the cross-section has been divided into layers as shown in Fig. 3. For each layer, it is possible to calculate its length l_i at any time step in accordance with the following relation:

$$l_i = r_i\, \alpha \tag{3}$$

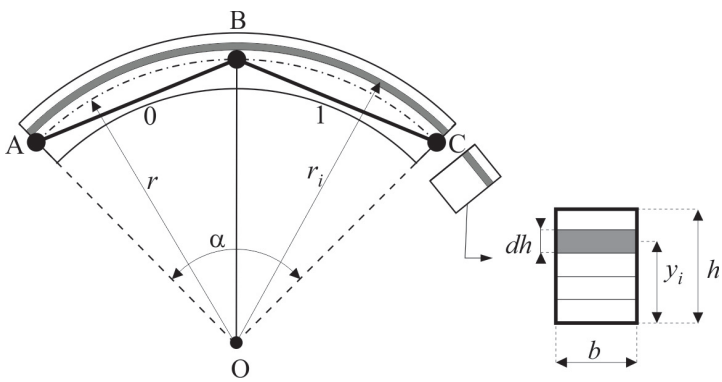

Fig. 3. Cross-section of the structures with layers
Sl. 3. Uslojeni poprečni presjek

Here, r_i is the radius of the curvature of the observed layer (see Fig. 3) given by:

$$r_i = r - \frac{h}{2} + y_i \tag{4}$$

In the previous relation, y_i is the distance between the centre of the layer and the bottom of the cross, while h is the height of the cross-section as shown in Fig. 3. Based on the length of the layers in initial $l_{i,i}$ and current $l_{i,c}$ configuration, it is possible to calculate the strain of the layer according to the following relation:

$$\varepsilon_i = \frac{l_{i,c} - l_{i,i}}{l_{i,i}} \tag{5}$$

Taking into account the constitutive law of material given in relation between stress and strain, based on the known strain ε_i, it is possible to obtain stress σ_i in the centre of the layer. It is important to note that an arbitrary relation can be chosen between strain and strain. Differential force dn_i acting at the centre of the layer can be obtained according to the following relation:

$$dn_i = b\, dh\, \sigma_i \tag{6}$$

Here, b and dh are the width and the thickness of the layer, respectively (see Fig. 3.). Total axial force acting on the centre of the gravity of the cross-section in the node B (see Fig. 4.) is obtained according to:

$$n_B = \sum_{i=1}^{n} dn_i \tag{7}$$

Here, index n in the summation relates to the number of layers.
The procedure described above is repeated for the nodes A and C, which yields axial force in node A n_A and axial force in node C n_C as shown in Fig. 4a. Finally, axial forces in finite elements 0 and 1 are given by:

$$n_0 = \frac{n_A + n_B}{2}\ ;\ n_1 = \frac{n_B + n_C}{2}, \tag{8}$$

respectively.

The moment at the centre of the gravity of the cross-section in the node B (see Fig. 4b.) is obtained according to relation:

$$m_B = \sum_{i=1}^{n} dn_i \left(y_i - \frac{h}{2} \right) \tag{9}$$

Here, h is the height of the cross-section.

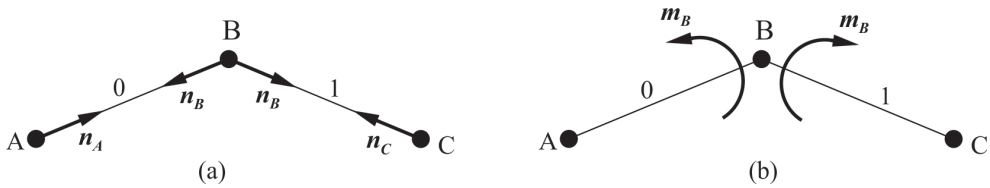

Fig. 4. (a) Axial forces in nodes A, B and C and (b) moment in node B

Sl. 4. (a) Uzdužne sile u čvorovima A, B i C i (b) moment u čvoru B

Axial forces in finite elements 0 and 1 are transferred in the form of equivalent nodal forces in nodes A, B and C as shown in Fig. 5a, while the moment in observed node B is transferred in the form of pair of forces in nodes A, B, and C as shown in Fig. 5b.

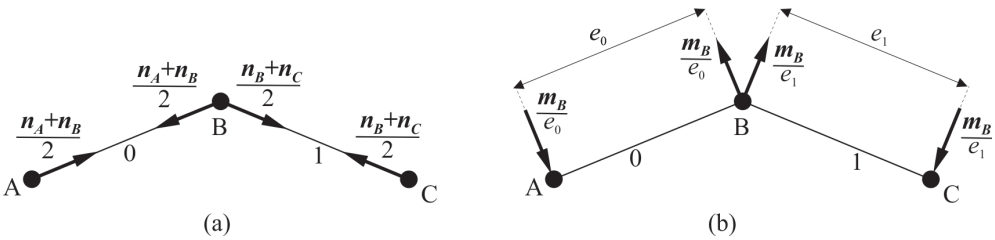

Fig. 5. Equivalent nodal forces due to: (a) axial force in finite elements 0 and 1; (b) moment in node B

Sl. 5. (a) Ekvivalentne čvorne sile uslijed: (a) uzdužne sile u konačnom elementu 0 i 1; (b) momenta u čvoru B

If node A is boundary node, axial force in node A equals n_B. Finally, if node C is boundary node, axial force in node C equals n_C. Equivalent nodal forces due to axial force in finite elements 0 and 1 in case when node A and C are boundary nodes are shown in Fig. 6a and Fig. 6b, respectively. The procedure described above is repeated for all nodes.

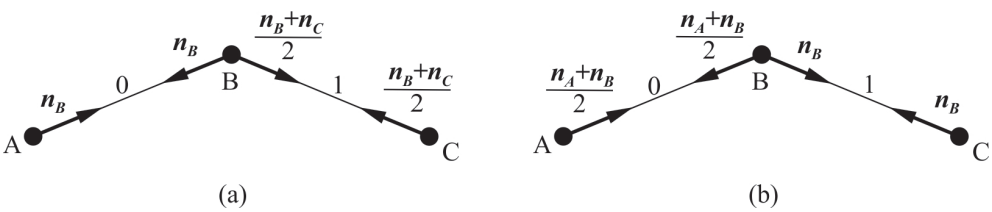

Fig. 6. Equivalent nodal forces due to axial force in finite elements 0 and 1 in case where boundary node is: (a) node A; (b) node B

Sl. 6. (a) Ekvivalentne čvorne sile uslijed uzdužne sile u konačnim elementima 0 i 1 u slučaju kada je krajnji čvor: (a) čvor A; (b) čvor B

2.3. Clamped boundary condition

In the context of the FDEM, based on which the presented numerical model has been developed, nodes only have translational degrees of freedom. Taking this fact into account, the question is how to achieve clamped boundary condition. In actual implementation, the clamped boundary condition, for example in node B (see Fig. 7.), can be achieved by implementing fictive node near the clamped boundary as shown in Fig. 7. As the fictive node, which lies in the tangent on the structure at the clamped boundary, tends to the clamped boundary, the tangent on the circle passing through nodes A, B and C converges to the tangent on the structure at clamped boundary as shown in Fig. 7. In the current configuration, there are some discrepancies between theoretical and calculated curvature, since the tangent on the structure at the boundary node does not coincide with the tangent of the circle passing through the fictive node A, and nodes B and C. It can be shown that if the length of the fictive element 0 (see Fig. 7) is over one thousand times smaller than the length of the finite element 1 (see Fig. 7), the discrepancy is smaller than 0.01 %.

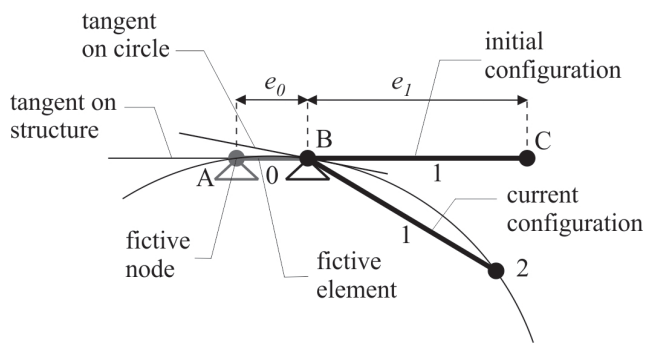

Fig. 7. Clamped boundary in actual implementation

Sl. 7. Upeti rubni uvjet u stvarnoj implementaciji

2.4. Nodal forces due to dumping

In the proposed numerical model, a viscous type of damping is adopted, in which the damping forces, whose intensity is proportional to the velocity and damping coefficient μ, are linearly distributed over the finite elements. The proposed numerical model differentiates the dumping forces, which act in direction of the construction line, and damping forces, which act in direction normally on the construction. For the purpose of calculating equivalent nodal forces due to dumping, the velocity of the nodes of the

finite element has been split into the components in direction tangential and orthogonal to the finite element as shown in Fig. 8. Equivalent nodal forces in nodes A and B are thus given by:

$$\begin{aligned}\mathbf{f}_{B,dump} &= -\mu_{nor}\left(\mathbf{v}_{B,nor}\frac{e_0}{3}+\mathbf{v}_{A,nor}\frac{e_0}{6}\right)-\mu_{\tan}\left(\mathbf{v}_{B,tan}\frac{e_0}{3}+\mathbf{v}_{A,tan}\frac{e_0}{6}\right)\\ \mathbf{f}_{A,dump} &= -\mu_{nor}\left(\mathbf{v}_{B,nor}\frac{e_0}{6}+\mathbf{v}_{A,nor}\frac{e_0}{3}\right)-\mu_{\tan}\left(\mathbf{v}_{B,tan}\frac{e_0}{6}+\mathbf{v}_{A,tan}\frac{e_0}{3}\right)\end{aligned} \tag{10}$$

Here, μ_{nor} and μ_{tan} are normal and tangential dumping coefficients.

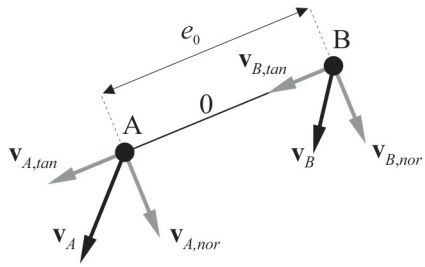

Fig. 8. Normal and tangential component of node velocity

Sl. 8. Normalna i tangencijalna komponenta brzine u čvoru

The procedure described above is repeated for all finite elements.

2.5. Time integration of equation of motion

The shape of a beam element and its position in space at any time step is given by the current coordinates of the finite element nodes x_i, where i is associated with the degree of freedom. Similarly, the velocity field and acceleration field have been defined by nodal velocities v_i and nodal accelerations a_i, respectively [12].

In the context of the FDEM, a time integration scheme in an explicit form is applied to each node and each degree of freedom. Nodal forces resulting from axial carrying mechanism, bending carrying mechanism, external loads and dumping forces are all added together, and a total nodal force f_i associated with each degree. The dynamic equilibrium for each degree of freedom is therefore given by:

$$m_i\, a_i = f_i \tag{11}$$

Here, m_i is the mass associated with each degree of freedom.

For the integration of the above equation, a central difference time integration scheme based on explicit integration of the governing equation for each degree of freedom has been employed. The scheme can be formulated as follows:

$$v_{i,t+\Delta t/2} = v_{i,t-\Delta t/2} + \Delta t\, f_{i,t} / m_i$$
$$x_{i,t+\Delta t} = x_{i,t} + \Delta t\, v_{i,t+\Delta t/2} \tag{12}$$

Here, Δt is a time step.

A schematic flowchart that describes the overall numerical procedure has been shown in Fig. 9. It is worth pointing out that the proposed numerical procedure does not require either stiffness or mass matrices to be assembled, which makes it suitable for parallel programming.

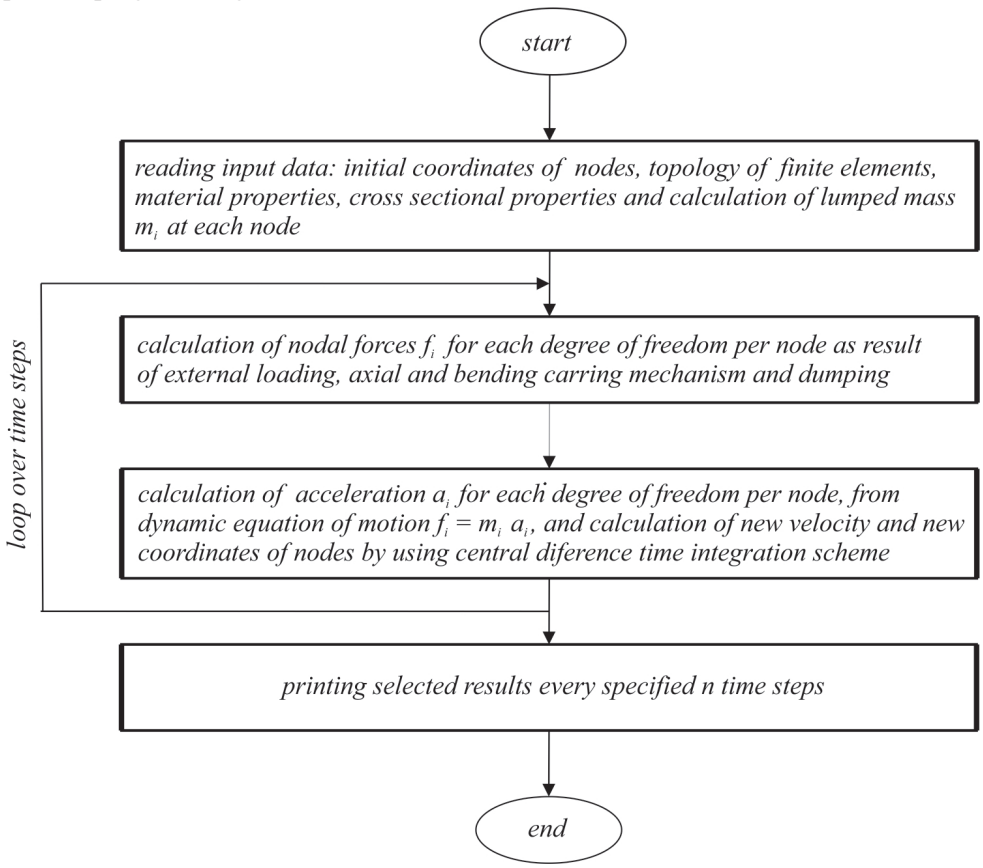

Fig. 9. A schematic flowchart of the overall numerical procedure

Sl. 9. Shematski dijagram prethodno opisanog numeričkog postupka

3. VALIDATION OF THE FDEM NUMERICAL MODEL

The model described above has been implemented into the open source FDEM package – Yfdem [12]. The validation of the model has been performed on several examples by comparing the obtained results with the known analytical and experimental results obtained in the literature.

3.1. Cantilever exposed to bending moment at the free end

The cantilever beam exposed to bending moment at the free end as shown in Fig. 10a, has been chosen in order to investigate the relative error of calculated moment in cross-section in dependence on the number of subdivisions per high of the cross-section.

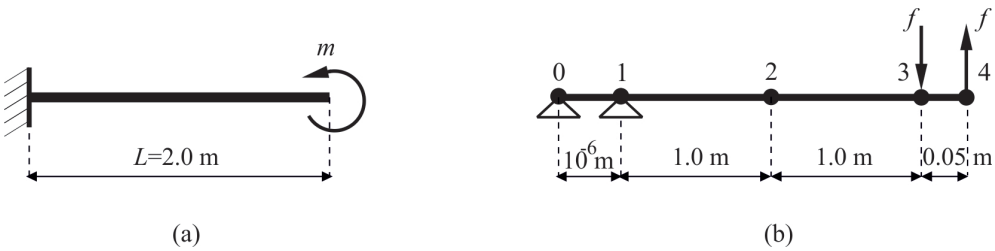

Fig. 10. Cantilever exposed to bending moment at the free end: (a) geometry; (b) discretization
Sl. 10. Konzola opterećena momentom na slobodnom kraju: (a) geometrija; (b) diskretizacija

The cantilever was discretized with four finite elements and five nodes as shown in Fig. 9b. The finite element 0 of length $1 \cdot 10^{-6}$ m with hinged nodes 0 and 1 has been used for modelling the clamped boundary condition in node 1, while the finite element 3 of length 0.05 m with a pair of forces in nodes 3 and 4 has been used for modelling of the bending moment in node 3, which equals:

$$m / kNm = 0.05 f / kN \tag{13}$$

The modulus of elasticity of the cantilever equalled E=210 GPa, while the width b and the height h of the cross-section were adopted in the amounts of 1.0 m and 0.1 m, respectively. The following relation explains the analytical relationship between bending moment and curvature in cross-section:

$$m_{an} = \frac{1}{r} EI \tag{14}$$

Here, I is the moment of inertia of the cross-section given by:

$$I = \frac{bh^3}{12} = \frac{1.0\,\text{cm} \cdot 0.1\,\text{cm}^3}{12} = 8.333 \cdot 10^{-5}\,\text{m}^4 \tag{15}$$

Including the relation (15) in (14) and taking into account the modulus of elasticity that equals E=210 GPa yields as follows:

$$m_{an}/(\text{N/m}) = 17500 \frac{1}{r/\text{m}} \tag{16}$$

The relation between the moment at the free end and curvature in node 2 obtained with the proposed numerical model for a different number of subdivisions n per height of the cross-section has been shown in Fig. 11. From the presented results, it can be seen that by increasing the number of subdivisions per height of the cross-section, the numerical solution converges to the analytical one.

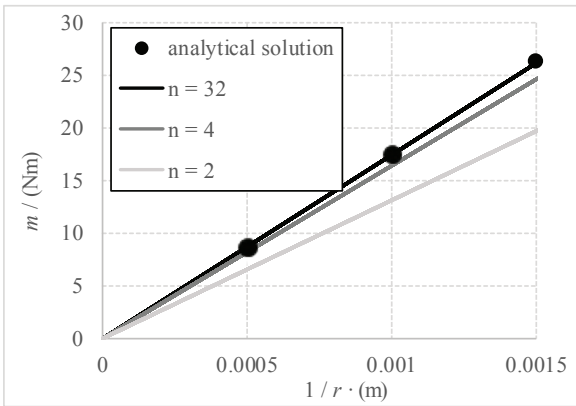

Fig. 11. Comparison of curvature in node 2 with analytical solution

Sl. 11. Usporedba zakrivljenosti u čvoru 2 s analitičkim rješenjem

Relative error in calculating the moment in node 2 in comparison with the analytical solution obtained according to the following relation:

$$\text{relativeerror} = \frac{m - m_{an}}{\text{m}_{\text{an}}} \cdot 100 \tag{17}$$

has been shown in Fig. 12. It can be seen that in a number of subdivisions higher than 30, relative error is less than 0.1 %.

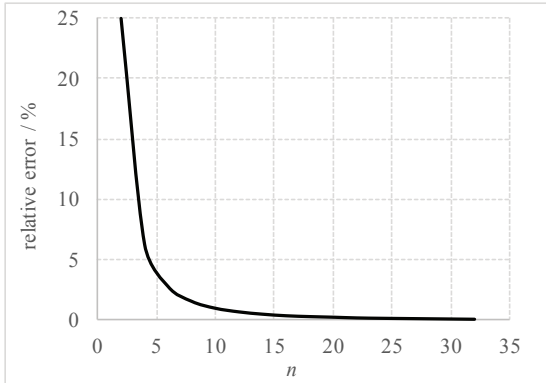

Fig. 12. Relative error of the moment in node 2 in comparison with analytical solution

Sl. 12. Relativna pogreška momenta u čvoru 2 u usporedbi s analitičkim rješenjem

3.2. A simply supported beam under self-weight

A simply supported beam under self-weight, whose geometry has been shown in Fig. 13, has been chosen to analyse relative error in numerical solution obtained with presented numerical model in dependence of the number of finite elements per beam length. The width of the cross-section equalled 100 cm, while the height of cross-section varied in the amounts of 50 mm and 200 mm. The modulus of beam elasticity equalled E = 210 GPa, while the density ρ and gravity constant g were adopted in the amounts of 7,850 kg/m^3 and 10 m/s^2, respectively.

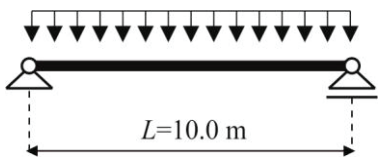

Fig. 13. Simply supported beam under self-weight

Sl. 13. Jednostavna greda opterećena vlastitom težinom

The discretization of the beam was performed by using 2, 4, 8 and 16 finite elements, which means that the lengths l of the finite elements were $L/2$, $L/4$, $L/8$ and $L/16$, respectively. Starting from an initially flat geometry, the beam oscillates due to its self-weight, and subsequently, as a result of damping, finds an equilibrium position as shown in Fig. 14.

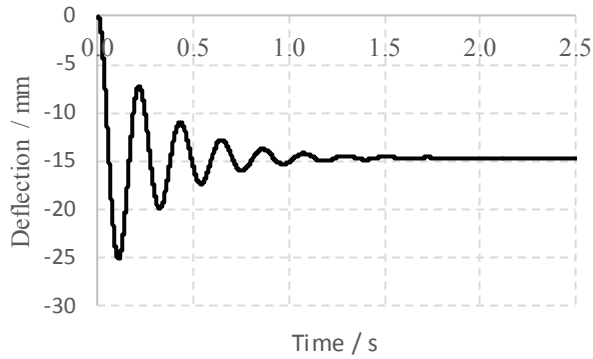

Fig. 14. Time-midspan deflection response for beam discretized with 16 finite elements and damping coefficient $\mu_{nor} = \mu_{tan}$ =10000 kNm²/s.

Sl. 14. Progib centra grede u vremenu za diskretizaciju od 16 konačnih elemenata i prigušenje $\mu_{nor} = \mu_{tan}$ =10000 kNm²/s.

The equilibrium deflections at the midspan of the beam obtained with presented numerical model together with numerical solutions obtained by the ABAQUS programme package have been shown in Table 1. The numerical solutions from ABAQUS have been obtained by using 100 three-noded quadratic beam finite elements. Relative errors of the numerical results obtained with the proposed numerical model in comparison with the numerical solutions obtained by ABAQUS have been shown in Table 2.

Table 1

Deflection at the midspan of the beam in (mm)

Beam thickness	50 mm	200 mm
FDEM (l=L/2)	279.73	17.538
FDEM (l=L/4)	244.84	15.346
FDEM (l=L/8)	236.12	14.798
FDEM (l=L/16)	233.94	14.661
ABAQUS	232.999	14.601

From the presented results, it can be observed that as the number of the finite elements increases, the numerical solutions converge to those obtained by ABAQUS and the error of approximation decreases with l^2. It has also been observed that the influence of beam thickness on error is negligible, which indicates that the presented numerical model does not suffer from the locking phenomenon related to the length to thickness ratio of the beam.

Table 2

Relative error of the beam in comparison with numerical solution obtained by ABAQUS in (%)

Beam thickness	50 mm	200 mm
FDEM (l=L/2)	20.06	20.11
FDEM (l=L/4)	5.08	5.10
FDEM (l=L/8)	1.36	1.35
FDEM (l=L/16)	0.40	0.41

3.3. Reinforced concrete beams

Reinforced concrete beams exposed to monotonic increasing loading condition, with the known experimental results taken from literature [16], have been used for additional validation of the presented numerical model. The experimental programme conducted by Alca et al. [16] included 12 reinforced concrete beams subjected to a four-point bending test as shown in Fig. 15. Three depths of beams have been used: namely 230 mm (small beam); 360 mm (medium beam); and 515 mm (large beam). These have been combined with two concrete strengths: lower strength concrete (cylinder strength of 50 MPa), and higher strength concrete (cylinder strength of 90 MPa).

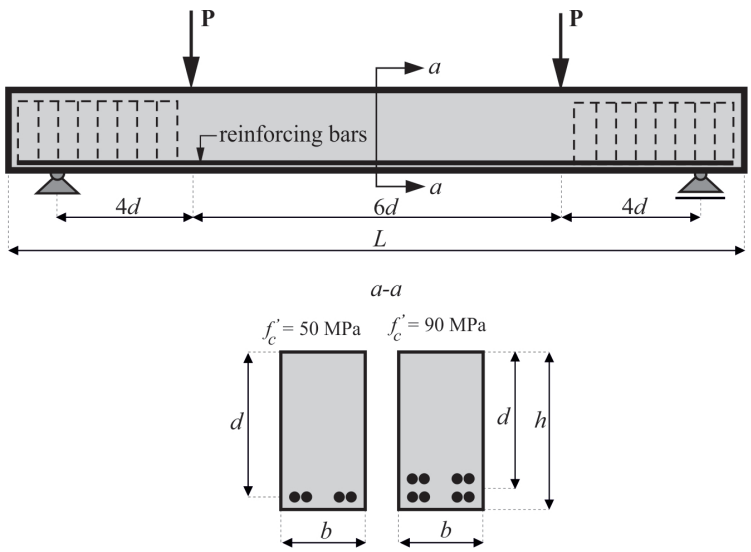

Fig. 15. Reinforced concrete beams exposed to monotonic increasing loading condition with cross-sections

Sl. 15. Jednostavna armirano betonska greda izložena monotono rastućem opterećenju sa poprečnim presjecima

In this work, only four beams were used, namely SL1, SH1, LL1 and LH1. Two letters and a number designate each beam. The first letter S or L refers to small or large beam. The second letter L or H refers to low or high strength concrete. The geometric characteristic of these beams have been summarised in Table 3.

Alca et al. [16] have tested two beams of each type to failure (letter 1 or 2). Material properties for the first set of beams have been presented in Table 4.

Table 3
Beam geometry

Beam	∅ / mm	*b* /mm	*d* / mm	*h* / mm	*L* / mm
SL1	16	150	230	282	3740
SH1	16	150	230	302	3740
LL1	35.7	335	515	630	8380
LH1	35.7	335	515	630	8380

Table 4
Beam material properties

Beam	f_c' / MPa	f_y /MPa	□ / %
SL1	51.1	410	2.32
SH1	90.1	410	4.64
LL1	54.2	409	2.32
LH1	90.3	406	4.64

For the purpose of numerical analysis with the presented numerical model, the structure has been discretized with 28 finite elements as shown in Fig. 16. The beams have been modelled from support to support, and the overhang beyond the supports has been ignored.

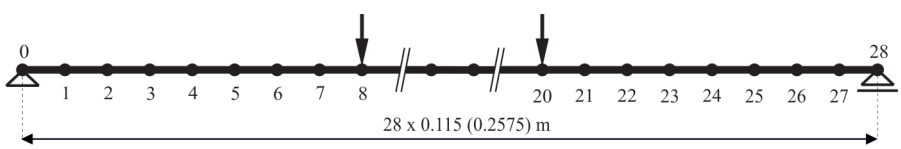

Fig. 16. Discretization of small and large reinforced concrete beams.
Values in brackets corresponds to large beam

Sl. 16. Diskretizacija velike i male armirano betonske grede. Vrijednosti u zagradi odgovaraju velikoj gredi

For all beams, the following approximation for the stress–strain curve for concrete has been adopted (as shown in Fig. 17a):

$$\sigma = E\varepsilon - \frac{E^2}{4f_s}\varepsilon^2 \tag{14}$$

Here, σ is stress, ε is strain, while f_s is compression strength of concrete, which is adopted in amount of 44.77 MPa for lower strength beams and 76.70 MPa for higher strength beams. Stress in each of the bars has been obtained from strain using the bilinear stress–strain curve for steel as shown in Fig. 17b.

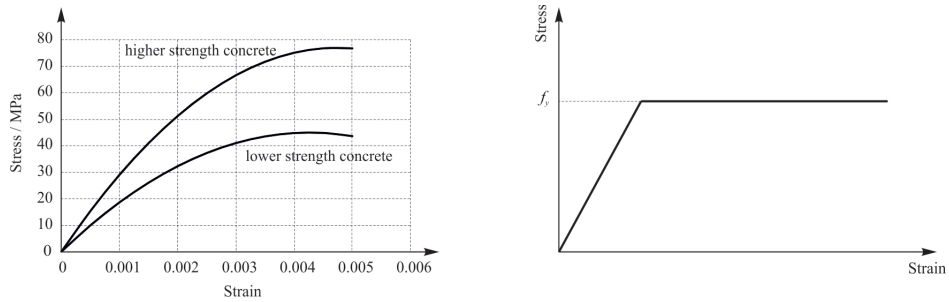

Fig. 17. Adopted stress strain curves for: (a) concrete; (b) reinforcing bars

Sl. 17. Usvojene krivulje naprezanje-deformacija za: (a) beton; (b) armaturne šipke

Fig. 18 shows the comparison of numerical results obtained with presented numerical model with experimental results from Alca et al. [16] for small and large beams, for both lower and higher strength concrete.

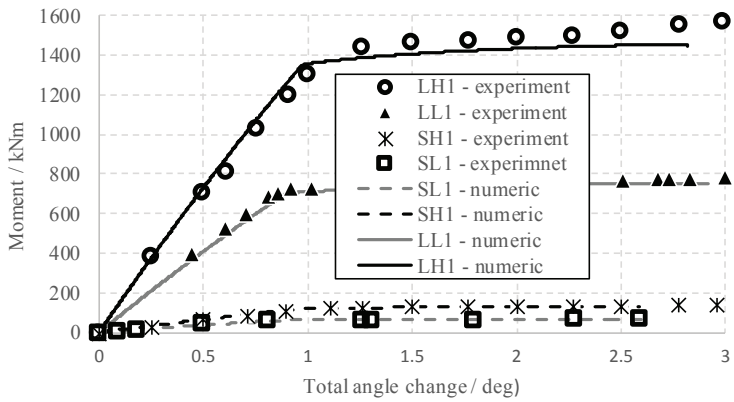

Fig. 18. Comparison of experimental and numerical moment-rotation curves

Sl. 18. Usporedba numeričke i eksperimentalne veze moment-rotacija

For both experimental and numerical results, the bending moment at midspan versus total angle change has been shown. For all beams, the total angle change in both experimental and numerical results has been measured over a length of 3.7*d*. In both cases, good agreement can be seen between the two sets of results. This applies to both bending moments and ultimate rotations.

4. CONCLUSIONS

This paper presents a new robust numerical model for the two-dimensional analysis of beam type structures. The model uses two-noded rotation free finite elements. Detailed information related to axial and bending carrying mechanism has been presented in the paper in brief, together with numerical procedure for the time integration of equation of motion. The proposed algorithms have been implemented into the existing open-source 'Yfdem.' Package, based on a combined finite-discrete element method. The performance of the model has been demonstrated on simple benchmark tests by comparing the results obtained by the proposed numerical model with known analytical, numerical and experimental results available from literature.

Based on the proposed numerical algorithms and presented benchmark tests, concluding remarks can be drawn as follows:

- The model is based on two-noded rotation free finite elements, which enables efficient representation of any arbitrary geometry.
- The model enables the analysis of flat beams and beams with large initial curvature.
- The proposed model takes into account arbitrary non-linear material model, and is also suitable for the analysis of reinforced concrete structures.
- Due to defined local coordinate systems in the initial and current configuration, the proposed numerical model takes into account finite displacements, finite rotations and geometrical non-linearity.
- The main advantage of the presented model lies in the simplicity of its formulation. The presented numerical model requires neither stiffness nor mass matrices to be assembled; this makes it suitable for parallel programming.
- The results obtained by the presented numerical model show good agreement with the analytical, numerical and experimental results available from literature.

Furthermore, the model is easily upgradable for the analysis of three structures and parallel programming, which is yet another advantage of using the FDEM model.

References

[1] Raveendranath P, Gajbir S, Pradhan B. Free vibration of arches using a curved beam element based on a coupled polynomial displacement field. Computers & Structures 2000: 74 (4); 583–590.

[2] Kim JG, Park YK. Hybrid-mixed curved beam elements with increased degrees of freedom for static and vibration analyses. International Journal for Numerical Methods in Engineering 2006: 68; 690–706.

[3] Tang YQ, Zhou ZH, Chan SL. An accurate curved beam element based on trigonometrical mixed polynomial function. International Journal of Structural Stability and Dynamics 2013: 13 (04); 2525–2540.

[4] Pan KQ, Liu JY. Geometric nonlinear dynamic analysis of curved beams using curved beam element. Acta Mechanica Sinica 2011: 27 (6); 1023–1033.

[5] Santos HAFA. A novel updated Lagrangian complementary energy-based formulation for the elastica problem: force-based finite element model. Acta Mechanica 2015: 226 (4); 1133-1151.

[6] Trogrlić B, Mihanović A. The comparative body model in material and geometric nonlinear analysis of space R/C frames. Engineering Computations 2008, 25: 155-171

[7] Phaal R, Calladine CR. A simple class of finite elements for plate and shell problems. I: Elements for beams and thin flat plates. International Journal for Numerical Methods in Engineering 1992: 35 (5); 955–977.

[8] Flores FG, Onate E. Rotation-free element for the non-linear analysis of beams and axisymmetric shells. Computer Methods in Applied Mechanics and Engineering 2006: 195 (41-43); 5297–5315.

[9] Zhou YX, Sze KY. A rotation-free beam element for beam and cable analyses. Finite Elements in Analysis and Design 2013: 64; 79–89.

[10] Smoljanović H, Uzelac I, Trogrlić B, Živaljić N, Munjiza A. A computationally efficient numerical model for a dynamic analysis of beam type structures based on the combined finite-discrete element method. Materialwiss. Werkstofftech 2018: 49; 651–665.

[11] Bangash T, Munjiza A. Experimental validation of a computationally efficient beam element for combined finite-discrete element modelling of structures in distress. Computational Mechanics 2003, 30: 366-373.

[12] Munjiza A. The combined finite-discrete element method. UK: John Wiley & Sons; 2004.

[13] Munjiza A, Knight EE, Rouiger E. Computational Mechanics of Discontinua. UK: John Wiley & Sons; 2012.

[14] Munjiza A, Owen DRJ, Bicanic N. A combined finite-discrete element method in transient dynamics of fracturing solids. Engineering Computations 1995; 12: 145-174.

[15] Munjiza A, Rougier E, Knight EE. Large strain Finite element method a practical course. UK: John Wiley & Sons; 2015.

[16] Alca N, Scott DBA, MacGregor JG. Effect of size on flexural behavior of high strength concrete beams. ACI Structural Journal 1997; 94: 59-67.

Sažetak

U ovom radu prezentiran je novi numerički model za analizu grednih konstrukcija. Model koristi dvočvorne konačne elemente sa translacijskim stupnjevima slobode u svakom čvoru i pri tome uzima u obzir materijalnu nelinearnost, velike pomake, velike rotacije i velike deformacije. Prezentirani numerički model je implementiran u numerički paket 'Yfdem' koji se bazira na kombiniranoj metodi konačnih i diskretnih elemenata. Prednosti novog numeričkog modela demonstrirane su na jednostavnim primjerima usporedbom rezultata s poznatim analitičkim i eksperimentalnim rješenjima iz literature.

Ključne riječi: numerički model, gredne konstrukcije, kombinirana metoda konačnih i diskretnih elemenata

Prof. DSc Ante Mihanović[*]; DSc Hrvoje Smoljanović;
Prof. DSc Boris Trogrlić; Prof. DSc Ante Munjiza[**]

University of Split, Faculty of Civil Engineering, Architecture and Geodesy;
Matice hrvatske 15, 21000 Split, Croatia
[*] član suradnik HAZU, [**] dopisni član HAZU
corresponding author
ante.mihanovic@gradst.hr

UDK / UDC 621:016Bazjanac, D.
DOI: 10.21857/ygjwrcj4xy

Pregledni članak / Review paper
Prihvaćeno / Accepted: 21. 6. 2018.

DAVORIN BAZJANAC – PRIGODOM 75. OBLJETNICE STJECANJA DOKTORATA TEHNIČKIH ZNANOSTI (1943. – 2018.)

Branko Hanžek

Sažetak

U radu je, u skraćenom obliku, prikazan životni put Davorina Bazjanca te je, na temelju sustavnog istraživanja, cjelovito istaknuta njegova stručna publicistička djelatnost. Nakon što je navedeno da je dosada dan popis njegovih 80 objavljenih radova koji su predočili njegovi učenici Stjepan Jecić, Ivo Alfirević i Osman Muftić, taj popis dopunjen je, objavljivanjem prvi put, popisom novih Bazjančevih radova. Navedeni se autori nadopunjuju tako da se iznose nazivi 127 dosad nespominjanih Bazjančevih autorskih bibliografskih referencija.

Ključne riječi: Davorin Bazjanac; životopis; doktorat iz tehničkih znanosti; autorska bibliografija.

1. UVOD

Do sada je o Davorinu Bazjancu pisano u spomenicama iz 1970. [1], 1989. [4] i 1995. [5], leksikonima iz 1983. [3] i 1996. [6], enciklopediji 1999. [7], knjigama 2002. [8] i 2004. [9], ljetopisu [10] i časopisu 1975. [2], a građa o njemu nalazi se i u arhivu [11]. Pravo sustavno istraživanje života s objavljivanjem učinjeno je u knjigama. Tamo su autori akademik Stjepan Jecić, prof. dr. Ivan Heidl, prof. dr. Ivo Alfirević, prof. dr. Osman Muftić i prof. dr. Andrija Mulc nadahnuto i autentično pisali o Bazjančevu životu i radu. Dakle može se pouzdano utvrditi da je njegov životopis potpuno poznat. Drugačije je s njegovom bibliografijom. Ako se želi sveobuhvatno prikazati njegov rad i istaknuti njegova važnost u povijesti znanosti (tehnike), nužno je objaviti i njegove potpune bibliografske podatke. Samo u takvoj potpunoj cjelovitosti moći će se istaknuti njegovo značenje za povijest tehničkih znanosti. Ovim radom učinjen je pokušaj da se naša javnost upozori na veličinu ličnosti Davorina Bazjanca.

Sl. 1. Davorin Bazjanac

2. KRATKI ŽIVOTOPIS

Vidoslav Bazjanac, općinski bilježnik, i njegova supruga Ana rođena Sekulić živjeli su u slavonskom selu Beravci i imali dvoje djece. Prvi im je potomak bila kći Marija, koja se udajom za trgovca Stanka Lakića odselila u Brčko, gdje je sa sinom Dragomirom dočekala starost. Drugi potomak, mlađi sin, Davorin Bazjanac, rođen je 22. rujna 1902. i već sutradan kršten je u Rimokatoličkoj župi sv. Ilije Proroka u Velikoj Kopanici pod imenom Martin Antun. Pučku školu i četiri razreda srednje škole završio je u Slavonskom Brodu. No, životne nedaće nisu ga mimoišle ni kao mladog. Kada mu je bilo 13 godina, umro mu je otac, a 1918. i majka. Za njegovu sestru i njega skrbio je prof. Stanković, koji je radio u maloj gimnaziji u Slavonskom Brodu. Budući da nije bio materijalno osiguran za daljnje školovanje, 1918. godine upisao se u kadetsku školu u Karlovcu, a ispit zrelosti položio je 1921. godine. Nakon dvogodišnjeg studija 1923. godine na Vojnoj akademiji u Beogradu dobiva čin artiljerijskog potporučnika. Slijedi dvogodišnji studij na Mašinskom odsjeku Tehničkog fakulteta u Beogradu i dvogodišnji studij na *Ecol d´ Application d´ Artillerie* u Fontainebleau u Francuskoj. Vraća se 1927. u Kraljevinu SHS i biva upućen na službu u Vojno-tehnički zavod u Kragujevcu, gdje je radio pet godina baveći se podizanjem nove tvornice pješačkog streljiva te rukovodeći izradom alata i balističkim ispitivanjem streljiva. U tom periodu, u više navrata, bio je u Čehoslovačkoj, gdje se upoznavao s tehnologijom proizvodnje oružja i oruđa. Godine

1932. odlazi na studij u Zürich, i to na čuvenu *Eidgenössische technische Hochschule* (ETH), koja je do danas dala 21 nobelovca. Godine 1932. oženio se Slobodom Marinković u Beogradu, a 1938. rodio im se sin Vladimir. Diplomu strojarskog inženjera na ETH dobiva 1935. godine. Pri kraju njegova studija na ETH gradio se u Zürichu novi laboratorij za aerodinamička ispitivanja sa zračnim tunelom i kanalom za supersoničko ispitivanja. Ponuđeno mu je da radi u tom laboratoriju, ali došlo je do zastoja u izgradnji supersoničkog kanala. Ipak, eksperimentalna ispitivanja izvršena su u zračnom tunelu 1936. godine. Ta su ispitivanja bila zamišljena kao eksperimentalni dio njegove disertacije. Godine 1936. vratio se u Beograd i do 1938. radio je u Ministarstvu vojske (podizanje novih tvornica ratne industrije). U međuvremenu je, 1937. godine, položio majorski ispit s temom autofretaže topovskih cijevi. Godine 1937./38. Bazjanac je u Beogradu na Vojnoj akademiji predavao predmet Nauka o oružju i balistika. Godine 1938. opet odlazi u Zürich da bi konačno utvrdio tekst svoje disertacije i položio usmeni doktorski ispit. Ipak, zbog rata, sve je odgođeno. U razdoblju 1939. – 1941. radio je na proizvodnji streljiva u Kragujevcu. Rat ga je zatekao na službenoj dužnosti kraj Beča te je sredinom 1941. zajedno s diplomatskim osobljem otpremljen u Beograd. Bio je bez posla do kraja 1941., kada je došao u Zagreb, gdje je poslan u zapovjedništvo zračnih snaga kao šef oružanog odjela. U Zagrebu mu je omogućeno da radi kao znanstvenik. Bio je pošteđen ratnih zbivanja na fronti i službovanja u vojarnama. Čak mu je omogućeno da ode u Švicarsku i okonča postupak postignuća doktorata tehničkih znanosti. Tamo je konačno utvrdio tekst svoje disertacije (mentor: prof. dr. J. Ackeret, komentor: prof. dr. H. Ziegler) pod naslovom: *Untersuchungen mit Hilfe der elektrischen Analogie über den Einfluss der Luftstrahlbegrenzung in Windkanälen auf Tragflügelmessungen (Istraživanje utjecaja oblika presjeka zračne struje u zračnim tunelima na mjerenja na aeroprofilima)* i položio doktorski ispit, a promoviran je 7. prosinca 1943. za doktora tehničkih znanosti.

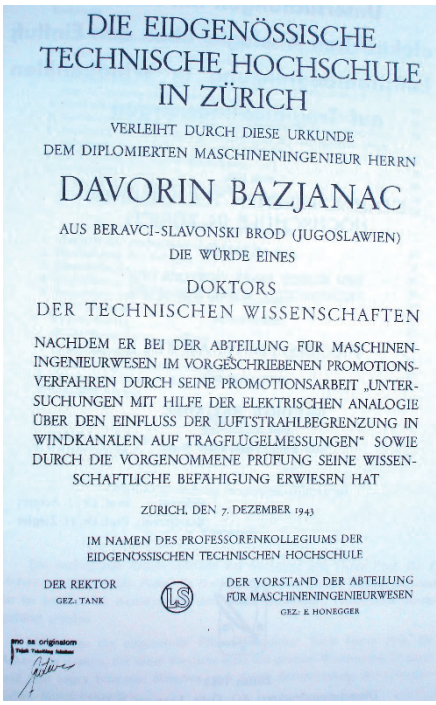

DIE EIDGENÖSSISCHE
TECHNISCHE HOCHSCHULE
IN ZÜRICH

VERLEIHT DURCH DIESE URKUNDE
DEM DIPLOMIERTEN MASCHINENINGENIEUR HERRN

DAVORIN BAZJANAC

AUS BERAVCI-SLAVONSKI BROD (JUGOSLAWIEN)
DIE WÜRDE EINES

DOKTORS
DER TECHNISCHEN WISSENSCHAFTEN

NACHDEM ER BEI DER ABTEILUNG FÜR MASCHINENINGENIEURWESEN IM VORGESCHRIEBENEN PROMOTIONSVERFAHREN DURCH SEINE PROMOTIONSARBEIT „UNTERSUCHUNGEN MIT HILFE DER ELEKTRISCHEN ANALOGIE ÜBER DEN EINFLUSS DER LUFTSTRAHLBEGRENZUNG IN WINDKANÄLEN AUF TRAGFLÜGELMESSUNGEN" SOWIE DURCH DIE VORGENOMMENE PRÜFUNG SEINE WISSENSCHAFTLICHE BEFÄHIGUNG ERWIESEN HAT

ZÜRICH, DEN 7. DEZEMBER 1943

IM NAMEN DES PROFESSORENKOLLEGIUMS DER
EIDGENÖSSISCHEN TECHNISCHEN HOCHSCHULE

DER REKTOR
GEZ.: TANK

DER VORSTAND DER ABTEILUNG
FÜR MASCHINENINGENIEURWESEN
GEZ.: E. HONEGGER

Sl. 2. Diploma Davorina Bazjanca o stjecanju doktorata tehničkih znanosti

Fig. 2 Davorin Bazjanac's doctoral diploma in the field of technical sciences

U disertacijskom je radu teorijski i eksperimentalno obrađen utjecaj što ga ograničenost ulaza zračne struje u zračnom tunelu ima na rezultate mjerenja, i to pomoću reoelektrične analogije po metodi Pérès-Malavard. Ta se analogija zasniva na analogiji diferencijalnih jednadžbi električnog strujnog polja i aerodinamičkog polja s obzirom na to da oba polja zadovoljavaju Laplaceovu diferencijalnu jednadžbu. Ta ispitivanja služila su za ocjenu korekcije izvedenog velikog strujnog kanala u zračnom tunelu aerodinamičkog instituta u Zürichu. Nakon kraja Drugoga svjetskog rata Bazjanac je upućen na rad u Srednju tehničku školu u Zagrebu, da bi 15. veljače 1946. bio izabran za honorarnog nastavnika mehanike na Tehničkom fakultetu Sveučilišta u Zagrebu. Predavao je slušačima strojarskog, elektrotehničkog i brodarskog odsjeka. Dana 30. lipnja 1948. postavljen je za izvanrednog profesora mehanike, a za redovnog profesora mehanike i nauke o čvrstoći izabran je 1954. na Tehničkom fakultetu u Zagrebu. Sve do odlaska u mirovinu 31. kolovoza 1973. predavao je profesor Bazjanac na više tehničkih studija. Kao nastavnik i znanstvenik nastojao je nastavu podignuti na potrebnu znanstvenu razinu. Od samih početaka oslanjao se na nastavna pomagala te je izdavao skripta, zbirke zadataka i kasnije udžbenike. Profesor Bazjanac bio je prodekan Tehničkog fakulteta godine 1948./49. te dekan i prodekan Strojarsko-brodograđevnog fakulteta (1958. – 1960.). Također je bio voditelj ili član komisije za ocjenu i obranu 12 disertacija i 10 magistarskih radova. Surađivao je i dugi niz godina s JAZU, najprije 1953. – 1955. godine. Godine 1973. kao član savjetodavnog odbora Centra za numerička istraživanja JAZU imenovan je za predstavnika Razreda za matematičke, fizičke i tehničke nauke u Međuakademijski odbor za astronautiku, zajedno s izvanrednim članom JAZU Vladimirom Matkovićem. Bio je i član niza stručnih društava (Društvo matematičara i fizičara NRH, Hrvatsko prirodoslovno društvo, Društvo inženjera i tehničara, Aerokozmonautičko društvo) te glavni osnivač Društva za mehaniku Hrvatske i dopisni član Međunarodne astronautičke akademije u Parizu. Za svoje požrtvovno djelovanje dobio je priznanja, među kojima se kao važnija ističu: Orden rada II. reda, Orden rada sa crvenom zastavom, Republička nagrada za životno djelo i Republička nagrada *Fran Tučan* za popularizaciju znanosti. Pred sam kraj, a ne manje važno, treba spomenuti da je Bazjanac govorio, čitao i pisao češki, ruski, francuski, engleski i njemački, a poznavao je i talijansku i poljsku stručnu terminologiju. Tako eminentna osoba koja je iza sebe ostavila mnoštvo zadovoljnih studenata i suradnika napustila nas je 1988. godine, u noći između 20. i 21. rujna, u Zagrebu. Kako bi se ovjekovječilo ime tog nadasve zaslužnog čovjeka, ustanovljena je 1995. godine Nagrada Fakulteta strojarstva i brodogradnje *Davorin Bazjanac* koja se dodjeljuje studentima za uspješnost u studiju. Nagrada se dodjeljivala u obliku pismenog priznanja za uzorni uspjeh i kao Dekanova nagrada iz redova dobitnika Nagrade *Davorin Bazjanac*. Te su

se nagrade sastojale od pismenog priznanja i novčane nagrade prema odluci dekana. Te 1995. godine uručena je i Nagrada *Davorin Bazjanac* i Dekanska nagrada. Prema važećem Pravilniku o dodjeli medalja, nagrada i priznanja (pročišćeni tekst), Zagreb, 2011., za Fakultet strojarstva i brodogradnje na Sveučilištu u Zagrebu [13], u čl. 16. navedeno je da se Nagrada *Davorin Bazjanac* dodjeljuje studentima prvih triju godina preddiplomskog studija za izvrsnost u studiranju u prethodnoj akademskoj godini. Osnovni su kriteriji: prosjek ocjena za prethodnu akademsku godinu veći od 4,20 i stečeno najmanje 60 ECTS bodova tijekom prethodne akademske godine, a dodatni su kriteriji: posebna dostignuća u promicanju ugleda Fakulteta, prosjek ocjena tijekom studiranja veći od 4,00, ukupno trajanje studija. Člankom 17. tog pravilnika uređeno je da se spomenuta nagrada sastoji od pisanog priznanja i novčanog dijela.

3. BIBLIOGRAFIJA DAVORINA BAZJANCA

Na više mjesta može se naći nepotpun popis bibliografskih jedinica Bavorina Bazjanca. Taj nepotpuni popis sastavili su njegovi učenici. U knjizi [8] prof. dr. Ivo Alfirević izrijekom je naveo 25 udžbenika, skripata i drugih publikacija, a podaci u ovom radu preuzeti su od njega. Prof. dr. Osman Muftić u spomenutoj je knjizi izrijekom precizirao 47 astronautičko-zrakoplovnih bibliografskih jedinica koje su također preuzete. Akademik Jecić u istoj je knjizi izrijekom upozorio na 8 objavljenih bibliogafskih jedinica koje se odnose na Davorina Bazjanca, što je također preuzeto. Sveukupno je preuzeto 80 autorsko-bibliografskih jedinica. Ostalih 127 bibliografskih jedinica dosad je bilo nepoznato javnosti, a do podataka o njima došlo se u oba arhiva [11] i [12] kao i u časopisu *Bilten dokumentacija inostrane stručne literature* [14], kasnije *Bilten dokumentacija stručne literature* [15].

Sl. 3. Naslovnica časopisa *Bilten dokumentacija inostrane stručne literature*

Fig. 3 Cover of the journal *Bulletin; list of Bazjanac's 207 bibliographic units*

Te ostale bibliografske jedinice prvi se put sada objelodanjuju. Ukratko: u ovom radu dan je cjelovit popis 207 Bazjančevih bibliografskih jedinica.

Udžbenici i skripta

1. Tehnička mehanika I, 1946. (skripta, 230 str.)
2. Zadaci iz mehanike, 1947.
3. Predavanja iz teorijske mehanike, II dio (Dinamika), 1948. (udžbenik preveden s ruskog „Nikolai, Lekcii po teoretičeskoj mehanike“, 300 str.)
4. Zbirka zadataka iz mehanike I (Statika), 1951. (skripta, 254 str.)
5. Zbirka zadataka iz mehanike IIb (Dinamika), 1952. (skripta, 366 str.)
6. Zbirka zadataka iz mehanike IIa (Kinematika), 1952. (skripta, 243, str.)
7. Tehnička mehanika V (Teorija oscilacija), 1953. (skripta, 270 str.)
8. Osnovi teorije mehanizama, I. dio, 1954., Tehnička knjiga (udžbenik, 211 str.)
9. Statika, 1958. (udžbenik, 376 str.)
10. Zbirka zadataka iz tehničke mehanike I (Statika), 1958.
11. Zbirka zadataka iz tehničke mehanike II (Kinematika), 1958.
12. Tehnička mehanika 1. dio, Statika, Tehnička knjiga, 1959.
13. Zbirka zadataka iz Statike, 1960., 4. prerađjeno i dopunjeno izdanje (skripta), 337 str.
14. Zbirka zadataka iz Kinematike, 1961., 2. prerađeno i dopunjeno izdanje (skripta), 247 str.
15. Zbirka zadataka iz Dinamike, 1963., 4. preradjeno i dopunjeno izdanje (skripta), 297 str.
16. Tehnička mehanika V (Teorija oscilacija), 1963., 2. izdanje (skripta), 270 str.
17. Osnovi teorije mehanizama,I. dio, 1963., 2. izdanje (udžbenik), Sveučilište u Zagrebu, 211 str.
18. Tehnička mehanika 1. dio, Statika, 1963., 2. prerađeno i dopunjeno izdanje (udžbenik, 398 str.)
19. Nauka o čvrstoći I, 1963. (skripta, 273 str.)
20. Nauka o čvrstoći II, 1963. (skripta, 272 str.)
21. Tehnička mehanika dio II, 1963.
22. Tehnička mehanika dio III, 1963.
23. Kinematika, 1966. (skripta, 242 str.)
24. Tehnička mehanika 1. dio, Statika, 1966., 3. izdanje (udžbenik), 398 str.
25. Nauka o čvrstoći, 1968., udžbenik, 758 str.
26. Tehnička mehanika 2. dio, Kinematika, 1969., udžbenik, Tehnička knjiga, 254 str.
27. Tehnička mehanika 1. dio, Statika, 1970., 4. dopunjeno izdanje (udžbenik), 431 str.
28. Osnovi teorije mehanizama, 1971., 3. izdanje (udžbenik), 211 str.
29. Zbirka zadataka iz Nauke o čvrstoći I, 1970. (skripta), 382 str.

30. Zbirka zadataka iz Statike, 1971., 5. prerađeno i dopunjeno izdanje (skripta), 431 str.
31. Zbirka zadataka iz Nauke o čvrstoći II, 1972., (skripta), 362 str.
32. Nauka o čvrstoći, udžbenik, 2. popravljeno izdanje, 1973., 758 str.
33. Tehnička mehanika, III dio (Dinamika), 1974., udžbenik, Sveučilište u Zagrebu, 530 str.
34. Tehnička mehanika 2. dio, Kinematika, 2. izdanje, 1977., Tehnička knjiga.
35. Zbirka zadataka iz Kinematike, 1980., 4. popravljeno izdanje (skripta)
36. Tehnička mehanika, III dio (Dinamika), 1980., udžbenik, 2. izdanje.

U izdanju Školske knjige, Zagreb:

37. Svemirski letovi, Biblioteka Obzor, Zagreb, 1970. (283 str.)

U izdanju Hrvatskog prirodoslovnog društva:

38. Suvremena astronautička istraživanja svemira, Mala knjižnica HPD, Zagreb, 1979., 80 str.

Znanstveno-popularne publikacije

1) Od Ikara do mlaznog aviona, 1958., Mala naučna knjižnica Hrvatskog prirodoslovnog društva, sv. 5, 32, str. 1958
2) Legenda o letećim tanjurima, 1958., Mala naučna knjižnica, HPD, sv. 6, 34 str.
3) Od vatrometne rakete do svemirskog broda, Mala naučna knjižnica HPD, sv. 7, str. 38
4) Zvučna barijera i suvremena avijacija, Mala naučna knjižnica HPD, sv. 8, str. 40
5) Raketa u službi nauke i tehnike, Popularno-tehnička knjižnica (Gradski odbor Narodne tehnike), br. 2, 1961. (str. 40)
6) Astronautika, Popularno-tehnička knjižnica, br. 3, 1961.

Napomena: Sve navedene publikacije objavio je pod pseudonimom „D. Vidoslavić“

Tekst i ilustracije za dokumentarne filmove:

1) Zemljini umjetni sateliti, 1958 (u izdanju Zora-filma – Zagreb)
2) Svjetska izložba u Bruxellesu, 1958 (u izdanju Zora-filma Zagreb)

Radovi i izvještaji

Tiskana disertacija:

1. Untersuchungen mit Hilfe der elektrischen Analogie über den Einfluss der Luftstrahlbegrenzung in Windkanälen auf Tragflügelmessungen, Zürich, 1943. (70 str.)
2. Analiza proračuna torzionih vibracija za sistem: Dieselmotor-trofazni generator, 1953., 136 str., naučno-istraživački rad izradjen i umnožen za potrebe generalne direkcije brodskih strojeva.
3. Primjena metode reoelektrične analogije za odredjivanje naprezanja u vratilima promjenljivog presjeka, Elektrotehnika, broj 3, 1965. (naučno-istraživački rad subvencioniran od strane Saveznog fonda za naučni rad). Koautor M. Kolaj, str. 211-242.
4. Bošković i suvremena fizika (prijevod s ruskog „Kuznecov, Boškovič i sovremennaja fizika"), Rasprave i gradja za povijest nauka JAZU, knjiga I, 1963., str. 158-161.
5. Uloga mehanike u suvremenim istraživanjima svemira, Uvodna konferencija na IX Jugoslavenskom kongresu racionalne i primjenjene mehanike u Splitu (1968). Objavljeno u Zborniku radova Jugoslavenskog kongresa za mehaniku, str. 1-15, i u Zborniku radova Fakulteta strojarstva i brodogradnje, 1970., str. 9-22.
6. O nekim problemima dinamike višestepenih raketa i svemirskih brodova pri ulaženju u atmosferu". Uvodna konferencija na X jubilarnom kongresu za mehaniku u Baškom Polju (1970). Objavljeno u Zborniku radova II Fakulteta strojarstva i brodogradnje, 1972., str. 89-106.
7. Eksperimentalno odredjivanje vibracija pogonskih sistema s pomoću električnih metoda, Strojarstvo, broj 12, 1970., str. 65-70 (naučno-istraživački rad subvencioniran od strane Saveznog fonda za naučni rad, koautori M. Kolaj i A. Vučetić).
8. O suvremenom razvoju raketodinamike i kozmičke balistike.
   Uvodna konferencija na XI Jugoslavenskom kongresu racionalne i primjenjene mehanike u Baškom Polju (1972). Skraćeni sadržaj te konferencije objavljen je u časopisu „Tehnika", Opšti deo, broj 9/1972, str. 193-198.
9. Ispitivanja dinamičkih naprezanja željezničkog kolosijeka.
   Naučno-istraživački rad subvencioniran od strane Republičkog fonda za naučni rad SRH uz vlastito učešće Fakulteta strojarstva i brodogradnje u Zagrebu. Nosilac zadatka: Prof. dr D. Bazjanac. Suradjivali su: prof. A. Vučetić i docenti S. Jecić, O. Muftić, I. Alfirević i I. Heidl. Zbornik radova II Fakulteta strojarstva i brodogradnje, 1970.
10. Eksperimentalna analiza naprezanja u anizotropnim materijalima s pomoću metode fotoelastične obloge. Timski naučno-istraživački rad subvencioniran od strane Republičkog fonda za naučni rad SRH. Nosilac zadatka: prof. dr. Davorin Bazjanac, Sudjelovali su: prof. A. Vučetić i docenti I. Alfirević, I. Heidl, S. Jecić i O. Muftić.

11. Električni giroagregat i njegova primjena za vuču vozila, „Elektrotehnika“, broj 2, 1959.
12. Izvještaj o učešću na Smotri britanskog zrakoplovstva u Farnboroughu, Ljetopis JAZU, knjiga 60, str. 256-266 (1955).
13. Izvještaj o studijskom boravku u inozemstvu radi upoznavanja novih metoda rada u institutima za ispitivanje materijala, Ljetopis JAZU, knjiga 61, str. 293-303 (1956).
14. Izvještaj o studijskom boravku u inozemstvu, Ljetopis JAZU, knjiga 62, str. 249-252 (1957).
15. Ženevska konvencija za primjenu nuklearne enargije u miroljubljive svrhe, Ljetopis JAZU, knjiga 62, str. 253-259 (1957).
16. Uloga naučnih i tehničkih kadrova u suvremenom tehničkom razvoju, Sveučilišni vjesnik, vol. II broj 1-2, 1956.
17. Glavni problemi astronautike, Mornarički glasnik, broj 2, 1957., str. 43-56
18. Umjetni sateliti i prodor u svemir, Časopis „Narodno sveučilište“ broj 3-4, 1957., str. 206-215.
19. Girotron novi tip giroskopa, Tehničke novine, broj 14, 15.7.1958.
20. Glavni problemi odašiljanja rakete na Mjesec, Tehničke novine, broj 12, 1958.
21. Medjunarodni astronautički kongres u Barceloni, Almanah Bošković, 1958., str. 139-152.
22. Medjunarodni astronautički kongres u Amsterdamu, Almanah Bošković, 1959. – 1960., str. 225-234.
23. Medjunarodni astronautički kongresi u Londonu (1959) i u Stockholmu (1960), Almanah Bošković, 1961. – 1962., str. 237-253.
24. Medjunarodni astronautički kongresi u Washingtonu (1961) i u Varni (1962), Almanah Bošković, 1963., str. 197-204.
25. Uloga astronautike u istraživanju svemira, Polet, broj 3, 1960.
26. Uloga astronautike u daljnjem razvoju nauke i tehnike, Nauka i društvo, broj 10, 1964. (Bilten Saveza inženjera i tehničara Hrvatske), str. 24-27.
27. Auguste Picard – istraživač stratosfere i morskih dubina, Industrijski radnik, 1963., broj 164, str. 6.
28. Prekretnica u civilnom zračnom saobraćaju, Industrijski radnik, 1964.
29. Zvučna barijera u suvremenoj avijaciji, Industrijski radnik, 1.VIII.1957., str. 10
30. Antigravitaciono letalo, Industrijski radnik, 1964.
31. Ukroćivanje termonuklearne reakcije – najvažniji naučni problem svih vremena, Industrijski radnik, broj 121, 1958., str. 4.
32. O ulozi raketne tehnike u suvremenim istraživanjima svemira, Zbornik radova I Jugoslavenskog aerokozmonautičkog kongresa, Beograd, 1973., str. 1-20.

33. Astronautika i znanstveno-tehnički napredak, Zbornik radova Simpozija prirodnih znanosti Hrvatskog prirodoslovnog društva, Zagreb, 1975., str. 45-47.
34. Razvoj satelitske tehnike, Zbornik radova Seminara „Sateliti – pomoć iz svemira“, Savez astronautičkih i raketnih organizacija Jugoslavije, Zagreb, 1977., str. 21-44.

Radovi u časopisu *Strojarstvo*

1. Eksperimentalne metode odredjivanja torzionih naprezanja, broj 9-10, 1964., str. 2-10 (naučno-istraživački rad subvencioniran od strane Saveznog fonda za naučni rad).
2. Medjunarodna izložba zrakoplovne i svemirske tehnike u Le Bourgetu, broj 9-10, 1967.
3. Utisci s XVIII medjunarodnog astronautičkog kongresa u Beogradu, broj 1-2, 1968.
4. X Jugoslavenski kongres racionalne i primjenjene mehanike, broj 7-8, 1970.
5. XI Jugoslavenski kongres za mehaniku, 1971., broj 9-12, str. 170.
6. Prikaz predavanja akademika W. Olzaka u JAZU o temi „Problemi neelastičnih ljusaka“, broj 7-8, 1970.
7. III Svjetski kongres za teoriju strojeva i mehanizama, broj 9-12, 1971., str. 170-171.
8. Simpozij o mehanici kontinuuma i srodnim problemima analize u Tbilisiju, broj 9-12, 1971., str. 171
9. In memoriam prof. dr inž. Konstantinu Čališevu, broj 9-12, 1970.
10. In memoriam prof. dr Stjepanu Timošenku, broj 4-6, 1972.
11. Prijevod s ruskog konferencije akademika I. I. Artobolevskog „Neki aktualni problemi suvremene teorije strojeva i mehanizama“, broj 4-6, 1972.
12. XIII Medjunarodni kongres za teorijsku i primjenjenu mehaniku, broj 1-2, 1973.
13. Rezultati XI Jugoslavenskog kongresa teorijske i primjenjene mehanike, broj 1-2, 1973.
14. Jugoslavenski simpozij: Mašine i mehanizmi, br. 3-4, 1973.
15. XII Jugoslavenski kongres racionalne i primjenjene mehanike, br. 5-6, 1973.
16. XXIV kongres Medjunarodne astronautičke federacije u Baku-u, broj 1/2, 1974.
17. Simpozij „Teorija i praksa brodogradnje“, 1974., 1-2, str. 61.
18. In memoriam prof. Dušanu Vitasu, broj 1, 1976.

Radovi u časopisu *Priroda*

1) Postanak i razvitak astronautike 1954., br. 5., str. 166-173.
2) O mogućnostima odašiljanja rakete na Mjesec, 1959., br. 1., str. 1-4.

3) O zakonitostima gibanja kozmičkih raketa, 1959., br. 9, str. 321-324; 1971., br. 10., str. 306-307.
4) Astronautika u 1960. godini, 1961., br. 3., str. 65-67 i str. 71.
5) Program istraživanja svemira u SSSR, br. 4/1961, str. 109-111.
6) Uloga nauke i tehnike u istraživanju svemira 1962., br. 5., str. 129-130.
7) O letu prvog američkog kozmonauta oko Zemlje 1962., br. 5., str. 144-147.
8) Susret u svemiru 1962., br. 9., str. 257-259.
9) Uloga astronautike u daljnjem razvoju nauke i tehnike, 1964., br. 5., str. 138-140.
10) Astronautika u 1964, br. 1, 1965., str. 1-4.
11) O najnovijim naučnim i tehničkim dostignućima astronautike, 1965., br. 9, str. 245-249.
12) Astronautika u 1965, br. 2, 1966., str. 42-44.
13) Keplerov „san“ o letu čovjeka na Mjesec, br. 2, 1966., str. 48.
14) Astronautika u 1966, br. 6, 1967., str. 161-164.
15) Istraživanja svemira u 1967., 1968., br. 5, str. 136-138.
16) Prvi umjetni Mjesečevi sateliti, 1968., br. 6., str. 166-169
17) O prvom letu čovjeka oko Mjeseca, 1969., br. 5, str. 140-144
18) Prvi ljudi na Mjesecu 1969., br. 9., str. 257-261
19) Let „Apolla 10“ oko Mjeseca, 1969., br. 9., str. 281-282
20) Istraživanja svemira u godini 1969., br. 5, 1970., str. 129 – 134
21) Istraživanja svemira u 1970. godini, br. 1, 1971., str. 1-3.
22) Istraživanje svemira u godini 1971., 1972., br. 5., str. 129-133.
23) Istraživanje svemira u godini 1972., 1973., br. 10., str. 289-292.
24) Istraživanje svemira u godini 1974., 1975., br. 6., str. 165-167.

Radovi u *Matematičko-fizičkom listu*

1. Raketa i ideja o letu u svemir, broj 1, 1956./57.
2. Raketa u službi nauke, broj 2, 1956./57.
3. Prvi umjetni Zemljini sateliti, broj 2, 1957./58.
4. O gibanju kozmičkih raketa, broj 2, 1959./60.
5. Prvi umjetni Mjesečevi sateliti, broj 1, 1967./68.
6 Prvi čovjekov let oko Mjeseca, broj 3, 1968./69.
7 Prvi ljudi na Mjesecu, broj 1, 1969./70., str. 5-11.
8. Druga čovjekova ekspedicija na Mjesec, broj 2, 1969./70, str. 49-51.

Radovi u časopisu *Savremena tehnika*

1. Mehanički i akustički afekti pri probijanju „zvučnog zida“ 1955., br. 8-9, str. 330-331.
2. Akustički efekti zvučne barijere, br. 1, 1956.
3. Girobus, br. 3, 1960.
4. O utjecaju astronautike na razvitak nauke i tehnike, str. 121-126, 1956.

Radovi u *Biltenu dokumentacija inostrane stručne literature*

1) Berman I. R.: Optjecanje okruglog cilindra s odvajanjem struje u ograničenom strujnom toku, 1950., br. 6-7-8, str. 489.
2) Ovsjannikov, L. L.: O strujanju plina s pravom prelaznom linijom 1950., br. 6-7-8, str. 490.
3) Pisarenko G. S.: Primjena metode nelinearne mehanike na problem disipacije energije u materijalu pri vibracijama 1950., br. 6-7-8, str. 495-496.
4) Lojcjanskij L. G.: Približna metoda integriranja jednadžbi laminarnog graničnog sloja u nestlačivom plinu 1950., br. 9-10, str. 9-10.
5) Lojcjanskij L. G.: Profilni otpor rešetke pri strujanju plina do kritičkih brzina 1950. br. 9-10, str. 12-13.
6) Geronimus, J. L.: Djelovanje sudara na slobodno tvrdo tijelo 1950., br. 11-12, str. 694.
7) Malkin, I. G.: Prilog teoriji oscilacija kvazilinearnih sistema s mnogim stepenima slobode 1950., br. 11-12, str. 698-699.
8) Mitropoljski J. A.: Polagani procesi kod nelinearnih oscilatornih sistema s mnogim stepenima slobode, 1950., br. 11-12, str. 699.
9) Butenin N. V.: Prilog teoriji prisilnih oscilacija u nelinearnom mehaničkom sistemu s dva stepena slobode 1950., br. 11-12, str. 699-700.
10) Malkin, I. G.: Oscilacije kvazilinearnih sistema s neanalitčnom karakteristikom nelinearnosti 1950., br. 11-12, str. 700.
11) Samojlovič, G. S.: Proračun hidrodinamičkih rešetaka 1951., br. 1, str. 4.
12) Rožanskij V. N: Prilog teoriji sklerometra na principu njihala 1951., br. 1, str. 23-24.
13) Abramjan, B. L.: Uvijanje i savijanje šupljih prizmatičnih štapova pravokutnog presjeka 1951., br. 2, str. 89.
14) Kočetkov, A. M.: O rasprostiranju elastično-viskozno-plastičnih valova smicanja u ploči 1951., br. 2, str. 89.
15) Zverev, I. N.: Rasprostriranje poremećaja u viskozno-elastičnom i viskozno-plastičnom štapu 1951., br. 2, str. 97.

16) Kajdanovskij, N. L.: Priroda mehaničkih autooscilacija, koje nastaju pri suhom trenju 1951., br. 2, str. 98.
17) Pruškov, B. T.: Količina topline rezanja koja se odvodi alatnim nožem 1951., br. 2, str. 134.
18) Sretenskij, L. N.: O prstenastim valovima na površini rotirajuće tekućine 1951., br. 7, str. 10.
19) Djačkov A. K.: Prilog problemu forsiranja kliznih ležaja 1951., br. 7, str. 26.
20) Čarnyj, I. A.: Dinamički proračun klipnjača dubokih naftnih pumpi s uračunavanjem sila trenja o cijevi pumpe 1951., br. 7, str. 36.
21) Popov, S. M.: O cilindrom obliku krivulje gubitka stabilnosti ploča iznad granice elastičnosti 1951., br. 7, str. 43-44.
22) Mežlumjan, R. A.: Granični uvjeti pri savijanju i uvijanju tankih ljusaka iznad granice elastičnosti 1951., br. 7, str. 44.
23) Muštari, H. M.: Kvalitativno istraživanje napregnutog stanja elastične ljuske pri malim deformacijama i proizvoljnim pomacima 1951., br. 7, str. 44.
24) Prokopov, V. K.: Ravnoteža elastičnog radijalnog-simetrično opterećenog šupljeg valjka debelih zidova, 1951., br. 7, str. 44

Radovi u *Biltenu dokumentacija stručne literature*

1) Erugin N. P.: O nekim problemima stabilnosti gibanja i kvalitativnoj teoriji diferencijalnih jednadžbi u cijelosti 1951., br. 8, str. 2.
2) Bulgakov B. V.: Diskriminantna krivulja i područja aperiodične stabilnosti 1951., br. 8, str. 4.
3) Sokolovskij, V. V.: Ravnoteža plastičnog klina u ravnini 1952., br. 1, str. 6.
4) Šimanov, C. N.: Prilog teoriji kvaziharmonijskih oscilacija 1952., br. 12, str. 14-15.
5) Moskovitin, V. V.: O sekundarnim plastičnim deformacijama 1952., br. 12, str. 24.
6) Šapiro, G. S.: Rasprostiranje elastično-plastičnih valova u osovinama promenljivog presjeka 1952., br. 12, str. 35.
7) Iljušin, A. A.: Proučavanje brzih procesa obrade užarenih metala pritiskom pomoću modela 1953., br. 1, str. 152.
8) Mihlin, S. G.: Veličina greške pri proračunu klasične ljuske kao ravne ploče 1953., br. 3, str. 8.
9) Panferov, V. M.: O konvergentnosti metode elastičnih rješenja pri rješavanju problema elastično-plastičnog savijanja ploča 1953., br. 3, str. 8.
10) Darevskij, V. M.: Rješenje nekih problema teorije cilindrične ljuske 1953., br. 4, str. 4.

11) Bejlin, K. A. i Džane Llidze, G. J.: Pregled radova o dinamičkoj stabilnosti elastičnih sistema 1953., br. 6, str. 5.
12) Kufarev, P. P.: O opterećenju kružnog luka 1953., br. 6, str. 5.
13) Kitover, K. A.: O primjeni specijalnih sistema biharmonijskih funkcija za rješavanje nekih problema teorije elastičnosti 1953., br. 7, str. 3.
14) Krejn, M. C.: O nekim novim problemima teorije oscilacije komandnih sistema 1953., br. 7, str. 5.
15) Kalandija, A. I.: Opći mješoviti problem savijanja elastične ploče 1953., br. 7, str. 8.
16) Hemmerling, E.: Mehaničko naprezanje cjevovoda za visoki parni pritisak 1953., br. 12, str. 33.
17) Sass, F.: Koljena od lijevanog čelika za osovine velikih diesel motora 1953., br. 12, str. 38.
18) Niemann, G.: Frikcioni mehanizmi. Svrsishodna primjena, oblikovanje i dimenzioniranje frikcionskih regulatorskih i drugih sličnih mehanizama 1953., br. 12, str. 40.
19) Langen, K.: Kut prenosa kod mehanizma kao tolerancija gibanja 1954., br. 2, str. 8.
20) Ertl, H.: Analiza duvaljke tipa „Roots“ 1954., br. 2, str. 37.
21) Pogonski elementi (Antriebselemente) 1954., br. 2, str. 40.
22) Amedick, E.: Ponašanje vijaka pri naizmjeničnom opterećenju 1954., br. 2, str. 42.
23) Schwaben, R. i Umstaten, H.: Prilog konstrukciji rotacionih viskozimetra 1954., br. 3, str. 2.
24) Lohmann, G.: Istraživanja o šumu valjkastih ležajeva (kraj) 1954., br. 3, str. 3.
25) Harz, G.: Jednostavan grafički postupak za određivanje obrtnog momenta kod četirizglobnih mehanizama 1954., br. 3, str. 6.
26) Simonis, F. V.: Mjenjačka kutija na principu oscilirajućeg momenta 1954., br. 3, str. 6-7.
27) Wunsch, G.: Funkcionalni studij prije konstruiranja, objašnjen na primjerima iz gradnje parnih kotlova 1954., br. 5, str. 7.
28) Niermeyer, H.: Dijagram naprezanja i proračun spojeva s prirubnicom 1954., br. 5, str. 38.
29) Witte, F. R.: Zavareni kotlovi kod parnih lokomotiva Njemačkih saveznih željeznica 1954., br. 6, str. 67.
30) Hausenblas, H.: Plinska turbina za pogon automobila 1954,. br. 6, str. 34.
31) Anders, H.: O pumpama za isisavanje para pod smanjenim pritiskom s pogledom na efikasne vakuumske uređaje 1954., br. 7, str. 45.
32) Hain, K.: Proračun zupčanih sistema izvedenih iz četverozglobnog kinematičkog lanca pomoću homolognih kutova 1954., br. 8, str. 60.

Članci i natuknice u enciklopedijama

1. Astronautika, Tehnička enciklopedija, sv. 1, str. 428-437, Zagreb, 1963.
2. Balistika, Tehnička enciklopedija, sv. 1, str. 672-684, Zagreb, 1963.
3. Balistički projektili, Tehnička enciklopedija, sv. 1, str. 670-672, Zagreb, 1963.
4. Astronautika, Enciklopedija fizičke kulture, str. 58-62.
5. Raketa, Enciklopedija Leksikografskog zavoda, 1. izdanje, sv. 6, str. 334-339, Zagreb, 1962.
6. Satelit, umjetni Zemljin, Enciklopedija Leksikografskog zavoda, 1. izdanje, sv. 6, str 622-629, Zagreb, 1962.
7. Rakete, Enciklopedija „Svijet oko nas“, 1963.
8. Svemirski letovi, Enciklopedija „Svijet oko nas“, 1963.
9. Raketa, Enciklopedija Leksikografskog zavoda, 2. izdanje, sv. 5, str. 377-382, Zagreb, 1969.
10. Satelit, umjetni Zemljin, Enciklopedija Leksikografskog zavoda, 2. izdanje, sv. 5, str. 623-631, Zagreb, 1969.
11. Telekomunikacijski sateliti, Enciklopedija Leksikografskog zavoda, 2. izdanje, sv. 6, str. 352-353, Zagreb, 1969.
12. Raketa, Opća enciklopedija Jugoslavenskog leksikografskog zavoda, sv. 6, str. 743-746, Zagreb, 1980.
13. Satelit, umjetni, Opća enciklopedija Jugoslavenskog leksikografskog zavoda, sv. 7, str. 295-299, Zagreb, 1981.
14. Telekomunikacijski sateliti, Opća enciklopedija Jugoslavenskog leksikografskog zavoda, sv. 8, str. 162-163, Zagreb, 1982.
15. Mehanika (Statika), Tehnička enciklopedija, sv. 8., str. 1.23., Zagreb, 1982.
16. D.Bazjanac, R.Galić:Sateliti, umjetni Zemljini, Tehnička enciklopedija 12, Hrvatski leksikografski zavod, Zagreb, 1992.
17. D. Bazjanac: Svemirske letejlice, Tehnička enciklopedija 12, HLZ, Zagreb, 1992.

Zaključak

Iako je životni put Davorina Bazjanca detaljno i sustavno istražen i objelodanjen, do sada nije temeljito istraženo publicističko područje Bazjančeva djelovanja. U knjizi: *Sjećanja na profesora Davorina Bazjanca* djelomično je pisano o objavljenim radovima Davorina Bazjanca. Autori su knjige njegovi bivši učenici Stjepan Jecić, Ivo Alfirević i Osman Muftić. Stoga je ovaj rad usredotočen na Bazjančevu autorsku bibliografiju kako bi i u tom području Bazjanac bio poznat u potpunosti. Budući da je najpotpuniji popis

njegovih radova do sada iznosio 80 referencija, u ovom radu on se dopunjuje s još 127 radova, pa ukupni popis njegovih radova čini 207 referencija. Na osnovi novih saznanja može se zaključiti da je Bazjanac imao važniju ulogu u povijesti tehničkih znanosti nego što se to dosad mislilo. Rad je pisan s namjerom da bude poticaj za daljnja dopunjavanja autorske bibliografije Davorina Bazjanca, ali i za buduću valorizaciju njegovih radova.

Literatura i izvori

[1] Spomenica Fakulteta strojarstva i brodogradnje, 1919-1969, Zagreb, 1970.

[2] Prof. dr Davorin BAZJANAC, dipl. inž., primio nagradu za životno djelo 1975., Strojarstvo, god. XVII, 1975., br. 6., str. 313-314.

[3] Hrvatski biografski leksikon, sv. 1, str. 559, Jugoslavenski leksikografski zavod, Zagreb, 1983.

[4] Fakultet strojarstva i brodogradnje Sveučilišta u Zagrebu u razdoblju od 1979. do 1989., Zagreb, 1989.

[5] Spomenica u povodu 75. obljetnice Zavoda za tehničku mehaniku 1920-1995. Građevinskog fakulteta i Fakulteta strojarstva i brodogradnje Sveučilišta u Zagrebu, Zagreb, 1995.

[6] Hrvatski leksikon, sv. 1., str. 77, Naklada leksikon d.o.o., Zagreb, 1996.

[7] Hrvatska enciklopedija, sv. 1., str. 674, Leksikografski zavod *Miroslav Krleža*, Zagreb, 1999.

[8] Sjećanja na profesora Davorina Bazjanca, Fakultet strojarstva i brodogradnje Sveučilišta u Zagrebu, Zagreb, 2002., 102 str.

[9] Slavonski korijeni profesora Davorina Bazjanca, Hrvatsko društvo za mehaniku, Zagreb, 2004., str. 23.

[10] Ljetopis JAZU za god. 1973. i 1974., knj. 78, Zagreb, 1978., str. 289.

[11] Arhiva Fakulteta strojarstva i brodogradnje Sveučilišta u Zagrebu.

[12] Arhiva Leksikografskog zavoda *Miroslav Krleža*.

[13] Pravilnik o dodjeli medalja, nagrada i priznanja (pročišćeni tekst), Zagreb, 2011., Fakultet strojarstva i brodogradnje Sveučilišta u Zagrebu

[14] *Bilten dokumentacija inostrane stručne literature*.

[15] *Bilten dokumentacija stručne literature*.

Summary

In this paper biographic nature of Davorin Bazjanac is given. On the base of systematic research his complete publicistic work is given. Upon presenting his 80 published references, shown by his students Stjepan Jecić, Ivo Alfirević and Osman Muftić, author adds for the first time a list of new references of Bazjanac. The contribution of mentioned authors is expanded by 127 more Bazjanac's bibliographic references not reffered before.

Keywords: Davorin Bazjanac; biography; PhD(technical science); author's bibliography.

Dr. sc. Branko Hanžek,
znanstveni savjetnik u Zavodu za povijest i filozofiju
znanosti Hrvatske akademije znanosti i umjetnosti,
Ulica književnika Ante Kovačića 5, Zagreb.
email: bhanzek@hazu.hr

UPUTE AUTORIMA

Časopis *Rad. Tehničke znanosti* objavljuje radove članova HAZU i drugih autora iz područja tehničkih znanosti i njezinih polja prema nomenklaturi o podjeli znanosti u RH.

Radovi se objavljuju prema sljedećoj klasifikaciji:

izvorni znanstveni članak,
pregledni članak (kritički osvrti s izvornim doprinosom autora),
stručni članak visoke razine s prijedlozima za struku.

Radovi se objavljuju, u pravilu, na jednom od svjetskih jezika, uz prošireni sažetak na hrvatskom. Ako je rad pisan na hrvatskom, sažetak se objavljuje na jednom od svjetskih jezika. Slike moraju imati dvojezične opise.

Pored naslova članka, ističu se imena autora, zanimanje, pripadna ustanova s adresom te se navode ključne riječi na oba jezika.

Radovi se dostavljaju Uredništvu u tri tiskana primjerka uz priloženu verziju u elektroničkom obliku (disketa, CD).

Uredništvo sačinjavaju svi redoviti članovi Tehničkog razreda HAZU.

Adresa Uredništva jeste: Hrvatska akademija znanosti i umjetnosti, Razred za tehničke znanosti, Zrinski trg 11, 10 000 Zagreb.

Uredništvo razmatra primljene radove i donosi odluku o pripadnosti rada tehničkim znanostima. Ako je mišljenje pozitivno, Uredništvo određuje dva recenzenta, od kojih je barem jedan usko vezan uz tematiku kojom se bavi rad. Drugi mora biti iz srodne znanstvene grane.

Uredništvo na osnovi primljenih recenzija prihvaća ili odbija rad, zahtijeva po potrebi izmjene, doradu i skraćivanje te odlučuje o tiskanju.

Radovi odabrani za tiskanje obavezno se lektoriraju.

Prema broju primljenih radova Uredništvo zaključuje opseg (broj radova) naredne knjige i šalje radove u tisak.

Sve pripremne radove za rad Uredništva, komunikaciju s autorima i s izdavačkim odjelom HAZU obavlja glavni urednik.

Objavljivanjem članaka u časopisu, autori su suglasni da se njihov članak u punom ili skraćenom obliku objavi na internetskom portalu HAZU ili drugim znanstvenim portalima s kojima HAZU surađuje.

Ako autor ne želi da se njegov članak objavi na internetu, molimo da to javi uredništvu časopisa.

Autori dobivaju jedan besplatan primjerak časopisa.

Rad 536. Technical sciences 19(2018)

Nakladnik
HRVATSKA AKADEMIJA ZNANOSTI I UMJETNOSTI
Trg Nikole Šubića Zrinskog 11, 10000 Zagreb

Za nakladnika
Akademik Dario Vretenar, glavni tajnik

Grafička urednica i urednica na portalu HRČAK
Nina Ivanović

UDK kategorizacija
Nataša Daničić

Digitalni identifikator objekta (DOI)
Kristina Polak Bobić

Naklada
200 primjeraka

Grafička priprema i tisak
Tiskara Zelina d.d.

Zagreb, srpanj 2019.

ISSN 1330-082